Aspects of Materials Research for Advanced and Future Generations of Gravitational Wave Detectors

Karen Anne Haughian

School of Physics and Astronomy,

University of Glasgow

Presented as a thesis for the degree of

Doctor of Philosophy

2011

Contents

List of Figures

List of Tables

'Gravity is a habit that is hard to shake off'

T. Pratchett

Acknowledgements

It is a pleasure to thank all the people who made this thesis possible.

First and foremost I would like to express my sincere gratitude to my academic supervisors, Professor Sheila Rowan and Professor Jim Hough. Both, for the opportunity to carry out this research and for their continued support and guidance, without which this thesis would not have been possible. I would also like to thank STFC for providing me with the funding to carry out my PhD studies.

My colleagues in the lab were tremendously helpful and supportive and this created an enjoyable atmosphere in which to carry out the research. In particular I would like to thank Stuart Reid for the time he has spent working with me, answering my many questions and enjoying Russian vodka together, Marielle van Veggel for her invaluable advice and Liam Cunningham for his extreme patience while teaching me to create models in ANSYS. I also received help and advice from Alan Cumming (along with random, crazy conversations), Iain Martin, Peter Murray and Ronny Nawrodt in various aspects of my research for which I am grateful. Great support was also provided by the research group technicians, Colin Craig, Stevie Craig and Steven O'Shea and from John Davidson who set-up and helped operate the 4 point strength tester in the mechanical engineering workshop. Thanks also go to Jamie Scott for his essential IT support.

I would like to thank my current and previous office mates Matt Abernathy, Nicola Beveridge, Chris Bell, Paul Campsie, Eleanor Chalkley, Keith Evans, Alastair Heptonstall and Rahul Kumar for making my PhD an enjoyable experience for which thanks also go to Matthew Edgar. Special thanks go to

Riccardo Bassiri for his friendship and support through the PhD process, for our countless laughs, sing-alongs and fun, death-defying travels together. I would like to thank all members of the Institute for Gravitational Research for providing a friendly environment in which to work and study.

On a personal note, I would like to thank all of my family and friends for their love and support and for the many fun times we have spent together throughout my PhD process. My most heart felt thanks go to my Mum and Dad, and my sister Helen, for their continuing love, support and encouragement throughout my studies.

Preface

This thesis is an account of work carried out in the Institute for Gravitational Research at the University of Glasgow between October 2007 and September 2011. The research presented here contributes to the design of low mechanical loss suspensions in gravitational wave detectors. In particular, methods of reducing the thermal noise levels of the suspensions to increase the sensitivity are studied. The mechanical losses of materials to be used as mirror substrates and of hydroxide catalysis bonds was investigated along with the strength of hydroxide catalysis bonds as a function of different parameters. These investigations were carried out at the suggestion of Professor Sheila Rowan and Professor Jim Hough.

Chapter 1 describes the nature of gravitational waves along with some of the potential sources. It also introduces the different noise sources which currently limit the sensitivity of the gravitational wave detectors. This work has been derived from current literature.

In Chapter 2 the theory of thermal noise is discussed. How thermal noise can be quantified is shown and thus how thermal noise affects the detection of gravitational waves. By understanding this process, methods can be developed to minimise thermal noise and so increase the sensitivity of the detectors. This work is derived from current literature.

Chapter 3 introduces the chemistry of hydroxy-catalysis bonding and its applications in gravitational wave detection. The focus of this research was to investigate the effect of different factors on the strength of a hydroxy-catalysis bond and find an optimal bonding and curing procedure to create the strongest bonds. The experimental results were obtained by the author with the help

of Dr Marielle van Veggel. Dr Alan Cumming and Dr Liam Cunningham carried out the welding of the Advanced LIGO design ears and supplied the information of maximum temperature to which the bond is elevated during this process and the length of time the bond is exposed to this heat.

For Chapter 4 the mechanical losses of bulk fused silica samples were investigated. A new type of fused silica, Suprasil 3001 was measured. The use of chemical etching to reduce surface loss was investigated as part of a joint project with colleagues at Moscow State University. The experimental results were obtained by the author in collaboration with Dr Stuart Reid, Professor Boris Lunin, Dr Sergey Torbin and Dr Kirill Tokmakov. The fibre which was chemically etched was profiled by Dr Angus Bell and Dr Alan Cumming.

In Chapter 5 the mechanical loss of bulk samples of silicon was investigated. Two orientations of silicon were studied. The mechanical loss of silicon which had a <100> orientation and silicon which had a <111> orientation was measured at room temperature. The mechanical loss of a hydroxy-catalysis bond which was created between silicon substrates of <100> orientation was measured and calculated. The mechanical loss measurements were taken by the author and Dr Peter Murray at the University of Glasgow and the Friedrich Schiller University in Jena, Germany. The finite element analysis of the samples was carried out by the author along with Dr Liam Cunningham. The oxidising and bonding of the silicon samples was carried out by the author and Dr Stuart Reid.

Chapter 6 contains a summary of the conclusions drawn from the work presented in this thesis.

Appendix A contains calculations of an estimate for the thickness of a hydroxy catalysis bond from the properties of the bonding solution. The thickness of the bond is important for the derivation of the mechanical loss of a hydroxy-catalysis bond from the measured mechanical loss of a bonded sample.

Appendix B includes a brief summary of work carried out by the author on methods of de-bonding hydroxy-catalysis bonds.

Summary

Gravitational waves were predicted by Einstein, in his General Theory of Relativity in 1916 [1]. These waves can be thought of as ripples in the curvature of space-time. They have not yet been directly detected but strong indirect evidence of their existence was provided by Hulse and Taylor when they measured the rate of decay of the inspiral motion of a binary system [2, 3]. Research towards direct detection of gravitational radiation from astrophysical sources has been carried out for many years through the design, construction and initial operation of a network of gravitational wave detectors. Direct detection of gravitational waves will provide insights into the astrophysical sources which produce them and will provide a new method of observing events in the Universe.

Gravitational waves are quadrupole in nature and produce strains in space-time, which have extremely small amplitudes. The largest most violent events in the Universe are expected to cause strains of approximately 10^{-22} at the Earth in the frequency band of a few Hz to a few kHz. Long baseline interferometry between suspended test masses is currently used to search for the induced strains in space-time, and thus the direct effects of gravitational waves of astrophysical origin.

There is currently a network of interferometer detectors running worldwide. A 600 m long detector, GEO600, was built near Hannover in Germany by a collaboration between the Institute for Gravitational Research at the University of Glasgow, the Albert-Einstein-Intitut in Hannover and Gölm, the University of Hannover and Cardiff University. There are three detectors in the United States of America forming the LIGO project. Two detectors, one of 4 km arm

length and one of 2 km arm length were constructed on a site near Hanford, Washington State, and one detector of 4 km arm length was constructed near Livingston Louisiana. A 3 km detector, Virgo, was built near Cascina, Italy, by a European collaboration involving France, Italy and more recently the Netherlands. Six data collecting science runs have taken place to date with different combinations of these detectors in operation during the various runs; no detections have yet been made.

An important noise source in the current operating frequency band of ground-based detectors is the thermal noise of the test mass mirrors in the interferometers, and the mirror suspension elements. The research presented in this thesis focusses on studies of techniques for quantifying and reducing the mechanical loss associated with the suspended mirrors and thus reducing the associated thermal noise thereby increasing detector sensitivity. In particular, experiments were carried out to study the loss of fused silica and investigate aspects of the hydroxy-catalysis bonding process used to joint elements of the test mass suspensions. In addition, silicon was investigated as a potential candidate for use as a mirror substrate material for use in future gravitational wave detectors.

In Chapter 1 the nature of gravitational waves is explained and some of the sources which are expected to produce the largest amount of gravitational wave radiation are described. The development of resonant bar detectors and interferometers is given along with the current status of detectors and that of planned future projects. Noise sources which cause limitations to the detector sensitivity are discussed and an important noise source, thermal noise, is described in Chapter 2.

Thermal noise is an important noise source in the current frequency band of gravitational wave detectors. Reduction of thermal noise is a major challenge but is possible through careful design of the mirrors and their suspension systems.

One technique aimed at minimising the thermal noise of a suspension sys-

tem involves the creation of a quasi-monolithic suspension system by the use of hydroxy-catalysis bonding. This is a high precision, high strength method of adjoining suspension elements. In Chapter 3 investigations were made of the strengths of hydroxy-catalysis bonds and on the effect on strength of various parameters associated with the most commonly used version of the bonding procedure, and of putting bonds through different treatments. It is shown that the average strength of a hydroxy-catalysis bond between silica substrates is $\sim$ 15 MPa and that somewhat elevated temperature treatment (similar to an airbake) can improve on this strength, but that thermal shock conditions can decrease the strength. These investigations provide information on processes which can be used in the suspension construction to produce the lowest loss, highest strength suspension system.

Chapter 4 details mechanical loss measurements of bulk silica at room temperature. Different types of fused silica are studied and techniques to reduce their mechanical loss are discussed along with the effect which time and heat treatments can have on the mechanical loss of a hydroxy-catalysis bond. It is shown that Suprasil 3001 is an acceptable choice of material for the mirrors in gravitational wave detectors and that the mechanical loss of silica can be reduced through heat treatment.

In Chapter 5 the mechanical loss of bulk silicon is studied, where silicon forms a potential candidate for future generation gravitational wave detectors. Silicon samples having two different crystal orientations, <100> and <111>, were studied. Both orientations were manufactured and polished by the same vendor and have equivalent doping levels. At room temperature it is seen that the crystal orientation <111> material yielded mechanical loss values which were slightly lower than the <100> material. It is shown that it is possible to further reduce the loss of the material through heat treatment. An upper limit of the mechanical loss of a hydroxy-catalysis bond between silicon substrates is determined and found to be within the range of 0.27 to 0.52.

The results presented in this thesis indicate that the mechanical losses

of silica suspensions in gravitational wave detectors can be reduced through methods such as heat treatments and, potentially, chemical etching. Silicon is seen to be an interesting candidate for the suspension material in future generation detectors run at cryogenic temperatures.

Chapter 1

Gravitational wave detection

1.1 Introduction

Gravitational waves were first predicted by Einstein in his General Theory of Relativity in 1916 [1]. These waves can be thought of as ripples in the curvature of space-time which are created by the asymmetric acceleration of mass, and are predicted to travel at the speed of light. At present these gravitational waves have remained elusive to direct detection techniques.

Efforts aimed at the direct detection of gravitational waves began with Weber in 1960 [4]. When, in 1969, he reported the coincident detection of a gravitational wave passing through both of his resonant bar detectors [4], various gravitational wave groups formed in an attempt to verify this reported detection. None of these new gravitational wave experiments could reproduce Weber's results [5]. Detectors of increased sensitivity, based on the use of Michelson-type laser interferometers have now been developed. There is currently a network of gravitational wave interferometers around the world and as upgrades to these detectors are implemented, the era of detection draws nearer. When gravitational waves are detected directly, the predictions made by Einstein should be confirmed and an entirely new field of astronomy created.

Although gravitational waves have yet to be experimentally observed directly, very strong evidence for their existence is provided from observations made by Hulse and Taylor. They discovered the binary pulsar PSR 1913 + 16

and observed its behaviour for many years [2, 3]. Their measurements showed that the rate of decay of its orbital period matched that of the decay which would be expected due to the emission of gravitational waves. This discovery won Hulse and Taylor the Nobel Prize in 1993.

1.2 Nature of Gravitational Radiation

Gravitational waves are produced by the acceleration of non-axisymmetric mass. The lowest order of gravitational radiation is quadrupole in nature as the conservation of mass precludes the existence of monopolar radiation and dipolar radiation is ruled out due to the conservation of momentum [5]. As gravitational waves propagate through space they create a strain in space-time, h, transverse to their direction of propagation. This has the effect of causing distances to be shortened in one direction while they are lengthened in the orthogonal direction. Gravitational waves consist of a superposition of two independent polarisations, h_+ and $h_\times$ which lie at 45° to one another. The effect that these polarisations would have on a set of free test particles positioned in the shape of a ring is shown in figure 1.1.

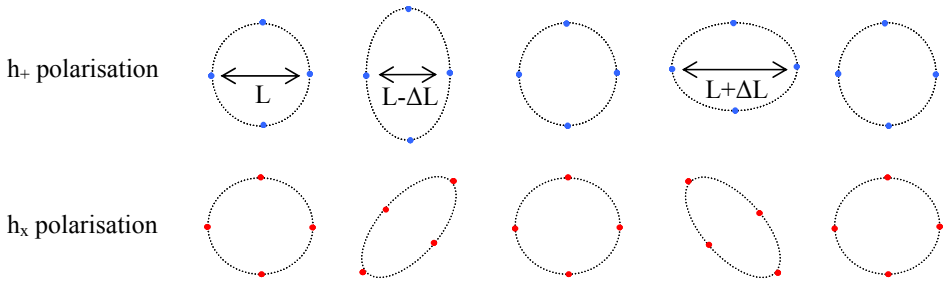

Figure 1.1: The effect of the passage of h_+ and $h_\times$ polarisations of gravitational waves on a ring of test particles when the incident waves are normal to the page.

The strain amplitude of a gravitational wave detected by a gravitational wave interferometer is defined as

$$h = \frac{2\Delta L}{L}, \tag{1.1}$$

where L is the distance between two test particles and ΔL is the change in this separation due to the passing gravitational wave.

Gravity is the weakest of the four fundamental forces. Any waves manually produced in a laboratory would be so minute they would be unmeasurable by the most sensitive gravitational wave detector currently in operation [5]. The production of gravitational waves which have an amplitude measurable on Earth requires sources of astrophysical masses and accelerations.

1.3 Sources of Gravitational Waves

A subset of the astrophysical events which are expected to produce gravitational waves are discussed below. The events discussed here can create waves with a frequency from a few tens of Hertz up to a few thousand Hertz. This is the frequency range at which the current detectors are the most sensitive.

1.3.1 Burst Sources

Burst sources, as suggested by the name, are events which cause a very brief rapid outburst of gravitational radiation as opposed to continuous signals. Two different types of this kind of source are discussed below.

1.3.1.1 Supernovae

Supernovae are among the most spectacular events in the Universe. They are extremely luminous stellar explosions. Due to their great luminosity, which can outshine a galaxy, it can appear from Earth that a bright new star has just been born when in fact a supernova can be described as the death of a star. At the end of a star's lifetime it can approach the Chandrasekhar limit [6]. As the star's mass can no longer be supported by electron degeneracy pressure the core collapses causing a stellar explosion. The product of this

stellar explosion is dependant on the mass of the star, small stars will become white dwarf stars, larger stars will become neutron stars or black holes. If the collapse of the star is symmetrical then no gravitational radiation will be emitted. However, if the star has angular momentum then the collapse can be asymmetric and a burst of gravitational radiation will be produced. The strain, h, of the gravitational waves produced from a core collapse supernova is estimated to be $\sim 1 \times 10^{-21}$ at a distance of 10 kpc from the source [7].

1.3.1.2 Coalescing Compact Binaries

A type of astronomical configuration is the binary system. Compact binary systems consist of two extremely dense objects, such as neutron stars or black holes, rotating around a common centre of mass. The orbit of the system decays as the system emits gravitational radiation. As the objects become closer, the frequency of the gravitational waves increase and over the last few seconds before the objects coalesce the frequency sweeps through the operating band of ground-based gravitational wave detectors, in the range of a few tens to a few hundred Hertz. At this point the amplitude may, depending on the sources distance, become large enough to be detectable from Earth.

The strain, h, produced from this type of source was estimated by Schutz to be [8]

$$h \approx 1 \times 10^{-23} \left(\frac{m_T}{M_\odot}\right)^{2/3} \left(\frac{\mu}{M_\odot}\right) \left(\frac{f}{100\text{Hz}}\right)^{2/3} \left(\frac{100\text{Mpc}}{r}\right), \qquad (1.2)$$

where $m_T = m_1 + m_2$, the sum of the mass of the two objects in the system, $\mu = m_1 m_2/(m_1 + m_2)$, the reduced mass of the system, f is the frequency of the emitted gravitational wave radiation and r is the distance between the coalescing system and a gravitational wave detector.

Compact binary systems with two neutron stars are the most commonly occurring, systems with one neutron star and one black hole are rarer and there is a possibility that two black holes could also form a binary system. Binaries containing black holes are important candidates for detection to gravitational

wave astronomers as their larger mass and density would mean they would emit gravitational radiation of a higher amplitude.

1.3.2 Continuous Sources

During the lifetime of a binary system a continuous stream of low frequency gravitational waves is emitted. It is not until a few seconds before the coalescence that the frequency of the waves reaches a high enough level to be observable by the current detectors and so they are only considered as periodic sources. There are, however, some stably rotating systems which produce a continuous flow of gravitational waves that could be detectable on Earth within the current frequency range. Some candidates of detection are outlined below.

1.3.2.1 Pulsars

During a supernova the star core collapses into itself with one possible end state being a very dense neutron star. These stars emit streams of electromagnetic waves at radio frequencies from both of their poles. For a neutron star rotating about an axis which is not through these poles, these radio waves sweep out a path in space which may periodically include the Earth. The discovery of these periodic radio signals by Hewish et al in 1967 [9] led to the name 'pulsar' being adopted for such objects. If the pulsar does not rotate axisymmetrically, then gravitational radiation will be emitted. The strain amplitude produced from a pulsar of rotation frequency f_{rot}, a distance r away from the detector is thought to be [10]

$$h \approx 6 \times 10^{-25} \left(\frac{f_{rot}}{500\text{Hz}}\right)^2 \left(\frac{1\text{kpc}}{r}\right) \left(\frac{\epsilon}{10^{-6}}\right) \tag{1.3}$$

where ϵ is the equatorial ellipticity of the star.

1.3.2.2 Low Mass X-ray Binaries

A compact object such as a neutron star can exist in a binary system with a normal star. The large gravitational field from the neutron star can allow it

to accrete mass taken from its companion and hence experience an increase in its angular momentum. X-rays are emitted from the neutron star due to the accretion of mass. As the angular momentum increases, the Chandrasekhar-Friedman-Schutz (CFS) [11] instability point can be reached. This is where the rotation becomes non-axisymmetric and gravitational radiation is emitted. Stars which exist at this instability point are known as Wagoner stars [12]. The strain amplitude expected from this type of system is related to the observed X-ray flux, L_γ [12] as,

$$h \approx 3 \times 10^{-27} \left(\frac{1\text{kHz}}{mf}\right)^{\frac{1}{2}} \left(\frac{L_\gamma}{10^{-8}\ \text{ergs cm}^{-2}\ \text{sec}^{-1}}\right)^{\frac{1}{2}}, \tag{1.4}$$

where m is the mode number and is ~ 4 and f is the frequency, expected to be ~ 500 Hz.

1.3.3 Stochastic Sources

The stochastic background is not as well understood as the other sources of gravitational waves discussed above. It is thought to have been created from a superposition over space, time and frequency of gravitational waves created by many different events distributed throughout the Universe. Such events could be the collapse of a population of black holes [5], waves produced just after the Big Bang in the inflationary period [5] or those arising from cosmic string production [13]. This stochastic background exists as random signals. It can therefore not be detected by one interferometer alone. By cross-correlating the output from two or more detectors it is possible to search for the stochastic background [14].

1.4 Gravitational Wave Detection

There are two types of ground-based gravitational wave detectors currently being operated and further developed; resonant bar detectors [15, 16] and laser interferometers [17–20]. As gravitational waves produce extremely small

strains in space the detectors must be very sensitive to enable the observation of these strains. There are also radio astronomy techniques being applied to search for gravitational waves; e.g. pulsar timing.

1.4.1 Pulsar Timing

Pulsar timing is the tracking of the arrival time at Earth of the periodic radio wave signals from pulsars. The separation between the Earth and a pulsar will be altered by a passing gravitational wave and this will affect the propagation of the radio signals thus affecting the time of arrival. When the actual time of arrival is compared to the predicted time of arrival for many pulsars, correlations due to the gravitational wave should be seen. Pulsar timing would be sensitive to gravitational wave sources from $\sim 10^{-9} - 10^{-8}$ Hz which is the frequency of waves we would expect to be produced by the coalescence of supermassive black holes [21]. Several pulsar timing projects are ongoing such as the IPTA (International Pulsar Timing Array) [22] which is a collaboration between three projects, EPTA (European Pulsar Timing Array)[23], NANOGRAV (North American Nanohertz Observatory for Gravitational waves) [24] and PPTA (Parkes Pulsar Timing Array)[25].

1.4.2 Resonant Bar Detectors

The first gravitational wave detectors were resonant bar detectors, originally a concept of Joseph Weber. In 1960, Weber constructed and ran the first bar detectors and in 1969, he reported a coincident detection [4]. Many institutions constructed bar detectors in an attempt at confirming Weber's suspected detection. A bar detector which made use of an interferometer to monitor the motion of the mass, created at the University of Glasgow is shown in figure 1.2. Weber's experiment consisted of two large cylindrical masses (of the order of a few tonnes) made from aluminium which were suspended under vacuum at room temperature [26–28]. The two bar detectors were separated by 2 km. If a gravitational wave of appropriate frequency and orientation passed through

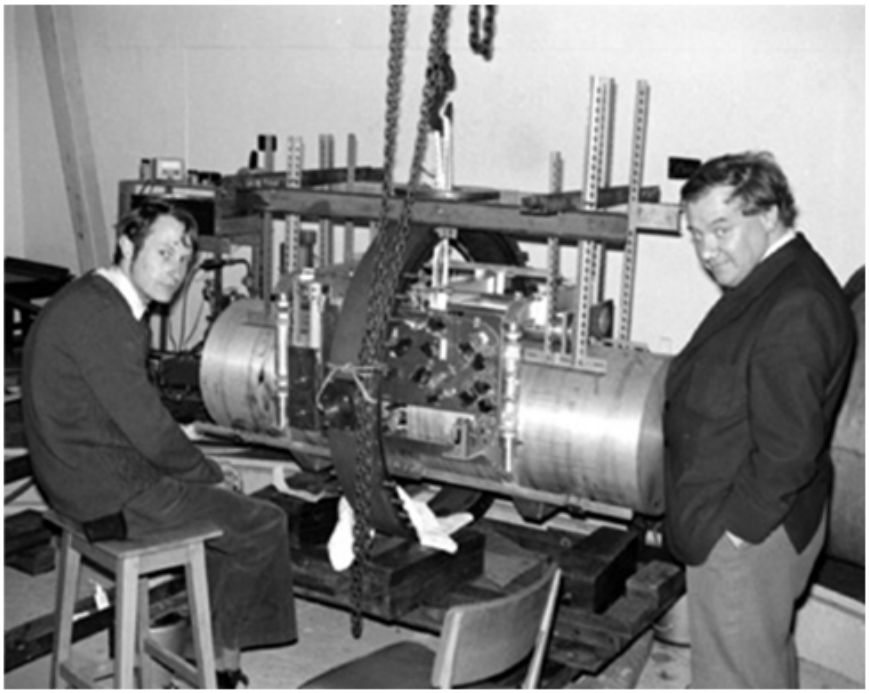

Figure 1.2: Jim Hough and Ron Drever working on the aluminium bar detector at the University of Glasgow.

the mass, the fundamental longitudinal mode of the bar would become excited causing small movements of the cylinders. A set of piezoelectric strain gauges were attached to the middle of the bar to record the motion over time thus transforming the effect of the gravitational wave into a electrical signal. It was found that the electronic noise of the detector and the thermal noise of the molecules making up the bar itself formed a limit to detector sensitivity [29]. The smallest gravitational wave strain amplitude detectable from this type of instrument at 1,600 Hz was h $\sim 10^{-16}$ $/\sqrt{\text{Hz}}$ which is much larger than the predicted strain size for astrophysical sources [5]. This led to scientists working to reduce the thermal noise by cooling the bars to cryogenic temperatures. Allegro [30], Auriga [15], Explorer [31] and Nautilus [16] are some of these cyrogenically cooled bar detectors, with strain sensitivities of h $\sim 10^{-20}/\sqrt{\text{Hz}}$ [32] over a band width of $\sim$ 100 Hz having been achieved. Of these, only Auriga and Nautilus are currently still operating [33].

Further increases to the sensitivity could be obtained by increasing the mass of the detectors. By changing the geometry of the detectors to a sphere it is easier to increase the mass without dramatically increasing the size of the experiment and this also provides a method of achieving directionality [34]. A spherical mass has five quadrupole modes as opposed to a bar which has one. Thus, if a gravitational wave passed through the sphere, the direction of the waves could be found by comparing the ratio of the excitation of each mode. This enables the direction of the source to be obtained. MiniGRAIL [35] and the Mario Schenberg Detector [36] are two spherical detectors which are currently operating with $\sim$ 60 Hz bandwidth and can measure strains of $h \sim 10^{-21}$ at $\sim$ 3,000 Hz.

One of the disadvantages of using bar and spherical detectors is that the frequency bandwidth observable is $\sim$ 100 Hz as only frequencies close to the resonance of the detector can be observed. A concept of creating a dual resonant mass detector was proposed by Cerdonio and others [37]. Their idea was to place a solid cylinder inside a hollow cylinder. The cylinders would be chosen to ensure the hollow cylinder had a resonant frequency two or three times less than that of the solid cylinder inside. If a gravitational wave passed through this detector the masses would be excited in anti-phase and thus the signal would be amplified. This instrument is predicted to achieve strain sensitivities down to 2×10^{-23} $/\sqrt{\text{Hz}}$ over a bandwidth of two kiloHertz [37]. However, this type of detector requires a complicated readout system which could add extra loss to the system reducing the sensitivity levels. Therefore, more research has to be carried out to ensure the practicality of this design.

1.4.3 Interferometric Detectors

A design of gravitational wave detector which is sensitive to a larger frequency band is the interferometric detector. The quadrupole moment of the gravitational waves make a Michelson-type laser interferometer a very useful tool for detection. Figure 1.3 shows a schematic of a simple Michelson interferometer.

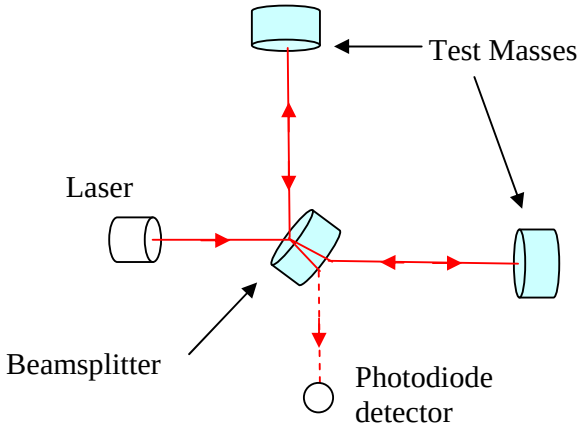

Figure 1.3: A schematic diagram of a simple Michelson interferometer.

The test masses in figure 1.3 can be thought of as the test particles in figure 1.1. Hence, as a gravitational wave passes through, the length of one of the arms, the distance from the laser to the end mirror, shortens while the second arm is lengthened. Then the shortened arm is lengthened and the lengthened arm is shortened.

Forward and Weiss carried out the first experimental work developing interferometers to search for gravitational waves [38, 39]. In these instruments an incident beam of light from a laser is split using a beam splitter; 50% of the light being transmitted and 50% being reflected. These two beams of light then travel down the orthogonal arms of the interferometer and are reflected back by the end test masses which have a reflective coating. The test masses are suspended in vacuum to reduce noise in the system. The beams recombine at the beam splitter and the resultant signal is detected at a photodiode detector. In the absence of noise sources and passing gravitational waves, the difference in arm lengths of the interferometer remain constant, such that the light from each arm will interfere at the output. A change in the difference in arm lengths caused by a passing gravitational wave would change the interference pattern at the output causing a change in the intensity of the light at the photodiode.

From equation 1.1 it can be seen that for a given amplitude 'h' of gravitational wave, an increase in the arm length of the detector will cause an

increase in the change in length caused by the gravitational wave, making the wave more easily detectable. However, due to the curvature of the Earth the length of the detectors on the Earth's surface are currently limited to ∼4 km [5]. To ameliorate the effects of this constrained arm length a range of interferometry techniques have been implemented to increase detector sensitivity. These will be discussed further below.

1.4.4 Improving the Sensitivity of Interferometric Detectors

Interferometers are most sensitive when the time for which the laser light is stored within the arms equals half of the period of the gravitational wave [5]. For this situation, the light would take a quarter of the period of the gravitational wave to travel from the beamsplitter to the end mirrors. Thus, the light would sense the end mirrors when they were maximally displaced due to the the passing gravitational waves. For gravitational waves between 100 Hz and 1 kHz detector arm lengths would have to be between 750 km and 75 km respectively. Building gravitational wave detectors this size would be impractical due to the large cost of the infrastructure and the curvature of the Earth causing extra noise in the system, this is discussed further in section 2.7.2.3. Therefore, concepts were developed to increase the optical path length without physically increasing the length of the arms to improve sensitivity.

1.4.4.1 Delay-line Interferometer

The incorporation of optical delay-lines in interferometric systems to improve sensitivity was proposed by Weiss in the 1970s [40]. In a delay-line interferometer an extended optical path is created by reflecting the laser light multiple times between additional mirrors placed in the arms of the interferometer typically with the reflected beams being spatially separated. There are two methods for creating a delay-line interferometer. The first is to fold the arm so the laser light reflects off a secondary mirror which is positioned at an angle

to the end test mirror near the beam splitter. This folded arm method was implemented for the GEO600 detector [19] and a schematic diagram of this layout is shown in the left image of figure 1.4. The second method of creating a delay-line interferometer is to insert the secondary mirror close to the beam splitter, facing the end test mirror. This method was developed at the Max-Planck-Institut für Quantenoptik [41] in Gärching, Germany [42]. By having the mirrors slightly curved, the laser light could enter through a hole in this secondary mirror, be reflected between the two mirrors without any overlapping beams and would exit through the same hole it entered. A schematic of this layout is shown in the right image in figure 1.4. The disadvantage of a delay-line is that the interferometer becomes more sensitive to scattered light.

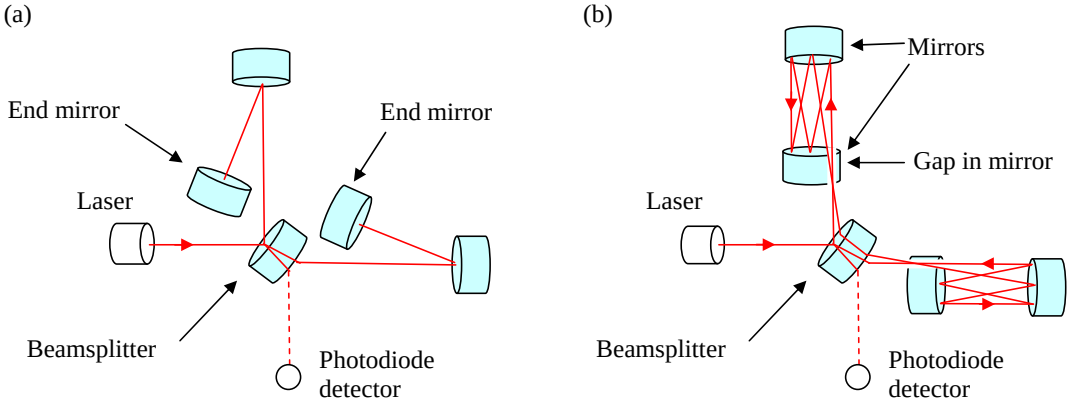

Figure 1.4: A schematic diagram of an interferometer in a delay-line configuration. The left image shows the optical path being extended by reflection from additional mirrors at an angle and the right image shows the optical path being extended through reflection against an input mirror.

1.4.4.2 Fabry-Perot Cavities

The method of enhancing detector sensitivity by using Fabry-Perot cavities in the interferometer arms was first developed in Glasgow in the 1980s [43] and is now used in the LIGO [17], Virgo [18] and TAMA-300 [20] detectors.

In this configuration the arms consist of partially transmissive mirrors situated near the beam splitter, facing highly reflective mirrors at the end of the interferometer arms. The laser light enters the cavity through the partially transmissive mirror. The reflected beams lie on top of one another allowing for smaller mirrors than those needed for the delay-line interferometers. In this configuration one of the cavities can be held on resonance by altering the frequency of the laser and the other arm length can be held on resonance by feedback of an appropriately amplified and filtered portion of the photodiode signal at the output to an actuator at the end mirror. This method artificially extends the path length of the detector and hence, amplifies the phase change of the laser light caused by any passing gravitational wave. A schematic of this layout is shown in figure 1.5. The use of Fabry-Perot cavities requires sophisticated systems to control the orientations of the mirrors and the lengths of the cavities.

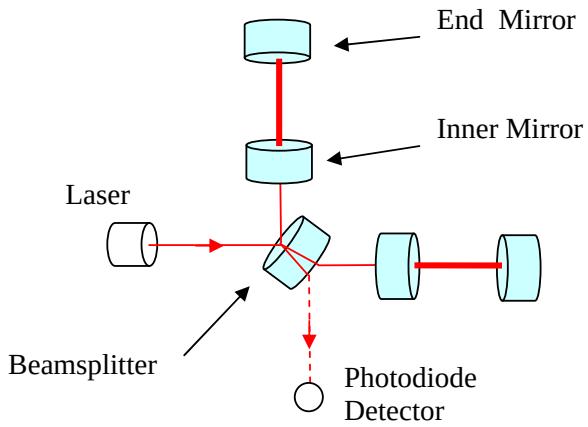

Figure 1.5: A schematic diagram of an interferometer with Fabry-Perot arm cavities.

1.4.4.3 Power Recycling

A method of increasing the output signal from the gravitational wave detector is that of "power recycling" [44]. A partially transmissive mirror is placed between the laser and the beamsplitter as shown in figure 1.6. This mirror

creates a cavity with the interferometer and the light which is transmitted through the beamsplitter, when travelling back towards the laser is reflected and is 'recycled'. This increases the stored laser power within the interferometer and hence increases the sensitivity as will be discussed in section 1.5.3. This technique is used in GEO600 and will be implemented in Advanced LIGO.

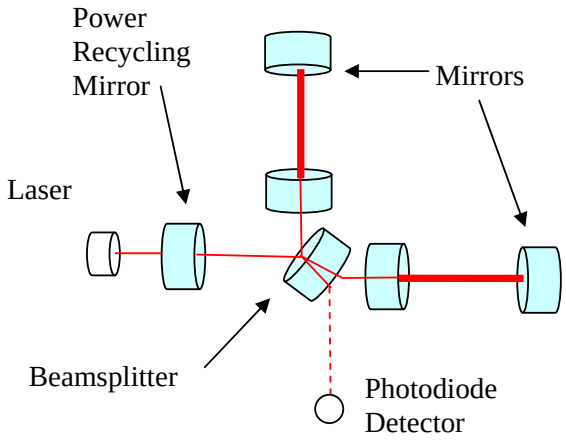

Figure 1.6: A schematic diagram of a simple Michelson interferometer a power recycling mirror.

1.4.4.4 Signal Recycling

Signal recycling works in a similar way to power recycling. A partially transmissive mirror is placed between the beam splitter and the detector output to recycle the signal light [45] as shown in figure 1.7. The interferometers are operated near a dark fringe thus, the light signal caused by a passing gravitational wave is small. The signal recycling mirror forms a cavity with the interferometer which can amplify the signal. By careful placement of this signal recycling mirror the frequency at which the detector is most sensitive can be altered. This allows possible targeted detection of different sources of gravitational waves.

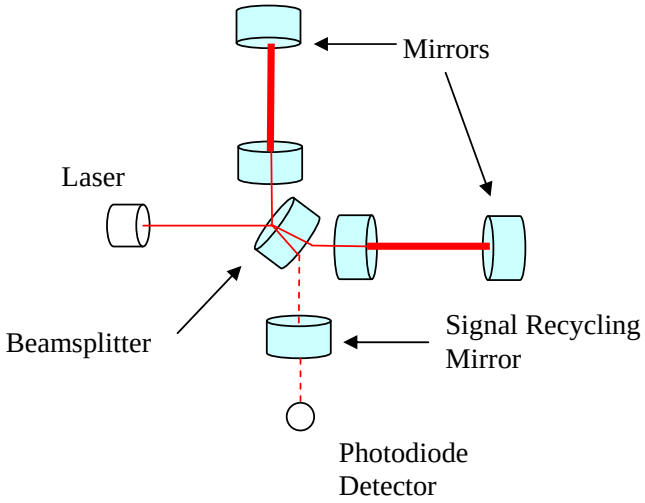

Figure 1.7: A schematic diagram of a simple Michelson interferometer with a signal recycling mirror.

1.5 Noise Sources

There are many noise sources which can limit the sensitivity of interferometric gravitational wave detectors. In this section a selection of these noise sources will be discussed, along with the effects of the noise and some methods of reducing the noise.

1.5.1 Seismic Noise

Seismic noise is noise caused by movement or vibration of the Earth's crust. This can be created by many sources, both natural and man-made such as the crashing of waves in the ocean or the flow of traffic. The level of seismic noise varies with the time of day and with location on the Earth. At a reasonably quiet location the seismic noise in all three directions is around $10^{-7} \times f^{-2}$ m/$\sqrt{\text{Hz}}$ [46], where f is the frequency in Hertz. To enable a gravitational wave to be detected, the displacement of each test mass is required to be less than $\sim 3 \times 10^{-20}$ m/$\sqrt{\text{Hz}}$ for a frequency of 30 Hz [46]. To meet this requirement the seismic noise must be reduced in the horizontal direction by a factor greater than 10^9 [46]. Noise in the vertical direction can couple

through to the horizontal axis so it is important to apply seismic isolation in this direction also. Horizontal seismic noise can be reduced by suspending the mirrors as pendulums. This attenuates the ground motion above the resonant frequency, f_0, of the pendulum by approximately $-{f_0}^2/f^2$ [5]. By increasing the number of pendulum stages the attenuation of the ground motion can be increased. The vertical motion of the mirrors can be reduced with the use of cantilever springs [47].

1.5.2 Gravitational Gradient Noise

Gravitational Gradient Noise can also be known as "directly coupled seismic noise" or "Newtonian noise". It results from the mirrors directly coupling to local fluctuations in the gravitational field caused by changing mass distribution of the surrounding area. This type of noise is thought to limit the performance of detectors at less than 10 Hz [46]. One method of reducing this noise is to build the detector underground. This is planned for the third generation detector the Einstein Telescope [48] and for the Large-scale Cryogenic Gravitational wave Telescope (LCGT) [49]. Gravitational gradient noise can be significantly reduced by placing the detector in space which is planned for the Laser Interferometer Space Antenna, LISA [50].

1.5.3 Photoelectron Shot Noise

Photoelectron shot noise, or photon shot noise [51] is caused by a combination of vacuum fluctuations and the amount of photons being emitted or absorbed fluctuating due to the photodiode and laser not being 100% efficient. Vacuum fluctuations occur within the vacuum system and enter the interferometer and this alters the number of photons, N, reaching the photo-diode detector situated at the output of the interferometer over an observation time, τ. Assuming that the number of photons reaching the diode in a time, t, follows Poisson statistics then the uncertainty in the number of photons is $\sqrt{\mathrm{N}}$. The intensity of light reaching the detector is dependent on the amplitude of the

gravitational wave passing through. Thus, shot noise is a limiting factor to the detector sensitivity. The sensitivity limit set by shot noise in a simple Michelson interferometer can be written as [5],

$$h_{shot}(f) = \left(\frac{1}{L}\right)\left(\frac{\hbar c\lambda}{2\pi P_{in}}\right)^{\frac{1}{2}} \text{ per } \sqrt{\text{Hz}}, \tag{1.5}$$

where L is the length of the interferometer arm, $\hbar$ is the reduced Planck's constant, c is the speed of light, λ is the wavelength of the laser, P_{in} is the input laser light power.

From equation 1.5 it can be seen that the limit to sensitivity caused by shot noise can be reduced by increasing the input power of the laser. Shot noise is the dominant noise source at higher frequencies ($\sim$ a few hundred Hertz).

1.5.4 Radiation Pressure

When photons are reflected from the mirrors in an interferometer, they transfer momentum to the mirrors and a force is applied to the face. As there is a fluctuation in the number of photons being reflected the force varies causing a variation in the mirror position. This in turn results in a phase change in the recombined beam. This effect is known as radiation pressure noise. The radiation pressure noise in a simple Michelson interferometer can be expressed as [5],

$$h_{r.p}(f) = \left(\frac{1}{mf^2L}\right)\left(\frac{\hbar P_{\text{in}}}{2\pi^3 c\lambda}\right)^{\frac{1}{2}} \text{ per } \sqrt{\text{Hz}}, \tag{1.6}$$

where m is the mass of the mirror, f is the frequency of a passing gravitational wave, L is the arm length of the detector, $\hbar$ is the reduced Planck's constant, P_{in} is the input power, c is the speed of light and λ is the wavelength of the laser light. From equation 1.6 it can be seen that in an interferometer radiation pressure noise decreases towards higher frequencies and increases as input laser power is increased.

1.5.5 The Standard Quantum Limit

Photoelectron shot noise and radiation pressure noise can be combined in quadrature to give a total optical readout noise. In a simple Michelson interferometer these two types of noise are uncorrelated and respond in an opposite manner to an increase of laser power. Therefore, it can be seen that an optimum power level which gives the minimum amount of noise, exists where $h_{shot}(f) = h_{r.p}(f)$. This sensitivity limit is known as the standard quantum limit [52, 53].

In some interferometer configurations coupling of the optical field to the mechanical system occurs in such a way as to introduce correlations between shot noise and radiation pressure noise. Studies suggest this should enable sensitivities better than that set by the standard quantum limit to be achieved at specific frequencies [54].

1.5.6 Thermal Noise

Thermal noise in an interferometric gravitational wave detector arises from the fact that each atom in the material used for the suspensions and test mass mirrors has some thermal energy and thus, some associated thermally driven motion. From the equipartition theorem we know that the average energy of each atom is $\frac{1}{2}k_BT$ per degree of freedom, where k_B is Boltzmann's constant, and T is the temperature in Kelvin [5]. Thermal noise is often described as arising in three main forms.

The first of these is Brownian noise [55]. The random movement of the atoms results in energy dissipation within the material. This type of noise can be reduced by using low mechanical loss materials to create the suspension elements and test masses. As the friction is reduced, the noise is reduced, thus increasing the sensitivity of the detector.

A second type of thermal noise is thermoelastic noise [56]. Statistical fluctuations in the local temperature can cause elements of the suspension material to expand or contract via the effects of its thermal expansion coefficient.

The third way in which thermal noise exists is as thermorefractive noise [57]. The temperature fluctuations in the material cause local fluctuations in the refractive index of the mirrors and thus can alter the phase of the laser light which passes through them.

Thermoelastic and thermorefractive noise can be correlated as "thermo-optic" noise. The total thermo-optic noise has been shown to be less than previously thought as these mechanisms can occur with a relative negative sign [58].

Thermal noise is the dominant noise source limiting detector sensitivity at the lower end of the current operating frequency band, between $\sim$ 50-500 Hz. The work in this thesis is aimed at reducing this type of noise. It is discussed in more detail in Chapter Two.

1.6 The Current Detector Network

Currently there is a network of laser interferometric gravitational wave detectors located around the world which has been operating to search for gravitational waves. These detectors have in many cases been developed from small prototypes with arm lengths of a few metres, leading to the design and construction of the much larger, currently operating detectors which have arm lengths of up to a few kilometres.

LIGO

The LIGO (Laser Interferometer Gravitational-wave Observatory) system consists of three interferometers in the United States of America. Two of which, a 4 km and a 2 km detector, are situated in the same vacuum system in Hanford in Washington State and the third, a 4 km arm length detector, is in Livingston, Louisiana. Photographs of these detector sites are shown in figure 1.8. All three of these interferometers have Fabry-Perot cavities in their arms. The mirrors of the first generation LIGO instruments were each made from fused silica of mass 10.7 kg, suspended on a single loop of metal wire.

Figure 1.8: Photographs of the LIGO detector sites. On the left is the Hanford detector site and the Livingston site is shown on the right.
[59]

The fifth "science" run (S5) - a data taking period for the detectors, was completed in 2007. LIGO achieved a strain sensitivity of 2.5×10^{-23} $/\sqrt{\text{Hz}}$ at 150 Hz. This sensitivity is shown in figure 1.9 [60]. LIGO was incrementally upgraded to Enhanced LIGO. This included improvements such as an increased laser power. In October 2010, the sixth science run was completed. This science run was completed in conjunction with the Virgo+ detector. The current status and planned upgrades to this detector are discussed in section 1.7.

Virgo

The Virgo detector has 3 km arms and was designed and built as a collaborative European project led by Italy and France. It is located near Cascina in Italy and has a sophisticated seismic isolation system which includes a multi-stage pendulum to suspend the mirrors. This allows for a reduction in the effects of seismic noise allowing the detector to be sensitive at frequencies down to 10 Hz. Virgo was completed in 2007 and it took five months of data during the period of LIGO's S5 science run, giving Virgo's first science data taking period, known as VSR1. An incremental upgrade to the hardware of the Virgo instrument, Virgo+ was effected by changing the mirror suspensions of Virgo to a quasi-monolithic system as in the GEO600 detector amongst other things. The current status and future plans for Virgo is discussed in section 1.7.

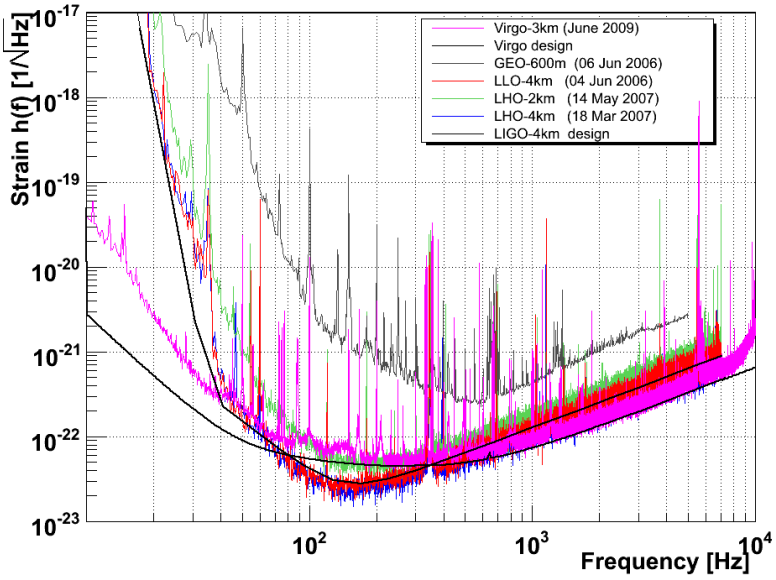

Figure 1.9: The sensitivity of the Virgo, LIGO and GEO600 detectors for a period of data taking during S5.

[61]

GEO600

GEO600 is a detector constructed and operated by a German-British collaboration [13]. It is situated near Hannover in Germany and has arms of length 600 m. A photograph of the detector is shown in figure 1.10. It uses a delay line configuration and advanced technologies such as power and signal recycling and a low mechanical-loss quasi-monolithic mirror suspension system as will be discussed later. Although its arm length is shorter than the largest of the other operating detectors, the advanced optical technologies and low loss mirror suspensions have allowed it to operate alongside the larger instruments during the first searches for gravitational waves carried out by the long-baseline detector network. Since 2002, GEO600 has been a part of the LIGO scientific collaboration and has participated in four science runs. In between the science runs various improvements were made to the detectors. The sensitivity reached by GEO600 in each of these runs is shown in figure 1.11 [62]. From

November 2007 until July 2009, GEO600 ran in "Astrowatch" mode collecting data while the larger LIGO detectors and the Virgo detectors were offline for incremental hardware upgrades. Section 1.7 describes the current status and future plans of the GEO600 detector.

Figure 1.10: A birds eye view of the GEO600 gravitational wave detector, located near Hannover in Germany.
[63]

TAMA

TAMA is a detector located in Tokyo at the National Astronomical Observatory [20]. It has arm lengths of 300 m and makes use of Fabry-Perot cavities and power recycling. Recently, a multistage pendulum design similar to Virgo was implemented within TAMA creating a more sensitive TAMA seismic attenuation system (TAMA SAS). This was developed jointly with LIGO and improved the sensitivity of TAMA at low frequencies by a factor of 10 [64]. Work on long baseline gravitational wave interferometers in Japan has a future focus on a 3 km arm length underground detector known as the Large-scale Cryogenic Gravitational wave Telescope (LCGT) as will be discussed in section 1.7.

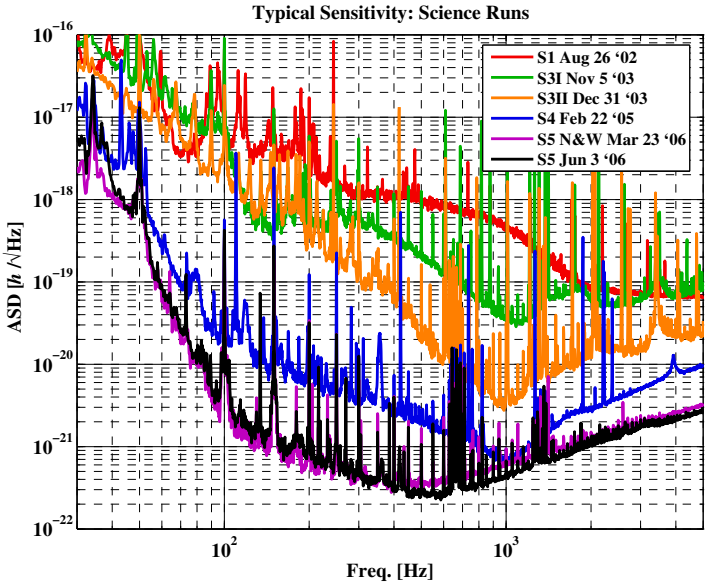

Figure 1.11: Sensitivity of the GEO600 gravitational wave detector for each of the five science runs it participated in as part of the LIGO scientific collaboration.

[63]

1.7 Second Generation Detectors

To further improve the sensitivity of the worldwide detector network, significant hardware upgrades to several of the instruments are being implemented. For the LIGO and Virgo instruments this should enable a sensitivity improvement of a factor of 10 to 15. It is predicted that with this increase in sensitivity, the most probable rate of detection of binary coalescences for the detector network increased from ~ 0.02 per year to ~ 40 per year [65].

GEO-HF

As GEO600 has a shorter arm length than LIGO and Virgo its ability to remain competitive in sensitivity across the full frequency band will decrease as LIGO and Virgo upgrades are implemented. Thus the upgrade to GEO600 will focus on improvements to sensitivity in the kHz region while maintaining its ability to be tuned into lower frequencies to enable it to run in "Astrowatch mode"

when the longer detectors are offline [66]. The changes made to GEO600 to increase sensitivity in the high frequency range include methods of beating the quantum limit and increasing the laser power to reduce photoelectron shot noise.

Advanced LIGO

Advanced LIGO is the planned upgrade to LIGO [67]. It will consist of three 4 km detectors, where the initial 2 km instrument is extended in length to form a third 4 km detector. Two of these will be situated at the original LIGO sites within the current infrastructure. The third may be situated in Australia, this is discussed further in section 1.7. Advanced LIGO will be a factor of 10 to 15 times more sensitive than LIGO and should allow sources down to 10 Hz to be observable. In order to achieve these aims, improved seismic isolation, suspensions, lasers and optics are required [67]. Techniques being implemented to achieve these goals include increasing the laser power, using signal recycling and suspending the mirrors in multistage pendulums with the bottom stage being a monolithic fused silica suspension. Chapters 3 and 4 of this thesis describe some of the work carried out by the author toward the construction of the monolithic suspension.

LIGO-Australia

A proposed project being considered for Australia is a collaboration with LIGO [68]. This would involve the transfer of the components of the 2 km detector from the Hanford, Washington site to Australia. Australia would provide the infrastructure to allow for the construction of a 4 km detector, nominally identical to the Advanced LIGO detectors allowing enhanced sensitivity and positional information to be obtained by the global network [68].

Advanced Virgo

Advanced Virgo [69] will incorporate a further set of upgrades after Virgo+. The goal is to increase the detector sensitivity by a factor of ~ 10 by increasing the mirror mass, increasing the input power and having a higher finesse in the arm cavities.

LCGT

The Large-scale Cryogenic Gravitational wave Telescope (LCGT) [49] is a Japanese detector which will consist of sapphire masses and suspension elements. Initially this telescope will be run at room temperature with plans to subsequently cool it down to cryogenic temperatures. The room temperature interferometer was granted funding in 2009 [70].

1.8 Third Generation Detectors

The second generation detectors should guarantee the first direct detection of gravitational waves. They will be sensitive enough to see the larger astrophysical sources such as binary systems coalescing. Once this first milestone is reached, there is a strong case to be made for improving sensitivities such that less intense/strong events can be studied, and to enable precision astrophysical measurements to be carried out on sources detected. Thus concepts for a third generation of detectors are being developed which would allow for better understanding and enhancement of the observational aspects of gravitational wave astronomy. The most probable number of observable binary coalescence should increase from 40 a year to millions per year [48]. In trying to further increase the sensitivity of the second generation detectors challenges again exist from, for example the thermal noise of the mirror substrates, coatings and suspensions. Therefore, one concept being considered for the third generation of detectors is to reduce thermal noise by cooling the mirrors and their suspensions down to cryogenic temperatures [48, 49]. This cooling is planned as

part of the concept for the Einstein Telescope which has been the subject of a design study carried out by a number of partners including the GEO600 and Virgo projects as a new European instrument [48]. As part of this study, identification of a material which has a low mechanical loss at low temperatures is required. Silicon is a good candidate material and its suitability is currently being studied.

1.9 Space-Based Gravitational Wave Detectors

Laser Interferometer Space Antenna (LISA) was, until earlier this year, a proposed joint ESA/NASA mission to fly a space based gravitational wave interferometer [50]. This formed one mission proposal under the ESA cosmic vision programme. ESA are currently exploring the possibility of flying each of the cosmic vision missions with European funding only, and NASA are thus re-evaluating their roles in the various joint studies.

By situating LISA in space, gravity gradient noise can be significantly reduced allowing for the possibility of operation at lower frequencies than is possible on Earth. A significant increase in the interferometer arm length is also possible. The original baseline LISA mission consisted of three separate drag-free space craft, housing mirrors and lasers and flying in a triangular formation following the Earth by 20° in a heliocentric orbit. The distance between each space craft was five million kilometres. The precise configuration is currently under review by European study teams,however relevant technology used in the drag free space craft envisioned for a space-based mission is to be tested on the LISA pathfinder mission [71]. This is due to be launched in 2013.

1.10 Conclusion

Over the last fifty years the gravitational wave community has increased considerably. Several long baseline interferometers operating in a world-wide network have carried out extended science runs, setting significant new upper

limits on the strength of gravitational waves from astrophysical sources, but as yet making no direct detections. The detection of gravitational waves will create a new branch of astronomy, teaching us more about our Universe.

The planned upgrades to increase the sensitivity of the current detectors are essential in advancing gravitational wave astronomy. However, there are many experimental challenges to overcome. Noise sources must be reduced, in particular, the thermal noise of the test mass mirrors and their suspensions. This is the main focus of the work presented in this thesis.

Chapter 2

Thermal noise

2.1 Introduction

As previously discussed in Chapter 1, thermal noise is a limiting factor to the sensitivity of gravitational wave detectors, at the lower end of the operating frequency range. This noise source originates from the thermally driven motion of the individual atoms in the test mass mirrors and their suspension.

The lower stages of gravitational wave detector mirrors are suspended as pendulums with a number of different resonant modes of oscillation. The Equipartition theorem states that each degree of freedom of a classical harmonic oscillator system has an average energy of $\frac{1}{2}k_bT$ Joules [72], where k_b is Boltzmann's constant and T is the temperature in Kelvin. This energy is stored in the translational, rotational and vibrational motion of the atoms which, when coupled in a solid excites the mechanical resonant modes of the overall system. The motion of each resonant mode combines resulting in thermally induced motion of the mirrors. This is known as thermal noise. This motion can be greater than the movement induced by a passing gravitational wave and so forms a limit to the sensitivity of gravitational wave detectors.

2.1.1 Brownian Motion

In 1827, a botanist named Robert Brown observed the random motion of pollen grains and dust floating in water [73]. He believed that the movement

was caused by a vital force within the particles themselves. It wasn't until 1905, when Einstein showed that this movement was caused by fluctuations in the rate of stochastic collisions of the particles with the surrounding water molecules, that this motion was fully understood [74]. He also showed that these collisions caused the pollen and dust to lose kinetic energy as they float in the water through friction with the water molecules [55], thus linking the fluctuations of position and energy dissipated.

This relationship was developed further by Callen et al [75, 76], and expressed as the fluctuation- dissipation theorem for linear systems in thermodynamic equilibrium. This theorem is an important tool in the study of thermal noise.

2.2 Fluctuation-Dissipation Theorem

The fluctuation-dissipation theorem relates the power spectral density of the fluctuating mechanical driving force $S_F(\omega)$ of a mechanical system to the dissipative (i.e real) part of the mechanical impedance $\Re[Z(\omega)]$ as follows [75, 76],

$$S_F(\omega) = 4k_B T \Re[Z(\omega)] \tag{2.1}$$

The mechanical impedance can be defined as F/v, where F is the force acting on an object which results in a velocity v of this object. Using this relationship the fluctuation-dissipation theorem can be expressed in a more useful form giving the expression for the power spectral density of thermal displacement, $S_x(\omega)$,

$$S_x(\omega) = \frac{4k_B T}{\omega^2} \Re[Y(\omega)] \tag{2.2}$$

where $Y(\omega)$ is the mechanical admittance, $(Y(\omega) = 1/Z(\omega))$.

The fluctuation-dissipation theorem therefore allows the amplitude spectral density of the thermal noise to be calculated from the real part of the mechanical impedance $\Re[Y(\omega)]$, or more specifically from the mechanical loss of the mechanical system (i.e the mirror suspension) as discussed further in section 2.4 and 2.6.

2.3 Sources of Dissipation

2.3.1 External Sources of Dissipation

There are a number of external sources of noise which contribute to the thermal noise of a suspension system in a gravitational wave detector, for example:

- gas damping [77] - residual gas molecules collide with the suspension elements and this friction provides a viscous damping effect;
- frictional losses - friction can occur at the contact points of the suspension elements and test masses. These are known as "slip-stick" losses [78];
- recoil damping [77] - energy can be dissipated from the suspension into the support structure.

To minimise thermal noise, these, and any other sources of external dissipation should be minimised as far as possible in the frequency range of interest.

2.3.2 Internal Sources of Dissipation - Anelasticity

Once the external damping is suitably minimised, the damping and thermal noise arising from the internal friction in the materials of the mirrors and fibres becomes of significant interest.

Internal damping exists in materials which act anelastically. An ideal elastic material obeys Hooke's law such that a force exerted on the material causes a stress, σ and this stress results in a strain, ϵ being instantaneously produced within the material. An anelastic material does not react instantaneously. Instead it reaches its new state of equilibrium after some finite relaxation time. Thus, for example, the application of a periodic stress at some angular frequency ω, will result in the development of a periodic strain, with the strain having the same angular frequency as the applied stress, but with a phase lag ϕ, with respect to the stress. This phase lag is known as the loss angle of a material, or mechanical loss factor - see for example Nowick and Berry [79].

Internal mechanical loss in a material can arise from a number of different causes. For example, if the internal stress in a material changes then material properties such as the density of defects in the material structure, or the local heat flow in the material can take some finite time to respond to the new stress state, with the strength of some of the relevant processes being dependent on, for example, temperature or frequency. Thus more generally, the mechanical loss in a material may be written as $\phi(\omega, \mathrm{T})$. A knowledge of the form of $\phi(\omega, \mathrm{T})$ for a material, combined with the use of the fluctuation-dissipation theorem allows the expected thermal noise from a particular system to be calculated.

2.4 The Loss Factor

It is important to know which forms of loss are present within the suspension in order to correctly model the system and calculate the amount of thermal noise expected. The mechanical losses associated with the components of the suspensions and mirrors in current and future gravitational wave detectors is extremely small, and difficult to measure directly at all frequencies. However, the level of the mechanical loss can be obtained by measuring the loss at the resonant frequencies, ω_0, of the various modes of the suspension and the test mass. The total dissipation of the system is dependent on the loss angle at any frequency of interest.

An alternative definition for the mechanical loss of an oscillating system is given by [80],

$$\phi(\omega_0) = \frac{E_{\text{lost per oscillation}}}{2\pi E_{\text{total}}} \tag{2.3}$$

where the total energy of the system is E_{total} and $E_{\text{lost per oscillation}}$ is the energy lost per complete cycle of oscillation. Thus, it can be seen that by exciting a suspension at a resonant frequency and recording the amplitude of motion of the sample as it decays, a loss value can be obtained. This is the method used in Chapters 4 and 5 to measure mechanical loss of different substrates.

2.5 The Form of the Internal Dissipation

It can be shown that a class of relaxation mechanisms have dissipation with a characteristic frequency dependent form resulting in loss peaks, known as Debye peaks, with the peak height and width related to the relaxation time τ, associated with the mechanism as shown in equation 2.4 [79].

$$\phi(\omega) = \triangle \frac{\omega\tau}{1+\omega^2\tau^2} \tag{2.4}$$

where $\triangle$ is a constant related to the magnitude of the dissipation.

However, in some experimental situations a clear frequency dependence to the measured loss is not observed, with the loss being approximated as frequency independent damping or 'structural' damping. In such cases it is postulated that the observed dissipation is the result of the superposition of a number of different mechanisms each peaking at a different frequency, with this frequency often being far from the measurement frequency.

The frequency range of interest for operation of current gravitational wave interferometers ($\sim$ a few 10's of Hz to a few 100 Hz) happens to be far from the majority of these loss peaks for the materials involved. However, there is a source of dissipation associated with gravitational wave detector test mass suspensions which is dependent on frequency and could result in loss peaks which are close to the frequency range over which gravitational wave detectors are operated. This is known as thermoelastic dissipation [56, 79] which is discussed in section 2.10.

2.6 Internal Dissipation Applied to a Harmonic Oscillator

The resonant modes of a pendulum suspension, which are described in section 2.7, can each be modelled as a damped harmonic oscillator which obeys Hooke's law,

$$F_{spring} = -kx \tag{2.5}$$

where F is the force applied to the system, x is the displacement caused by F and k is the spring constant. For low loss systems, systems in which $\phi(\omega) \ll 1$, the delay in reaching a new state of equilibrium caused by the anelasticity of the material can be added into this model by introducing an imaginary term into the spring constant such that [81],

$$F_{spring}(\omega) = -k(1 + i\phi(\omega))x \tag{2.6}$$

This imaginary term, $\phi(\omega)$, represents the phase lag in radians and is known as the mechanical loss of the material.

The equation of motion of this harmonic oscillator of mass m, subject to an internal thermal driving force $F_{\text{thermal}}(\omega)$ which acts on the system, is,

$$F_{thermal}(\omega) = m\ddot{x} + k(1 + i\phi(\omega))x \tag{2.7}$$

or expressed in terms of velocity,

$$F_{thermal}(\omega) = i\omega mv - i\frac{k}{\omega}(1 + i\phi(\omega))v \tag{2.8}$$

If we divide the fluctuating force by velocity an expression for impedance is obtained, such that,

$$Z(\omega) = i(\omega m - \frac{k}{\omega}) + \phi(\omega)\frac{k}{\omega} \tag{2.9}$$

The admittance is then calculated to be,

$$Y(\omega) = \frac{1}{Z(\omega)} = \frac{\frac{k}{\omega}\phi(\omega) - i(\omega m - \frac{k}{\omega})}{(\frac{k}{\omega}\phi(\omega))^2 + (\omega m - \frac{k}{\omega})^2} \tag{2.10}$$

This admittance can then be substituted into the fluctuation-dissipation theorem to give an expression for the power spectrum of thermal motion, $S_x(\omega)$,

$$S_x(\omega) = \frac{4k_BT}{\omega^2}\Re(Y(\omega)) \text{ per Hz} \tag{2.11}$$

$$= \frac{4k_BT}{\omega^2}\frac{\frac{k}{\omega}\phi(\omega)}{(\frac{k}{\omega}\phi(\omega))^2 + (\omega m - \frac{k}{\omega})^2}, \tag{2.12}$$

as $\omega_0^2 = \frac{k}{m}$ the equation can be reduced to,

$$S_x(\omega) = \frac{4k_BT\phi(\omega)\omega_0^2}{m\omega(\omega_0^4\phi(\omega)^2 + (\omega_0^2 - \omega^2)^2)}. \tag{2.13}$$

By expressing the fluctuation-dissipation theorem in this form it can be seen that at the angular resonant frequencies, ω_0 the power spectral density thermal noise is at a maximum and is proportional to $1/\phi(\omega_0)$. Thus, for materials with a low mechanical loss the dissipation peaks are tall and narrow, centred around the resonant frequency, resulting in a low level of thermal noise being exhibited at frequencies far from the resonant frequency. This off resonance thermal noise is of importance for achievable sensitivities of gravitational wave detectors and for this reason the suspensions in current detectors are made from fused silica which is known to have a low mechanical loss [82]. The quasi-monolithic suspension system which has been implemented in GEO600, (versions of which are being implemented in the advanced detectors) utilises fused silica fibres to suspend silica mirror substrates. A low loss bonding technique to joint the suspension elements to the mirrors is required to keep the loss of the suspensions at a low level and the technique of hydroxy-catalysis bonding is of interest for this purpose [83, 84]. Measurements of the strength of hydroxy catalysis bonds and the mechanical loss of the bonds between fused silica substrates and of bulk silica itself are presented in Chapter 3 and 4, respectively.

2.7 Interferometer Suspension and Mirror Thermal Noise Sources

Current and future gravitational wave detectors have been designed to ensure that the frequencies of the resonant modes of the mirrors and their suspensions, at which the thermal noise peaks, are located outside of the operational band of the detectors. There are two main types of resonant modes in a pendulum suspension system. These are the internal resonant modes of the mirror substrates and the set of resonant modes associated with suspension structure and assembly.

2.7.1 Internal Resonant Modes

Internal resonant modes of the test mass mirrors used in interferometers exist such that the position of the centre of the mass remains fixed while the body of the mass vibrates and alters shape. The resonant modes in which the position of the front face of the mass sensed by the laser light is altered will contribute to the thermal noise of the interferometer. The resonant frequencies of the masses are typically of the order of 10 kHz [46] meaning they are far away from the operating frequency band of current gravitational wave detectors which is from a few tens to a few hundred Hz. Thus, the contribution from this type of resonant mode to the thermal noise sensed in the system is got by evaluating the incoherent sum of the noise in the tails of the resonant peaks.

The thermal noise of each test mass is increased by the addition of the reflective coatings used to form mirror surfaces, as discussed in section 2.9.

2.7.2 Suspension Modes

Certain resonant frequencies of the suspension structure can couple to motions of the mirror faces.

2.7.2.1 Pendulum Modes

The mirrors in gravitational wave detectors are suspended as pendulums in order to isolate them from seismic vibrations. The pendulum modes of a suspension can move the position of the front face of the suspended mass, thereby altering the path length of one of the arms of the interferometer and so introducing noise. It is possible to ensure that the frequency of the pendulum mode is below the detection frequency band by careful design. The pendulum mode frequency can be lowered by increasing the length of the long suspension fibres. The loss, $\phi_{pendulum}(\omega_0)$, of a pendulum having mass m, and length l with n suspension elements is related to the loss of the suspension fibre material,$\phi_{material}(\omega_0)$, by [81],

$$\phi_{\text{pendulum}}(\omega_0) = \phi_{\text{material}}(\omega_0)\frac{\zeta n\sqrt{TYI}}{2mgl} \tag{2.14}$$

where ζ denotes how the fibre can bend. It is 1 if the fibres are constrained in such a way as to allow bending at the top or 2 if the fibres are constrained in a way that allows bending at the top and bottom [85]. T is the tension of each suspension element, Y is the Young's modulus of the material and I is the moment of cross-sectional area of the fibre. The loss of the pendulum mode is lower than that of the material of the suspension fibre due to the fact that some of the energy associated with the pendulum is stored in the lossless gravitational field, whilst some is stored in the bending of the fibres. This reduction in pendulum loss over that from the fibre material is known as "dissipation dilution" [86].

2.7.2.2 Violin Modes

The "violin" modes of the fibres are a series of resonant modes of the suspension fibres that lie within the operating frequency range of current interferometers. Like the pendulum mode, the losses of the violin modes are lower than that of the material used for the suspension elements, such that associated peaks in thermally induced motion are very narrow. Thus the energy is stored in narrow peaks at the resonant frequencies. This allows for the noise to be removed from the signal.

2.7.2.3 Vertical, Torsional and Tilt Modes of the Pendulum

Ideally these modes would not cause noise in the interferometer as the laser beam should be pointed directly into the centre of the front face of the mass and vertical, torsional or tilting movements would not change the path length of the detector arm. However, these modes can couple to horizontal motion [47] where there are misalignments in the positioning of the laser beam in the centre of the mass.

2.8 Thermal Noise Resulting from Spatially Inhomogeneous Mechanical Dissipation

The method of calculating the total thermal noise for a mass described in section 2.6, i.e. via summation of the levels of off resonant thermal noise associated with each resonant mode, is only a good approximation when the loss is distributed homogeneously throughout the volume of a material. This is not true in practical situations such as for the mirrors in gravitational wave interferometers. We know them to have inhomogeneous loss due to localisation of defects within the materials, for example, and the use of surfaces which have an increased level of loss compared to that of the bulk material [87]. Levin derived a formula for the power spectral density of thermal noise at the face of a mirror sensed optically with a laser beam using a direct application of the fluctuation-dissipation theorem to the system [87]. This method allows the spatial distribution of the loss and the shape of the wavefront of the sensing laser beam to be taken into account. The radius of the laser beam was described to be the distance to where the intensity of the light falls to $1/e$ of the maximum intensity. The power spectral density of thermal displacement, $S_x(\omega)$, calculated this way can be represented as,

$$S_x(\omega) = \frac{8k_BT}{\omega^2}\frac{W_{\mathrm{diss}}}{F_0^2}, \tag{2.15}$$

where F_0 is the maximum magnitude of a notional oscillatory force applied by the laser beam to the front face of the mirror and W_{diss} is the associated power dissipated in the mirror described as [87],

$$W_{\mathrm{diss}} = \omega \int_{\mathrm{volume}} \varepsilon(x,y,z)\phi(x,y,z,\omega)dV \tag{2.16}$$

where ε is the energy density of the elastic deformation under the peak applied force F_0.

For a loss which is distributed homogeneously throughout a mass which has an arbitrarily large radius and length compared to the radius of the sensing

laser beam the spectral density of Brownian noise can be expressed as [87],

$$S_x(\omega) = \frac{4k_B T}{\omega} \frac{1-\nu^2}{\sqrt{2\pi} Y r_0} \phi_{\text{substrate}}(\omega) \tag{2.17}$$

where ν is Poisson's ratio, this is the ratio of the transverse strain to the longitudinal strain in the direction of an applied force, Y is the Young's modulus, $\phi_{\text{substrate}}(\omega)$ is the mechanical loss of the material and r_0 is the radius of the laser beam at which the intensity has fallen to $1/e$ of the maximum. Approximating the mass as arbitrarily large gives the value of the spectral density to within 10% of the actual value for a mass of a given size. [88]. This expression shows that the level of thermal noise is directly related to the temperature of the substrate, the elasticity and mechanical loss of the material and the radius of the laser beam sensing the face of the substrate. Thus, these form important parameters to be considered in schemes aimed at reducing the overall thermal noise of a detector suspension. As the noise is directly related to the deformation of the surface due to the notional applied force from the laser, as seen in equation 2.15, it can be seen that loss located closer to the location of the sensing beam will have a greater contribution to the total thermal noise than loss further away. This makes the loss of the mirror coatings an important parameter and this is currently the dominant source of thermal noise in the most sensitive frequency band of current ground-based detectors. Another source of noise which is important due to its proximity to the surface of the mirror is the noise due to the hydroxy-catalysis bonds which are used to join the mirrors and the ears welded to the suspension fibres. The mechanical loss of these bonds are studied and discussed further in Chapter 4 and 5.

2.9 Reflective Coatings

Multi-layer dielectric reflective coatings are applied to the test mass substrates in gravitational wave detectors in order to make them highly reflective to the laser light used. The planned coatings for Advanced LIGO will be formed from

alternating layers of silica and titania doped tantala [89]. The large difference in the refractive index of silica and tantala creates a highly reflective surface. Tantala has a larger mechanical loss than that of silica and it has been shown that the loss can be reduced by doping the material with titania [90]. The thermal noise in a coated mirror, $S_x^{\text{total}}(f)$, can be approximated as [91],

$$S_x^{\text{total}}(\omega) = \frac{4k_BT}{\pi^{\frac{1}{2}}\omega}\frac{1-\nu^2}{r_0 Y}(\phi_{\text{substrate}} + \frac{2}{\sqrt{\pi}}\frac{(1-2\nu)}{(1-\nu)}\frac{d}{r_0}\phi_{\text{coating}}) \tag{2.18}$$

where k_B is Boltzmann's constant, T is the absolute temperature of the coated mass, ω is the angular frequency, ν is Poisson's ratio, r_0 is the laser beam radius where the amplitude has fallen to 1/e, Y is the Young's modulus, $\phi_{\text{substrate}}$ is the loss of the substrate material, d is the thickness of the coating and ϕ_{coating} is the loss of the coating. The Advanced LIGO requirement for coating loss is $\phi_{\text{coating}} = 2 \times 10^{-4}$ [89] while the loss of the substrates are required to be $\phi_{\text{substrate}} =< 3 \times 10^{-9}$ [89]. Current research has been targeted at investigating techniques to reduce the mechanical loss of the coatings by heat treating the material and doping the coatings with different materials [92–94]. Investigations have also been carried out on alternative coating materials as possible candidates for the mirror coatings and on the possibility of replacing the coatings with waveguide structured surfaces [95–97]. This work in ongoing in order to find the optimum coating for the third generation detectors. The use of waveguide structured surfaces in place of optical coatings could be a method of significantly reducing the thermal noise levels. However, further development is required to improve on the optical properties and to enable the production of waveguides which are the size required.

2.10 Thermoelastic Dissipation

Thermoelastic loss arises in both the fibres [79, 98] and the mirrors [56] of the suspensions used in gravitational wave detectors.

Statistical temperature fluctuations in the fibre material result in temperature gradients and thus heat flow and dissipation (and associated thermal noise), where the characteristic time for this process is a function of the diameter of the fibre.

In the bulk material of the mirrors, statistical temperature fluctuations within the body result in movement of the mirror surfaces via coupling through the linear coefficient of thermal expansion, α, of the substrate material. The amount of thermoelastic noise, $S_{TE}(\omega)$, expected for a half-infinite mass at room temperature was derived by Braginsky [56] to be

$$S_{TE}(\omega) = \frac{16}{\pi} \frac{k_B T^2 \alpha^2 (1+\nu)^2 \kappa}{\rho^2 C^2 r_0^3 \omega^2} \tag{2.19}$$

where ν is Poisson's ratio, κ is the thermal conductivity, ρ is the density, C is the specific heat capacity and r_0 is the radius of the laser beam where the intensity has fallen to $1/e$ of the maximum intensity.

Liu and Thorne created a correction factor which allowed for the calculation of thermoelastic noise in finite mirrors [88].

Equation 2.19 shows that thermoelastic dissipation is greater in materials which have a higher expansion coefficient. Silicon is being studied for third generation gravitational wave detectors and as this material has a higher thermal expansion coefficient than silica, thermoelastic noise could become a significant noise source in future detectors. Thus, the mechanical loss of silicon is of great importance and is studied in Chapter five.

2.11 Combined Thermal Noise in a Detector

In order to estimate the sensitivity of a gravitational wave detector, the contribution of thermal noise from every separate component of each mirror suspension must be combined. This includes the thermal noise from the suspension modes, the thermal noise from the internal modes of the test mass, the noise from the fibres and from the reflective mirror coatings. A plot showing the

expected values of thermal noise within an Advanced LIGO mirror is shown in figure 2.1. This plot shows that suspension noise and quantum noise provide significant contributions to the total noise levels of a gravitational wave detector. The noise of the current suspensions have been reduced as much as possible and thus, to further decrease suspension noise, cooling to cryogenic temperatures is being considered for third generation detector suspension systems. Quantum noise can be reduced by increasing the power of the laser beam. At cryogenic temperatures silica has noise peaks and if the laser power was increased thermal distortion of the silica mirrors would occur thus, silica would become unsuitable as a suspension material. Concentration has moved to Silicon and Sapphire as possible candidates for the suspension material of future detectors and this will be discussed further in Chapter 5.

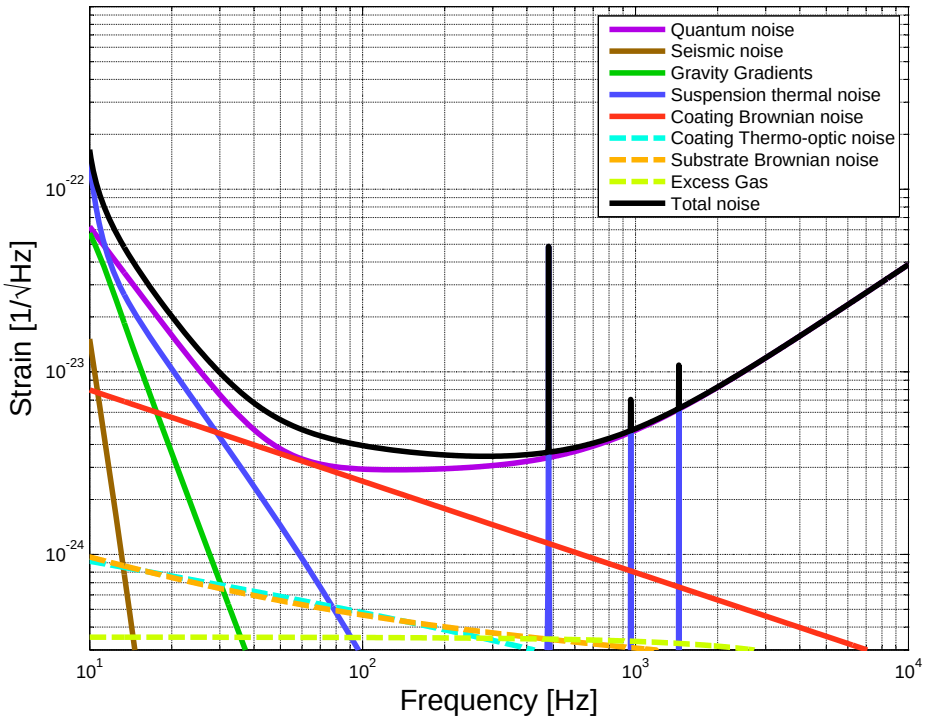

Figure 2.1: Limiting noise sources for a variety of Advanced LIGO tunings. [99]

2.12 Conclusion

Thermal noise is an important limiting factor to the sensitivity of current ground based gravitational wave detectors. The fluctuation-dissipation theorem is a very useful tool in designing and constructing gravitational wave detectors as it allows for a calculation of the predicted levels of thermal noise from the mechanical losses of the suspension. Thus, experiments were carried out to quantify the loss of the mirrors and the hydroxy-catalysis bonds between suspension elements, both for silica and silicon as suspension materials.

It is possible to lower the thermal noise within the gravitational wave detectors by careful design of the suspension and suspension elements. Thus, increasing the detector sensitivity. Methods of reducing the mechanical loss were investigated in this thesis.

Chapter 3

Strength of Hydroxy-Catalysis Bonds

3.1 Introduction

Hydroxy-catalysis bonding is a technique for jointing materials between which a silica-like network can be created. It was first patented by D. H. Gwo at Stanford University for use in the Gravity Probe B mission [100–102] and has been developed further by researchers at the University of Glasgow. This technique involves the placing of an aqueous alkaline bonding solution, typically sodium or potassium hydroxide or sodium silicate, between surfaces to be jointed, enabling a chemical bond to be formed (as discussed in more detail in Section 3.2). It has been used in the construction of ultra low loss, quasi-monolithic fused silica suspensions for interferometric gravitational wave detectors [83, 103]. The first of these suspension systems was installed in the GEO600 detector and variants of this design were created for use in the Advanced LIGO detectors and for upgrades to the Virgo detector [104] that are currently being installed. In addition, hydroxy-catalysis bonding is planned for use in future space-based gravitational wave missions [50]. It has already been used to bond optical components for a technology demonstration mission known as LISA Pathfinder [71]. This technique enables the joints created to be strong, stable and precisely aligned.

In each of the quasi-monolithic suspension systems which are being implemented in Advanced LIGO, a 40 kg mass of fused silica will be suspended on four silica fibres. At their thinnest point the fibres have a diameter of 400 μm. These fibres will be welded on to small silica prisms, 'ears', which will be attached to the masses by way of hydroxy-catalysis bonds. This design is an upgrade to the suspension design used in the initial LIGO detectors which used a 10.7 kg mass suspended using a steel wire loop [105]. By replacing the steel wires with silica fibres, the suspension losses are reduced as silica has a lower intrinsic mechanical loss than steel. The frictional "stick and slip" [78] losses which could have occurred where the silica masses contact the steel wire, are removed due to the ears being attached with hydroxy-catalysis bonds which create chemical bonds between the jointed surfaces. Although the bond material has a higher loss than bulk silica [106], the effect of the loss is kept to an acceptable level for advanced detector suspensions as the bond layer can be extremely thin (< 100 nm). However, as coatings are further developed, the coating loss is reduced and thus, substrate and bond loss could contribute more significantly to the total thermal noise. Chapters 4 and 5 describe methods of quantifying and reducing bond loss. Figure 3.1 shows a representation of the lower stage of this suspension structure.

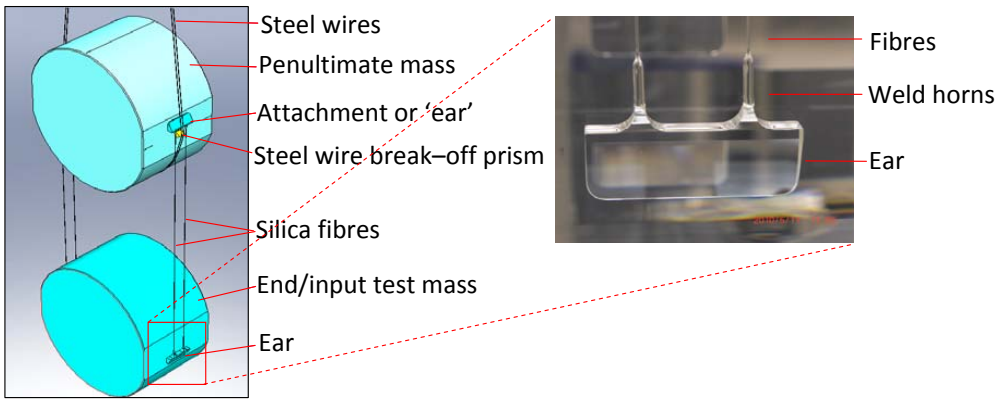

Figure 3.1: Schematic diagram of a silica test mass suspended on silica fibres and a photograph of a silica ear bonded to a test mass.

The fibres are not directly welded to the masses. Welding the fibres directly to the large masses would be more difficult than welding them to a component of similar dimensions to the fibre diameter such as the weld horns of the ears. Thus, each mass is supported via ears attached to a bonded area on the mass. The fibres are then welded using a CO_2 laser to 'weld horns' on the ears. The strength of the bonds is an important parameter as they keep the whole mass suspended. In order to meet the Advanced LIGO specifications on total allowable noise, the area of the bond has to be such that a shear strength of no less than ~ 0.17 MPa is required [107]. In the experiments presented in this Chapter the tensile strength is measured. An assumption is made that the samples tested have properties that are isotropic, and thus that we can assume that the shear and tensile strengths are equivalent.

There have been significant studies of the properties and underlying chemistry of silicate bonds, largely targeted at testing their suitability for advanced gravitational wave detectors. In this chapter the results of strength tests of silica-silica bonds are presented and discussed, where the bonds underwent different treatments in order to study the underlying factors that govern their final robustness. The different treatments were intended to mimic processes which will be carried out on the suspension systems for gravitational wave detectors. The effects on bond properties of different heat treatments, loading conditions and volumes of bonding solution were studied. The strength difference of bonds created between different types of silica material was also investigated.

A spread in strength in each set of results is to be expected as the resultant strength of an individual bonded fused silica sample is dependent on the inherent resistance to fracture of fused silica, and on the size and severity of any flaws there may be within the bulk silica or within the bond. To help identify this spread and its dependence on visual defects, the visual quality of the bond was noted for each sample and will be discussed in the analysis.

3.2 The Chemistry of Hydroxy-Catalysis Bonding

Hydroxy-catalysis bonds are used in the suspensions of gravitational wave detectors to minimise the effects of thermal noise. To minimise the thermal noise from the bond material itself, the volume of bonding material should be as small as possible. Hydroxy-catalysis bonds have typically been created between two oxide materials that have a peak to valley (PV) flatness of $\lambda/10$ (where $\lambda = 633$ nm). To create the hydroxy-catalysis bond, an alkaline bonding solution such as an aqueous potassium hydroxide solution or sodium silicate solution is placed on one of the surfaces and the other surface is brought into contact with the first. Before use, the bonding solution is put into a centrifuge and filtered to remove any larger particles that would prevent the surfaces from aligning themselves suitably close to each other. This is particularly important for sodium silicate solution, where particles can reside in the solution. Only a very small amount of bonding solution is required to create a strong bond (typically of order 0.4 μl/cm^2 [100]). If the bonding surfaces are sufficiently flat, clean and very hydrophilic, the bonding solution will spread out between the two surfaces and a series of chemical processes will begin. These chemical processes result in a strong, rigid, molecular network being formed between the two surfaces, hence jointing the two substrates. The thickness of typical bonds using the above procedure has been measured to be as thin as 61 $\pm$ 4 nm [106]. A calculated estimate of bond thickness can also be made from the properties of the bonding solution. This is shown in Appendix A. The steps of the chemical process for the bonding of fused silica, are discussed below, using sodium silicate solution as an example [100–102].

3.2.1 Hydration and Etching of the Silica Surface

A hydroxide solution such as a sodium silicate solution has a high concentration of OH^- ions. The clean bonding surface is hydrophilic and hence it will attract

OH^- ions to fill any open bonds on the surface of the silica. Any contamination on the surface will inhibit this hydration process. After the surface is fully hydrated, extra OH^- ions will attach to the silicon atoms of the surface forming weak bonds. Due to the increased number of bonds on each silicon atom, the original Si-O bonds will become weaker and therefore can be liberated from the bulk, i.e. the OH^- ions are etching the surface. This then creates a quantity of silicate, $Si(OH)_5^-$ molecules, free in the solution. Overall the number of free OH^- ions in the solution will decrease. A schematic of this process is shown in figure 3.2.

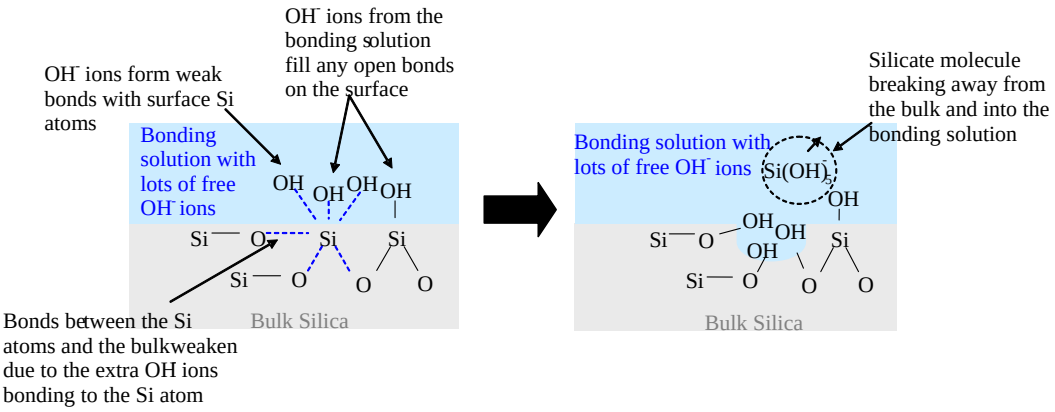

Figure 3.2: Hydration and etching process of hydroxy-catalysis bonding.

3.2.2 Polymerisation

As the number of free OH^- ions decreases the pH decreases. When the pH falls to below ~ 11 [108], the silicate ion dissociates to form siloxane, $Si(OH)_4$. These $Si(OH)_4$ molecules begin to polymerise to form siloxane polymer chains and water.

3.2.3 Dehydration

The water freed during polymerisation migrates or evaporates over time and the bond becomes stronger and more rigid. It has been found that the bond

reaches its maximum strength after curing at room temperature for $\sim$ 4 weeks [109]. The polymerisation and dehydration processes are shown in figure 3.3.

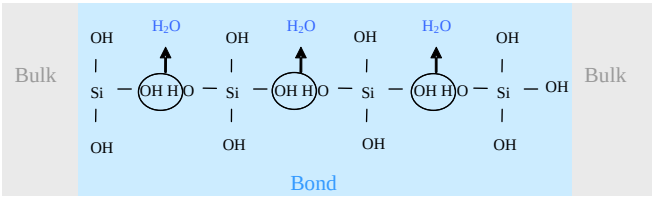

Figure 3.3: Formation of a Siloxane chain.

3.3 Bonding Procedure

Surface preparation and figure have been observed to be crucial factors in forming reliable, strong bonds between silica components [101, 102]. The effects of surface flatness on strength is not investigated here. However, every bonding surface was checked to ensure that the PV global flatness was $\lambda/10$ or better. The flatnesses of the surfaces were checked using a ZYGO GPI XP/D interferometer [110] before bonding. An image of the typical output from the interferometer is shown in figure 3.4.

The surfaces must not have any contaminants on them as this might inhibit the hydration and etching process or prevent the surfaces from becoming suitably close (same effect as the surfaces not being suitably flat). Thus, the following cleaning routine is used before bonding:

- Rinse with de-ionised water;
- Rub with a cerium oxide paste for $\sim$ 20 seconds using a cleanroom wipe;
- Rinse with de-ionised water to remove the cerium oxide;
- Rub with bicarbonate of soda for $\sim$ 20 seconds using a cleanroom wipe to remove any micro-particles of cerium oxide which may have been electrostatically stuck to the surface;

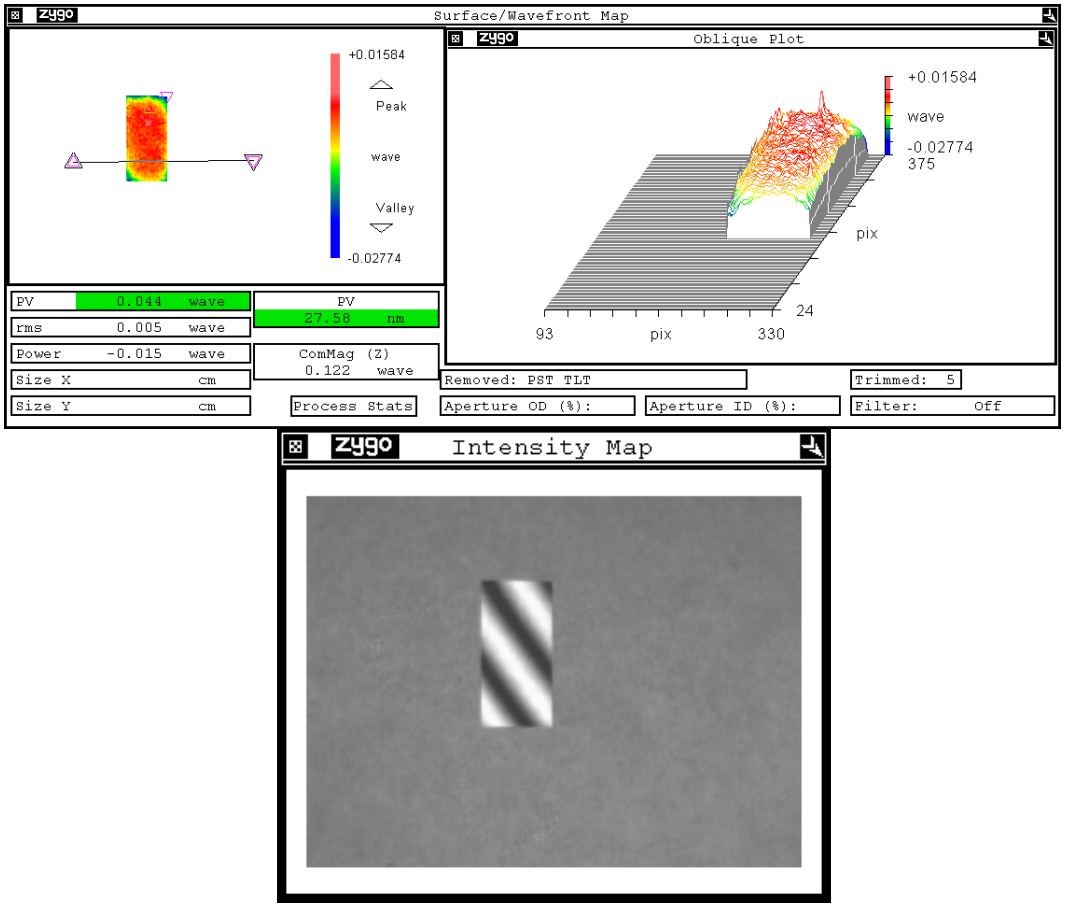

Figure 3.4: Flatness measurement from the ZYGO interferometer including a value for the flatness of the surface, the profile of the surface and an interferogram.

- Rinse with de-ionised water to remove the bicarbonate of soda;
- Repeat the bicarbonate of soda clean and de-ionised water rinse;
- Rinse with methanol;
- Wipe with a methanol soaked clean room cloth.

The bonding solution is filtered using a UNIPREP medical filter which has a 0.2 µm nylon membrane. Then the solution is centrifuged and the amount required for bonding is taken from close to the surface of the solution with a pipette. This is also to ensure that no particles or contaminants are in the

bond. The surfaces are then checked one last time using a high intensity goose neck light. The light allows any specks on the surface to be clearly seen. If any specks are present the surface is wiped again with methanol to remove them. When the surfaces are clean the bonding solution is placed onto one of the bonding surfaces after which the second sample is gently placed on top, the chemical processes then commence. The bond is left to cure at room temperature for 4 weeks. De-bonding these samples is possible for a period of time, however, the chemical bonds when formed, are strong and set quickly. A brief discussion of investigations into de-bonding methods is given in Appendix B.

Currently, sodium silicate solution is the bonding solution selected for use in gravitational wave detectors. This is a commercially available solution in which the composition is such that, by volume, 14% is sodium hydroxide, 27% is silicate and 59% is de-ionised water. The solution is typically diluted with de-ionised water at a ratio of 1 part sodium silicate solution to 6 parts water, and approximately 0.4 μl of solution for every cm^2 of the bonding area is used.

3.4 Strength Testing Procedure

The strength tests of hydroxy-catalysis bonds reported here, were carried out using a 4-point strength testing set-up at room temperature. The maximum stress, σ_{max}, of a sample being tested in the 4-point strength testing set-up is defined as [111],

$$\sigma_{max} = |\frac{cM}{I}| \tag{3.1}$$

where c is the maximum distance from the neutral axis to the highest or lowest point of the cross-section, M is the bending moment at the cross-section and I is the moment of inertia of the cross-section.

A photograph, and schematic diagram of this ideal set-up are shown in figure 3.5.

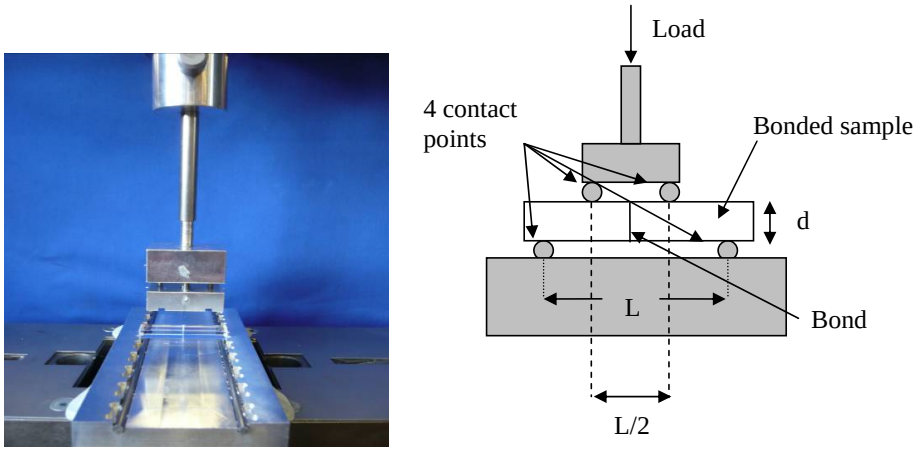

Figure 3.5: Photograph and schematic diagram of the 4 point strength tester.

This set-up is designed to allow the study of tensile strength of the bond [112]. In the ideal strength tester there are four lines of contact; two on the bottom of the sample a distance, L apart and two contact points on the top of the sample which are situated a quarter of the span, L, inwards from the lower contact points. The set-up has enough degrees of freedom such that the alignment can be achieved by applying a preload of 5 N ($<$ 2% of the average breaking force), this ensures that the load is distributed evenly and symmetrically between the rods by applying a pressure which is large enough to overcome the friction of the material. The force is zeroed before continuing with the test. The top section of the set-up is lowered at a constant rate of 2 mm a minute, thus applying a direct load to the sample until it breaks. The samples should break at the bond on the bottom of the sample, where the tensile stresses will be at a maximum located around this area. The compressive stresses will be at a maximum in the bond at the top of the sample. An image obtained using ANSYS finite element analysis software of the distribution of stresses throughout the sample and within the bond is shown in figure 3.6. It can be seen that the stress changes from a compressive stress to a tensile stress down the length of the bond as required. Very close to the edges of the sample the stress increases much more rapidly due to edge effects. However,

for calculation of bond strength we assume a linear stress distribution.

This strength testing process gives the force at which the bonded sample broke.

An equation for the tensile strength of the bonds broken in a set-up with the dimensions shown in figure 3.5 can then be derived from equation 3.1 to be [112],

$$\sigma_{tensile} = \frac{3}{4}\frac{FL}{bd^2} \tag{3.2}$$

where F is the breaking force of the sample, L is the separation between the two lower contact points and b and d are the width and thickness of the sample respectively.

3.5 Results and Analysis

3.5.1 Introduction

Bonds created for the purpose of jointing elements of the suspension in a gravitational wave detector are required to be of extremely high quality and preferably with no defects visible to the eye. Thus, bonds are inspected visually as soon as they are created. If there were, for example, an area of more than approximately 10% of the bond area which was not fully contacted or showed evidence of contaminants, bubbles or fringes, the bond would be rejected and the surfaces would be separated soon after bonding. The correlation between the visual quality and strength of a bond was confirmed by observations made while carrying out the experiments presented in this thesis. A hydroxy-catalysis bond can be de-bonded fairly easily within a few hours of the start of the bonding process. For example, in the construction of a test mass suspension, after an ear is removed, the bonding surface on the test mass may be recleaned and a new bond can be created. Bonds which had defects and would therefore not be of a high enough standard of quality to be used in gravitational wave detectors are included in the results presented here for statistical analysis and to investigate the effect of visual quality. Therefore,

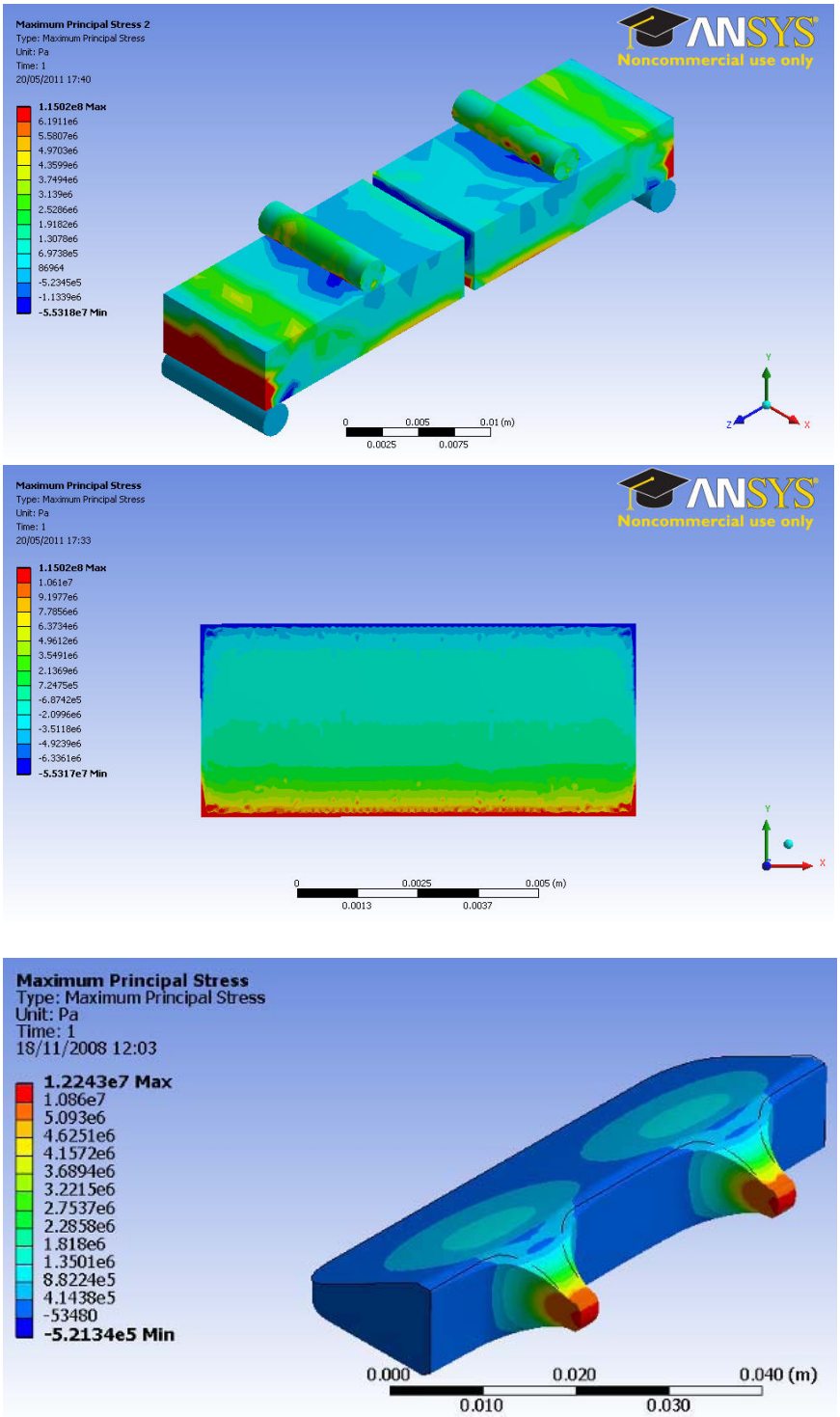

Figure 3.6: ANSYS picture of the distribution of stress while the force is being applied by the strength tester set-up. The top image shows the stress throughout the whole sample, the middle image shows stress through the bond and the stress in the ear is shown in the bottom image. The stress values are relative, blue signifies a compressive stress while red signifies a tensile stress.

it should be noted that the data sets presented here have a larger standard deviation than the bonds which would be used in gravitational wave detectors. The appearance and quality of the bond in each sample used here was noted before the strength was tested. The results were analysed first as a complete data set and then again using only the bonds which were optically without defects over more than 90% of the bond surface. By only selecting the bonds which are without defects over 90% of the bond area, a value for strength and standard deviation is obtained which is more representative of the bonds which would be used in a gravitational wave detector. The average strength is presented along with the standard error in the value. The standard error $= \frac{(\text{standard deviation})_{\text{N-1}}}{\sqrt{\text{N}}}$ where N is the number of samples tested.

For the strength tests carried out, two different sizes of samples were used. The reasoning behind using the second geometry of sample is explained in section 3.6. For the first set of tests discussed the dimensions of the samples and strength tester were such that $L = 18$ mm, $b = 10$ mm, $d = 5$ mm were used, such that the bonding surface was the face of dimension 5 mm by 10 mm. The strength tester and samples were not in the exact ratio shown in figure 3.5 and thus, the equation for calculating the tensile stress, derived from equation 3.1 is [112],

$$\sigma_{tensile} = \frac{15}{18}\frac{FL}{bd^2} \tag{3.3}$$

These samples were created between Corning 7980 samples which had been polished on all sides. An amount of $0.4\mu l/cm^2$ of the bonding surface of a 1:6 concentration of sodium silicate solution was used to form the bonds. This sample set forms the reference bonds. The results are shown in figure 3.7 and table 3.1.

8 out of the 9 bonds were visually perfect over 90% of the bond area, the average strength of these bonds are shown in table 3.1. The standard deviation of the bonds that had no defects over 90% of the bond surface was 4.8 MPa which is slightly less than the standard deviation of all the bonds. We might expect this to be the case, i.e that the strengths of the remaining samples were

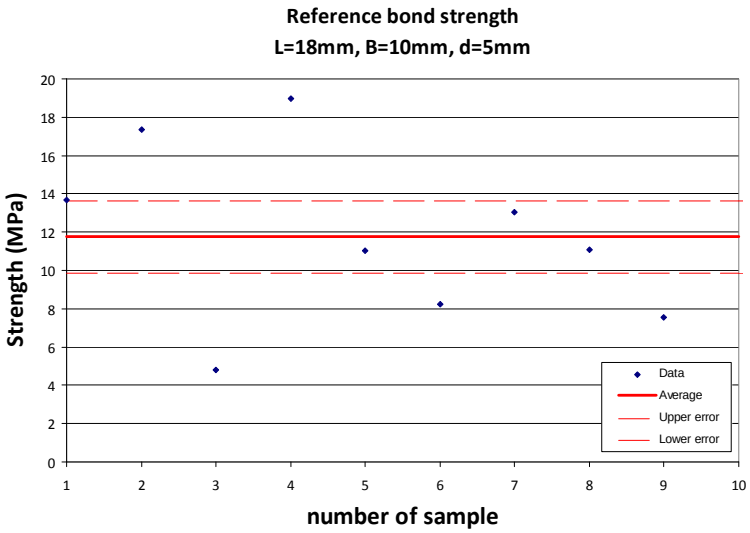

Figure 3.7: Reference strengths obtained for bonds created between samples with L=18mm, b=10mm, d=5mm (all samples).

	All Samples (MPa)		No defects over >90% (MPa)	
	Strength	Standard Deviation	Strength	Standard Deviation
Shorter Samples	11.7 ± 1.9	5.7	11.5 ± 1.7	4.8

Table 3.1: Strength of reference samples

not at the extremes of the values obtained.

The effects of different heat treatments were tested using this size of sample as will be discussed in section 3.5.2.

3.5.2 3 Minute Heat Treatment

The procedure of welding the fibres to the ears, as discussed in section 5.1, and the cleaning procedure of the suspension system before installation both involve the application of heat to the suspension. The amount of heat at the bond and any subsequent effects on bond strength are thus of interest.

Before the welding procedure had been carried out on ears of the final design for Advanced LIGO, it was estimated that it would take $\sim$ 3 minutes

to weld the fibres to the weld horns of the ears. An oven was preheated to the temperature required, the bonds were then placed inside for 3 minutes and then removed and left to cool at room temperature. This was repeated for a variety of temperatures in an attempt to simulate a range of possible thermal loads from welding and determine the effect such treatments might have on the bond strengths. 0.4 µl of bonding solution was used for every cm^2 of bonding surface. The commercially available bonding solution described in section 3.3 was diluted such that there was 1 part sodium silicate bonding solution to every 6 parts de-ionised water. This volume amount and concentration of solution was used for all samples which underwent 3 minute heat treatments. The results are shown in figure 3.8 and table 3.2.

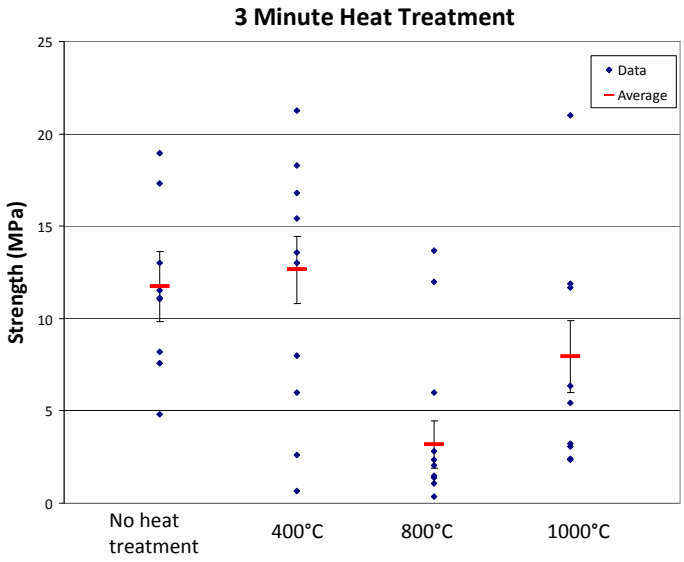

Figure 3.8: Strength of reference bonds and the strength of bonds which were thermally treated for 3 minutes at a variety of temperatures (all samples).

The average strengths for the bonds which underwent a range of heat treatments are shown in Table 3.2, along with the strengths of reference bonds which underwent no heat treatment. The average strength of bonds heated at 400°C was observed to be within error of the average strength of the reference bonds

	All Samples (MPa)		No defects over >90% (MPa)	
	Strength	Standard Deviation	Strength	Standard Deviation
Reference bonds: no heat treatment	11.7 ± 1.9	5.7	11.5 ± 1.7	4.8
400°C	12.6 ± 1.8	5.8	12.3 ± 2.0	6.0
800°C	3.2 ± 1.3	4.0	3.3 ± 2.7	3.8
1000°C	7.9 ± 1.9	6.1	14.1 ± 2.3	4.6

Table 3.2: Strength of samples which have been thermally treated at different temperatures for 3 minutes

of this size. The standard deviations were also very similar showing that a heat treatment for 3 minutes at 400°C does not seem to have any significant effect on bond strength. The bonds heat treated at 800°C and 1000°C were observed to have average strengths significantly weaker than the reference bonds.

If only the bonds which had no visual defects over >90% of the bond area before the heat treatments were carried out were considered, then the strength of the bonds which were heated at 1000°C was within error of the reference samples' strength. Although the bonds were bonded over 90% of their area or more before the heat treatment, they developed a cloudy appearance as a result of the heat treatments. This could be due to the stresses in the silica substrates increasing rapidly and the bond being slightly pulled apart over some areas. It was observed that bonds which were visually perfect over 100% of the bond surface before the heat treatments, were not visually affected by the heat to the same extent as the bonds that had bubbles, specks of contamination or areas which were not fully bonded. Bonds which were not 100% bonded are more likely to have areas which could debond if stresses are increased. This could explain the large increase in average strength of the sample set heated to 1000°C when only the samples which have no visual defects over >90% of the bond area are considered. Removing the samples which had no visual defects in the 800°C data set does not result in an increase in average strength of

the same type as is seen when considering the 1000°C set with and without samples having defects. It should be noted that there were only two samples in this set in which the bond had no visual defects over more than 90% of the bond area before the thermal treatments, four samples had >90% in the 1000°C case. Thus, it is recommended that more samples are tested at these temperatures to confirm and quantify the effect of the higher temperature heat treatments.

3.5.3 Suspension Cleaning Procedure

After the whole suspension is fabricated it will be put through a cleaning procedure which consists of the suspension being heated to 120°C for 48 hours under vacuum [113]. An initial experiment was carried out where the strength of bonds heated in air at the slightly elevated temperature of 150 °C for 48 hours was studied. This was to quantify an extreme of the scenario associated with this cleaning procedure. The bonds were created using 0.4 μl per cm^2 of a 1 part sodium silicate to 6 parts water bonding solution. After the 4 week curing time, they were put through the cleaning procedure in order to quantify the effect this has on the bond area and hence the bond strength. Figure 3.9 and table 3.3 shows the resultant strength of the bonds after undergoing this treatment.

This treatment appears to increase both the average strength and standard deviation of the bonds. Eight of these ten bonds had no optical defects over more than 90% of the bonded area. If only these bonds are considered, then this heat treatment is found to increase the strength of the bonds from the reference bonds by approximately a factor of two and the standard deviation decreases from 4.8 MPa to 3.2 MPa. This decrease in the standard deviation indicates that the heat treatment also increases the likelihood of having strong bonds. A possible reason for this increase in strength is that stresses were being removed from the sample and water was being evaporated from the bond. It was noted that this slow heat treatment did not seem to degrade the bonds

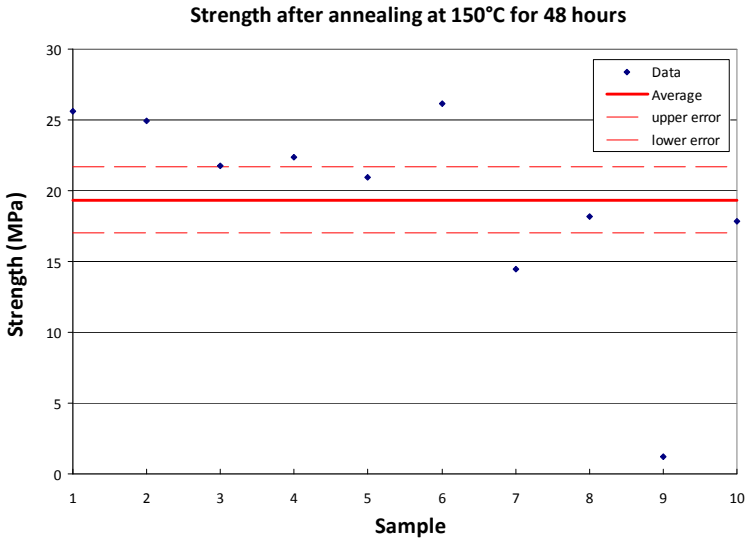

Figure 3.9: Strength of bonds which have been heated to 150 °C for 48 hours (all samples).

	All Samples (MPa)		No defects over 90% (MPa)	
	Strength	Standard Deviation	Strength	Standard Deviation
Reference	11.7 ± 1.9	5.7	11.5 ± 1.7	4.8
Cleaning conditions	19.3 ± 2.3	7.4	22.2 ± 1.1	3.2

Table 3.3: Strength of samples which have undergone simulated cleaning conditions, 150°C for 48 hours in air

visually although the shorter thermal treatment did reduce the transparency of the bonds. The strength results shown in table 3.3 show that the hydroxy-catalysis bonds are strengthened by the baking.

3.5.4 Ground Surfaces - Except the Bonding Surface

Samples which were ground on all surfaces except the bonding surface were tested and compared to samples polished on all surfaces to investigate the effect of the surface finish on strength. The reference bonds along with bonds that were heat treated are combined together to form these data sets. Ap-

proximately the same number of polished as ground bonds underwent each treatment. Thus, the data is shown to provide a comparison between ground and polished samples and not to provide an absolute value for strength of bonds between ground or polished samples. This comparison was carried out as a test to see if ground material would break on micro-cracks on the surface, possibly at the contact points of the strength testing set-up instead of in the bond. In both these cases the bonding surface was polished to a flatness of $\lambda/10$. All the samples used in obtaining the results shown in figure 3.10 were created using 0.4 µl for every cm^2 of the bond surface from a bonding solution formed from a 1:6 concentration of sodium silicate solution to de-ionised water bonding solution.

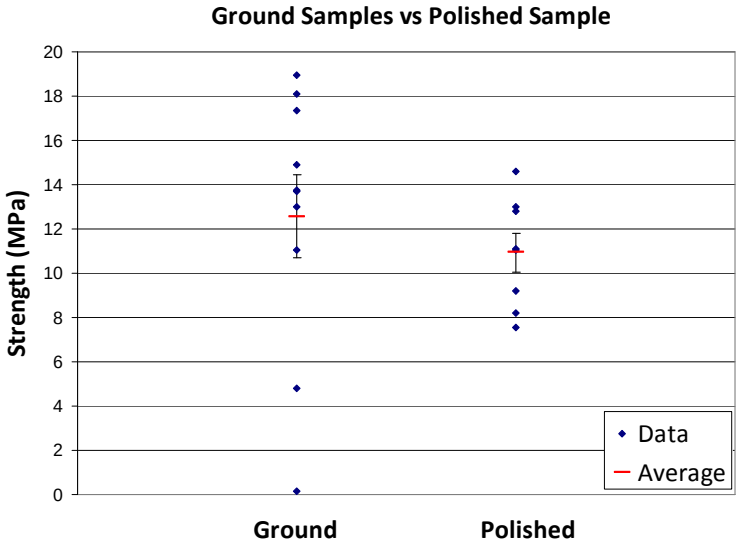

Figure 3.10: Strength of bonds created between ground and polished blocks (all samples).

The average strength of the sample set in which all surfaces except the bonding surfaces were ground is within error of the average strength of the samples which were polished on all surfaces. The results given in table 3.4 and figure 3.10 show that the surrounding surface polish does not appear to be a factor in strength determination but can affect the reliability of the strength.

	All Samples (MPa)		No defects over 90% (MPa)	
	Strength	Standard Deviation	Strength	Standard Deviation
Polished	10.9 ± 0.9	2.5	10.9 ± 0.9	2.5
Ground	12.6 ± 1.9	6.0	14.0 ± 1.6	4.6

Table 3.4: Strength of samples which are ground on all surfaces except the bonding surface and samples which are polished on all surfaces

When only the samples that were visually clear over >90% of the bonding area were taken into account, the large difference in the standard deviation of the ground and polished sets is removed. Thus, the surface finish of the sides of the sample which are not bonded does not effect the measured strength.

3.6 Altering the Geometry of the Samples

It could be seen during the above heat treatment tests, that a large subset of the samples were breaking at the points of contact instead of in the bond area. An example of this is shown on the left hand side of figure 3.11. It was postulated that the samples were breaking in this way as the geometry of the sample was such that stresses induced by the strength testing set-up were forming at the points of contact. This gave a lower overall breaking force for the sample. To reduce stresses at the contact points, longer samples were designed such that, a longer lever arm is created between the vertically applied stresses and the bonds therefore decreasing the stress at the points of contact for which the same stress is applied in the bond from the load. The longer samples had dimensions of $L = 38$ mm, $b = 10$ mm, $d = 5$ mm and the geometry of the testing set-up did not have the same ratio as shown in figure 3.5. Thus, deriving from equation 3.1, the tensile strength could be obtained from the relation [112],

$$\sigma_{tensile} = \frac{21}{34}\frac{FL}{bd^2} \tag{3.4}$$

	All Samples (MPa)		No defects over 90% (MPa)	
	Strength	Standard Deviation	Strength	Standard Deviation
Shorter Samples	11.7 ± 1.9	5.7	11.5 ± 1.7	4.8
Longer Samples	13.7 ± 1.3	4.1	14.8 ± 0.8	2.3

Table 3.5: Tensile strength of the shorter and longer reference samples

These samples could be seen to break predominantly in the bond area more often and diagonal fractures could not have originated from the line contacts. Images of the location of these breaks are shown in figure 3.11.

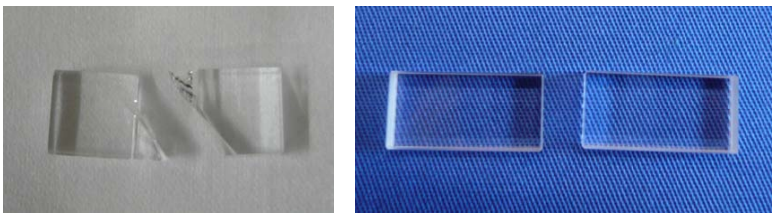

Figure 3.11: Left) Shorter sample broken at contact points due to high stresses and Right) longer sample broken in bond area).

Using these longer samples the average strength of the reference samples (constructed using 0.4 μl/cm^2 of 1:6 concentration of sodium silicate solution to de-ionised water) stayed the same within the standard error, however, if only the samples that had no visual defects over >90% of the bonding surface increased as expected. The results are shown in figure 3.12 and table 3.5 and compared to the results from the shorter samples.

3.6.1 Welding Conditions

After the previous tests were completed the welding process was carried out on a real Advanced LIGO-design ear. A thermocouple was placed on the bond surface during the welding procedure to investigate the temperature to which the bond was heated. These measurements showed that the bond surface was heated to a maximum of 350°C during the process which lasted between 3 and

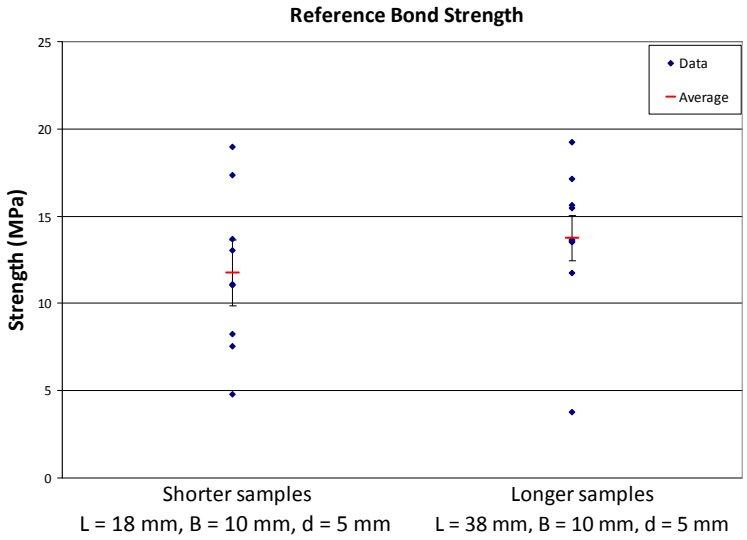

Figure 3.12: Reference strengths obtained for bonds created between samples with L=18mm, b=10mm, d=5mm and samples with L=38mm, b=10mm, d=5mm (all samples).

	All Samples (MPa)		No defects over 90% (MPa)	
	Strength	Standard Deviation	Strength	Standard Deviation
Reference	13.7 ± 1.3	4.1	14.8 ± 0.8	2.3
Welding conditions	12.3 ± 2.6	8.2	16.5 ± 2.0	5.4

Table 3.6: Strength of samples which have underwent simulated welding conditions, 350°C for 12 minutes

12 minutes [114]. Thus studies were carried out to simulate this type of heat treatment. Bonds were created using the longer design of fused silica samples, using 0.4 µl of bonding solution per cm^2 of surface area with a concentration of 1:6 sodium silicate solution to de-ionised water. The bonds were placed in an oven, which had been preheated to 350°C for 12 minutes and then removed and allowed to cool at room temperature in order to investigate an extreme of the scenario associated with the welding procedure. The result is shown in figure 3.13 and table 3.6.

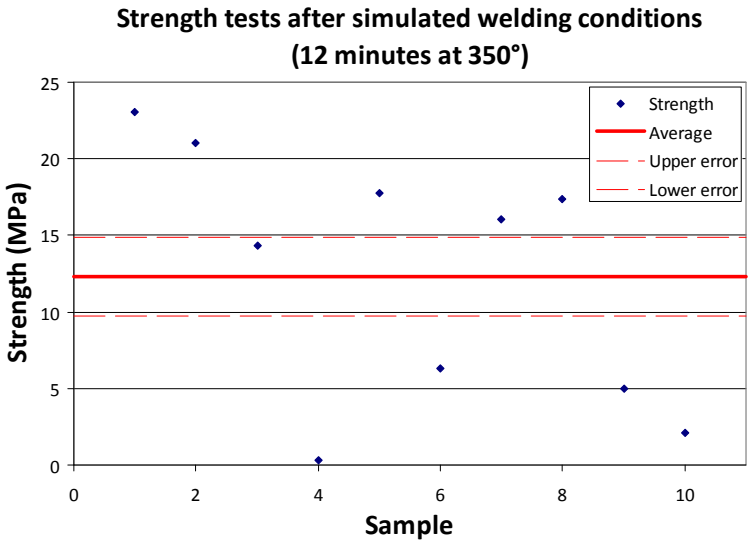

Figure 3.13: Strengths of bonds which have been heat treated at 350° for 12 minutes to simulate the thermal conditions which would be caused by the welding procedure (all samples).

Bonds number 4, 9 and 10 were not optically defect free over 90% of the bond area. The average strength of the sample set with and without these bonds is shown in table 3.6. For the bonds which had no visual defects over 90% of the bond area, the average strength is within error of the results for the reference bonds and the standard deviation was ~ 3 MPa greater for the bonds which underwent the welding conditions. Since the average strength for the complete sample set is lower than that for the bonds which have areas of $>$ 90% appearing to be free of defects, it can be seen that the strength of bonds which are not visually as good, is found to degrade more than those of bonds observed to have better optical appearance. As only bonds which are observed to have a bond area which is free of defects over 90 % of the area are accepted for use in the construction of the suspensions for gravitational wave detectors, these results show that the hydroxy-catalysis bonds are expected to remain strong during the fibre welding process.

Vacuum Baked Bonds

As discussed in section 3.5.3 the cleaning process of the suspension mirrors for Advanced LIGO involves heating the suspension to 120°C under vacuum. To further investigate the effect of this treatment on the strength of the hydroxy-catalysis bonds, a set of the longer bonded samples was placed under vacuum after the 4 weeks curing time. Two different sets of bonds, both created with 0.4 $\mu l/cm^2$ of 1:6 concentration of sodium silicate bonding solution to de-ionised water, were placed under differing vacuum pressures, the results are shown in figure 3.14. It should be noted that all bonds in these two sets had no optical defects over more than 90% of the bond surface, except for 1 bond in set 2. The results are shown in figure 3.14 and table 3.7 and it can be seen that both data sets lie within error of the reference set. Thus it can be determined that this difference in pressure does not alter the strength of the bonds. A third set, bonded with the same type and amount of solution was placed under vacuum at a pressure of 4×10^{-3} mbar and heated to 150°C for 48 hours. The strength results are shown in figure 3.14 and table 3.7 and it can be seen that this treatment increases the average strength over that of the reference sample strength. It should be noted that as discussed earlier in this chapter a set of shorter samples were baked in air at this temperature (see section 3.5.3). This air bake was shown to increase the strength over that of the relevant reference sample strength. It can be seen from the results here that baking under vacuum also appears to improve bond strength. To quantify the relative effects of baking in air and baking under vacuum it is recommended that a set of the longer samples undergo the exact Advanced LIGO cleaning procedure and are then strength tested. The procedure involves placing the samples under vacuum at $\sim 10^{-5}$ mbar and then heating to 150°C for 48 hours. This would form the basis for future work.

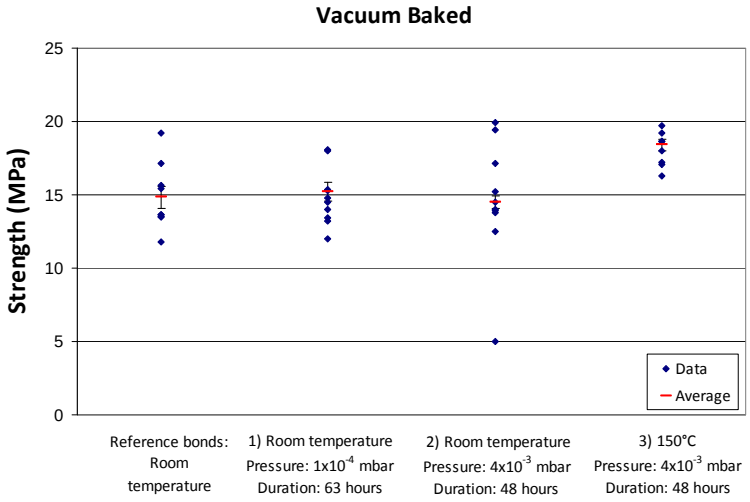

Figure 3.14: Strength results, where all bonds have been cured at room temperature and then baked under vacuum (all samples).

	All Samples (MPa)		No defects over 90% (MPa)	
	Strength	Standard Deviation	Strength	Standard Deviation
Reference bonds: room temperature	13.7 ± 1.3	4.1	14.8 ± 0.8	2.3
1×10^{-4} mbar	15.2 ± 0.6	2.0	15.2 ± 0.6	2.0
4×10^{-3} mbar	13.5 ± 1.0	3.2	14.5 ± 0.4	1.3
150°C at 4×10^{-3} mbar	18.4 ± 0.4	1.2	18.4 ± 0.4	1.2

Table 3.7: Strength of samples which have been baked under vacuum, where all bonds were formed over >90% of the bond area

3.6.2 Effect of Concentration of Bonding Solution

As discussed in section 3.3, the concentration of sodium silicate solution used to bond elements of gravitational wave detector suspensions is one part sodium silicate solution to every six parts de-ionised water, i.e. 1:6 concentration. To study the effect of solution concentration on bond strength a set of the longer blocks was used to create bonds using a different concentration of sodium silicate solution to de-ionised water. Bonds were created using a solution which

consisted of one part sodium silicate solution to every 4 parts de-ionised water, i.e. 1:4 concentration. The volume per unit area of the bond surface and type of bonding solution, 0.4 $\mu l/cm^2$, sodium silicate solution was kept the same as was used for the 1:6 reference samples. The strengths obtained for the samples made from the 1:4 solution are shown in figure 3.15 and table 3.8.

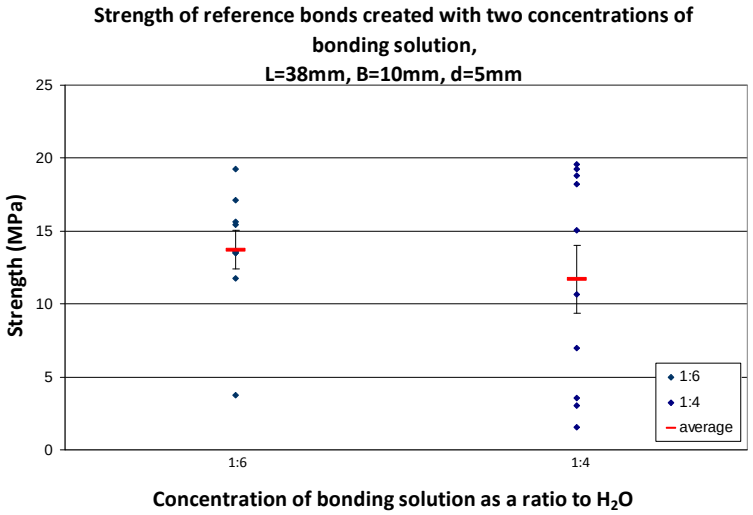

Figure 3.15: Strength results of varying concentration of bonding solution (all samples).

It can be seen that the average strength of the bonds created using these two different concentrations are not significantly different. However, the bonds created using the more concentrated solution have a larger standard deviation. A larger spread in strength values means they are effectively less reliably strong. By increasing the concentration of the bonding solution, we have added more sodium silicate to fill the bond. For some of the 1:4 concentration samples, this filling has worked very well resulting in higher strengths but for some of the other samples the extra silicate seemed to inhibit strong chemical bonding resulting in poorer bond quality and thus a lower tensile strength. This could be due to the 1:4 concentration of bonding solution having a higher pH than the 1:6 concentration of bonding solution. As the pH is higher, the bond will take longer to form and thus some areas of the bond could start to form before

	All Samples (MPa)		No defects over 90% (MPa)	
Concentration	Strength	Standard Deviation	Strength	Standard Deviation
1:6	13.7 ± 1.3	4.1	14.8 ± 0.8	2.3
1:4	11.7 ± 2.3	7.4	16.9 ± 1.4	3.5

Table 3.8: Strength of samples created with differing concentrations of bonding solution

others area. This could cause an uneven bond. These results suggest the weaker solution produces more consistently reliable bonds. It is recommended that a set of bonds with a 1:8 concentration of sodium silicate solution to de-ionised water is strength tested. To observe if a weaker concentration of solution further increases the reliability of the bond strength or does not have enough silicate to form strong bonds.

Bonds formed with these concentrations of bonding solution between silica substrates have previously been strength tested by E. Elliffe [109]. Elliffe also found that the strength of bonds created using a 1:6 concentration of bonding solution and a 1:4 concentration of bonding solution were within error. However, the values of the strength measured by Elliffe are not comparable to the strength values presented in this thesis as a different experimental geometry was used.

3.6.3 Effect of Loading During Curing

When bonds are first created it is not uncommon for bubbles to appear in the bond area. Generally these move out of the bond over time by migrating to the bond edges, but occasionally they can remain inside the bond. It has been seen that bonds with no visual defects are stronger on average than those with bubbles present. Bonds were created using 0.4 μl per cm^2 of a bonding solution, formed from a ratio of 1:6 sodium silicate to de-ionised water and small weights were placed on top of one of the bonding surfaces, compressing the bond slightly. The aim of this experiment was to find an optimum force

which may help push all bubbles out of the bond area giving a bond which has no visual defects and hence an increased bond strength (with the possibility that the improved optical appearance may be of interest in other applications). In this experiment the longer samples were used and hence, the strengths should be comparable to results of the sample set displayed in figure 3.12. Weights of 10 grams, 20 grams and 40 grams were used as loads. A bonding jig was designed to hold the samples rigidly and prevent the bonds being weakened due to any misalignment of the loads applied. The bonding jig and a schematic diagram showing how it works are shown in figure 3.16.

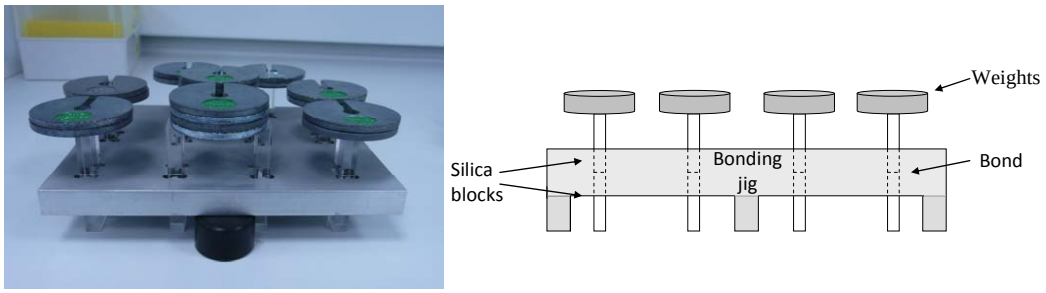

Figure 3.16: Left) Silicate bonds under a load of 10 grams, Right) a schematic showing more clearly how it works.

The results are shown in figure 3.17 and table 3.9. It can be seen from this that the amount of load which is applied to a bond during the curing process does not affect the resultant strength of the bond as they are all within error of the reference strength. However, it can be seen that loading a bond at the level of 40 grams here appears to help reduce the standard deviation of the strength results obtained, creating more reliably strong bonds. The standard deviation of the reference bonds was 4.1 MPa. The bonds loaded with 10 grams had a standard deviation of 5.6 MPa. This increase could be due to the weights not being distributed evenly over the sample due to difficulties in alignment of the load. The standard deviation of the 20g and 40g sets were smaller at 3.8 MPa and 1.8 MPa, respectively. It is possible that the force applied by a 10 gram mass was not large enough to compensate for any misalignment of the load.

The visual quality of the bonds was noted during each week of the 4 week curing process and it was found that the most effective time period for the loads to reduce the presence of bubbles was in the first week. After the first week of curing the visual quality of the bonds remained constant. The bonds which were placed under the largest load of 40 grams were the best bonds visually after the curing period. 9 of the 10 bonds in this set would have been accepted for use in a gravitational wave detector, 5 of the 20 gram set would have been accepted and 6 of the 10 gram set would be accepted.

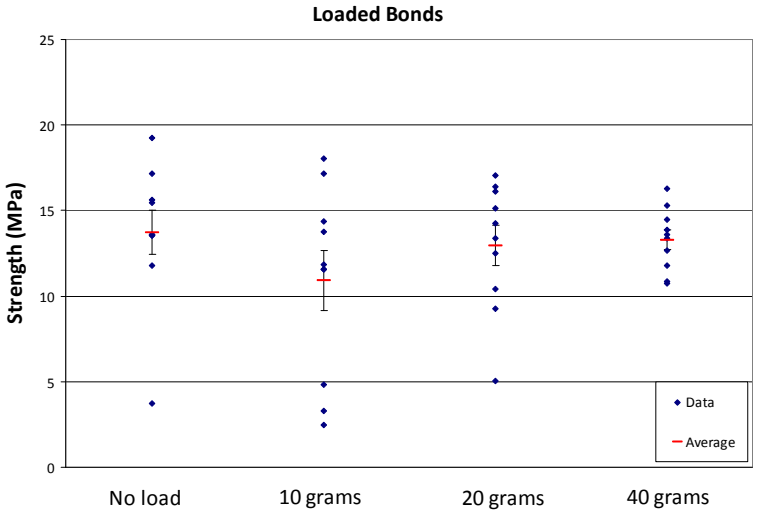

Figure 3.17: Strength of bonds under different amounts of force during the curing time (all samples).

3.6.4 Effect of the Volume of Solution Used in Bonding Procedure

The volume of bonding solution used in Advanced LIGO suspension construction is 0.4 μl/cm^2 of the bonding surface, as this amount is enough to fill the space between two surfaces which are $\lambda/10$ flat. For this reason the 0.4 μ l/cm^2 data set is the same set used as reference bonds and thus the other sets with varying amounts of solution can be compared to this set. The effect on bond

	All Samples (MPa)		No defects over 90% (MPa)	
	Strength	Standard Deviation	Strength	Standard Deviation
Reference strength i.e no load	13.7 ± 1.3	4.1	14.8 ± 0.8	2.3
10g	10.9 ± 1.8	5.6	14.5 ± 1.1	2.7
20g	13.0 ± 1.2	3.8	14.5 ± 0.8	1.7
40g	13.3 ± 0.6	1.8	13.1 ± 0.6	1.8

Table 3.9: Strength of samples which have been cured under a load.

strengths of using different volumes of solution was explored. The type of bonding solution used to create the bonds was kept constant; 1:6 concentration of sodium silicate to de-ionised water.

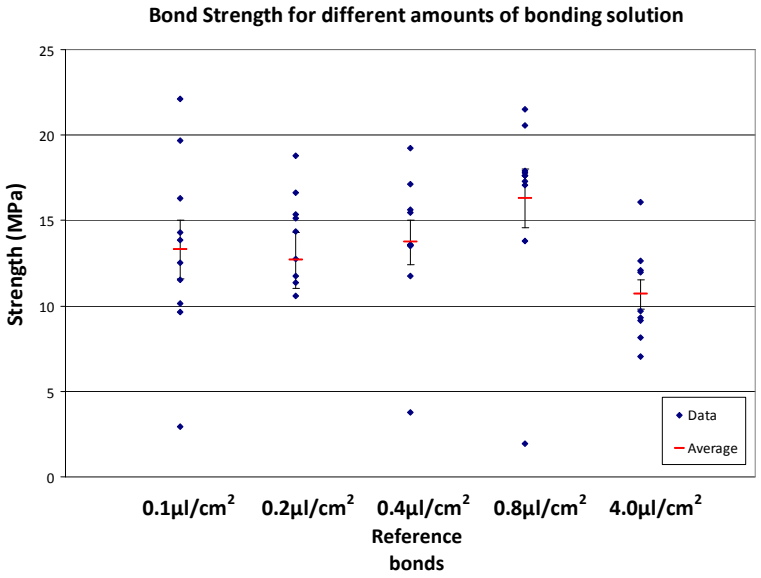

Figure 3.18: Measurements of the strength of bonds created with a varying amount of bonding solution (all samples).

All the results are shown in figure 3.18 and table 3.10 and the strength of the bonds with no defects over more than 90% of the bonding surface are shown in figure 3.19. For the bonds which have no defects over 90% of the

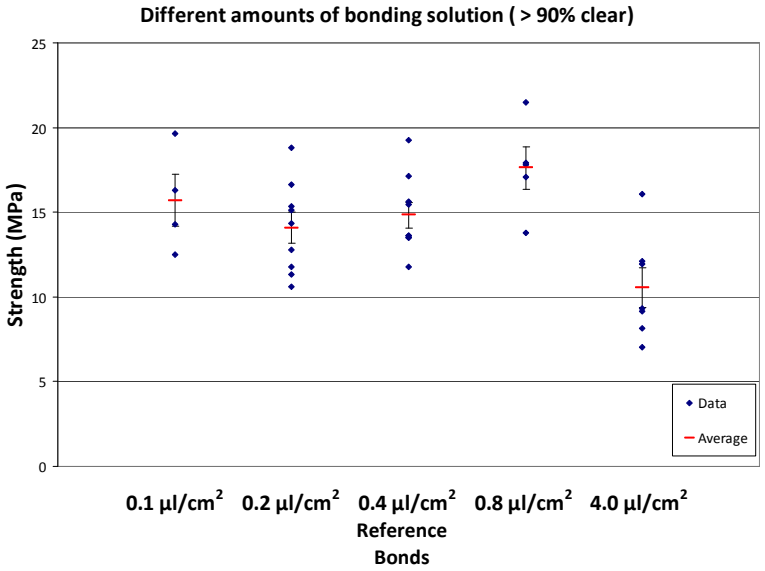

Figure 3.19: Strength of bonds which had no optical defects over >90% of the bond surface and were created with a varying amount of bonding solution.

	All Samples (MPa)		No defects over 90% (MPa)	
	Strength	Standard Deviation	Strength	Standard Deviation
0.1 µl/cm^2	13.3 ± 1.7	5.4	15.7 ± 1.5	3.1
0.2 µl/cm^2	12.7 ± 1.6	5.1	14.1 ± 0.9	2.7
Reference bond: 0.4 µl/cm^2	13.7 ± 1.3	4.1	14.8 ± 0.8	2.3
0.8 µl/cm^2	16.3 ± 1.7	5.5	17.6 ± 1.2	2.8
4.0 µl/cm^2	10.5 ± 1.2	3.1	10.5 ± 1.2	3.1

Table 3.10: Strength of samples which have been created using different volumes of bonding solution

bonding area, the average strengths of all of the data sets is within error with the exception of the 0.8 µl/cm^2 and 4.0 µl/cm^2. For the bonds which looked optically perfect over an area greater than 90% of the bond surface the sample set created using 0.8 µl/cm^2 of bonding solution had an increased strength. As the 4.0 µl/cm^2 did not have an increased strength this suggests that there may be an optimum amount of solution in this range which provides the strongest

bonds. This could be due to the fact that there is an optimum ratio of OH^- ions per unit area which allows for strong siloxane chains to be formed. Volumes of solution greater than the optimum could cause the siloxane chains to be deformed and therefore be weaker. An increase in the time taken for the pH to fall and the siloxane chains to be created could mean that the curing time would be extended. The increase in the amount of water in the bond would also cause an increase in the curing time as it would take longer for the water to migrate out. Thus, for the same period of curing time, bonds with less solution may be stronger but the bonds created with more solution may become stronger over greater periods of time. Further studies of the strength of bonds created using volumes of solution between 0.8 $\mu l/cm^2$ and 4.0 $\mu l/cm^2$ are of interest, including tests after different lengths of curing time.

Increasing the volume of bonding solution may increase the bond thickness which could increase the mechanical loss of the system. A low mechanical loss is very important for gravitational wave detectors and hence this must also be taken into account when deciding on the optimum amount of bonding solution to be used.

3.6.5 Effect of the Type of substrate Material on Strength

3.6.5.1 Quality of Material

The strength tests presented in this section were carried out in order to investigate how, if at all, bond strength is affected by the type of fused silica used as the substrate which is being bonded. Fused silica produced by different manufacturers can have properties which vary depending on manufacturing process, such as homogeneity, optical absorption and water content [115, 116]. By acquiring material from different suppliers we obtain material which has been created through different methods of manufacturing. Surface preparation and polishing of the samples can introduce machining micro-cracks which would reduce the overall sample strength. This makes the manufacturing process potentially important to the strength of the material. Strength tests were

performed using the longer type of samples to evaluate the strength of bonds created between two different types of fused silica, Corning 7980 [117], made by Corning, and Suprasil 312 [118], made by Heraeus. These materials were chosen as they are the material from which the mirrors in current gravitational wave detectors, such as LIGO, are made from. All of the samples tested were polished by Gooch and Housego [119]. Suprasil 312 has less bubbles or inclusions within the bulk of the fused silica than Corning 7980 and larger optical homogeneity throughout the bulk of the material. Both types of material were bonded using 0.4 μl/cm^2 of 1:6 sodium silicate bonding solution as described in section 3.6.2. The results obtained are shown in figure 3.20 and table 3.11 and the Corning 7980 set is the reference set for the longer samples shown previously and discussed in section 3.6.

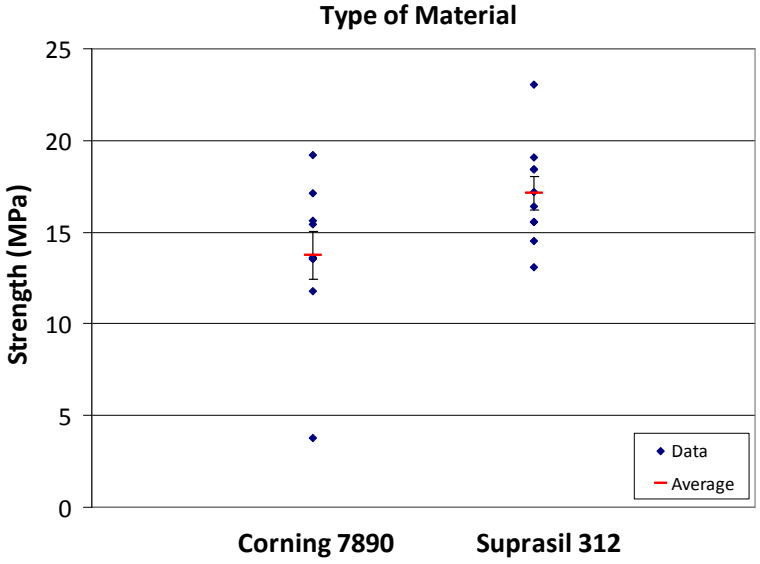

Figure 3.20: Strength Corning 7980 and Suprasil 312 fused silica (all samples).

Figure 3.20 shows that Suprasil 312 has an average strength which is slightly higher than the strength of Corning 7980. The standard deviation of Suprasil 312 is slightly smaller than the standard deviation of Corning 7980. However, the larger spread in Corning 7980 is mostly due to one weak sample. If any bonds which were less than 90% visually perfect before breaking are omitted

	All Samples (MPa)		No defects over 90% (MPa)	
	Strength	Standard Deviation	Strength	Standard Deviation
Corning 7980	13.7 ± 1.3	4.1	14.8 ± 0.8	2.3
Suprasil 312	17.1 ± 0.9	2.8	16.9 ± 0.8	2.1

Table 3.11: Strength of samples which have been created between Corning and Suprasil fused silica

from consideration then the standard deviations of the Corning and Suprasil sets are at a similar level. Thus, bonds created between Suprasil 312 and Corning 7980 have a similar reliability of strength. However, bonds created between Suprasil 312 substrates are slightly stronger. This could be due to differences within the bulk of the material or to differences in the quality of the bonds created between differing substrates.

3.6.5.2 Bulk Silica Strength Tested

Bulk pieces of silica were strength tested in the 4 point strength testing machine to allow for a comparison of bond strength to bulk fused silica strength and to investigate if the difference in strengths found in section 3.6.5.1 were due to the bulk material or difference in bond quality. All of the bulk samples were polished by Gooch and Housego[119]. The resultant strengths of these samples are shown in figure 3.21 and the values are given in table 3.12.

Figure 3.21 shows that Suprasil 312 and Corning 7890 have average strengths which are of the same level. In figure 3.20 it can be seen that the spread of strengths is smaller for Suprasil 312 than for Corning 7980. This could be due to the fact that Suprasil 312 is of a higher quality and therefore has less bubbles, inclusions or micro-cracks within the material which would be weak points in the structure. As Corning 7980 has a lower homogeneity we know that there can be a larger variation between each individual sample and it might therefore be expected to have a larger spread in strengths obtained for the different samples.

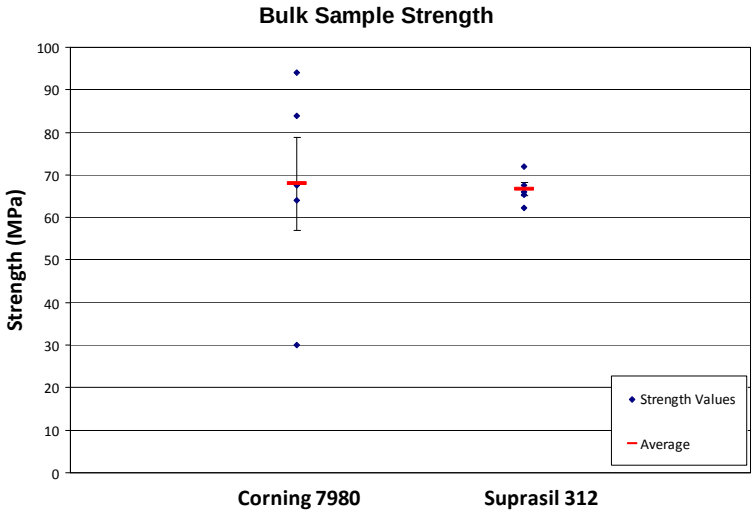

Figure 3.21: Strength of two different qualities of fused silica.

	All Samples (MPa)	
	Strength	Standard Deviation
Corning 7980	67.9 ± 10.9	24.4
Suprasil 312	66.6 ± 1.6	3.6

Table 3.12: Strength of bulk fused silica samples

From figure 3.21 and figure 3.20 it can be seen that bulk fused silica had a strength approximately ~ 4 times greater than the bonded silica samples. The published value for the tensile strength of Suprasil 312 fused silica is 50 MPa [116], which is somewhat lower than obtained in these experiments.

3.6.5.3 Bulk Silica with Chamfers

Pieces of silica were also manufactured to be identical in geometry to the bonded samples. These were the long bulk pieces as discussed above in section 3.6.5.2 with a small chamfer sawed into their surfaces where the bond would be located (± 0.2 mm deep). This permits a more accurate comparison to the strength of the bonded samples due to the closer match in geometries. Both sets of results are given in table 3.13 and shown in figure 3.22.

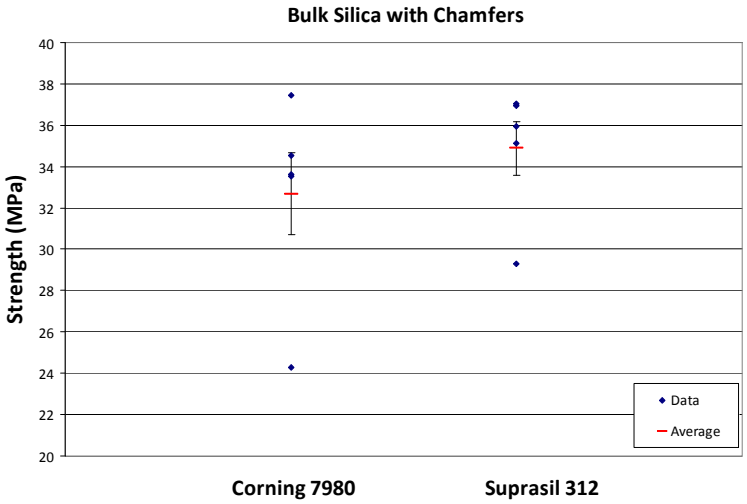

Figure 3.22: Strength of bulk Corning 7980 and Suprasil 312 samples with grooves machined in to represent the chamfer of the bonded sample (all samples).

	All Samples (MPa)	
	Strength	Standard Deviation
Corning 7980	32.7 ± 2.0	4.4
Suprasil 312	34.9 ± 1.3	2.9

Table 3.13: Strength of bulk fused silica samples with chamfers sawed in to imitate the bonded samples

As expected from the analysis shown in figure 3.6 the strength of the samples with grooves were less than that obtained from the bulk samples without the grooves imitating the chamfer. Stress builds at the edges of the chamfer which creates a weak point in the sample. This is the location at which the sample is most likely to break. The strengths are greater than the bonded samples showing that bonds are not as strong as pure silica.

3.7 Conclusion

Hydroxy-catalysis bonding is a very reliable way to construct low loss suspension systems for gravitational wave detectors. The bonds are extremely strong, being measured to be $\sim$ 15 MPa, very durable and can withstand significant amounts of heat without their strength being degraded. The results of experiments carried out to observe the effect of different heat treatments on the strength of bonds are as follows;

- 3 minute thermal treatments at 400°C, 800°C and 1000°C are not seen to effect the clarity of optically clear bonds;
- The clarity of bonds which are not clear over 100% of the bond area are degraded by the 3 minute heat treatments;
- Heat treating at 150°C for 48 hours, the treatment that will be carried out for the suspension cleaning procedure of gravitational wave detectors, has been seen to significantly improve bond strength;
- Heat treating for 12 minutes at 350°C, the heat treatment the bonds will experience when the fibres are being welded to the ears of gravitational wave detectors, does not effect strength, however this treatment does increase the spread of the strength values measured;
- Heating to 150°C under vacuum increases the strength of the bonds by a factor which is less than that of heating at atmospheric pressure.

Thus, the bond strength will not degrade due to procedures carried out on the suspension systems of gravitational wave detectors.

Experiments were carried out to observe any effect of loading the bonds during their curing time,

- Loading the bonds with 40 g weights, i.e. applying a pressure of $\sim$ 2.5 Pa, was observed to increase the clarity of the bonds;

- Applying a load which is > 20 grams to the bonds decreased the spread of strength results obtained.

Loading the hydroxy-catalysis bonds during their curing time can be used as a method of increasing the success rate of creating clear, strong bonds.

Different formulations of the bonding solution were used in studies of bond strength,

- Decreasing the amount of bonding solution to $0.1\mu l/cm^2$ does not effect bond strength;
- Increasing the amount of solution to $0.8\mu l/cm^2$ increases the bond strength;
- Increasing the amount of solution tenfold to $4.0\mu l/cm^2$ decreases the average strength of the bonds;
- Increasing the concentration of the bonding solution to a 1:4 ratio of sodium silicate to de-ionised water increases the bond strength.

Increasing the amount of bonding solution to $0.8\mu l/cm^2$ and increasing the concentration of the bonding solution to a 1:4 ratio of sodium silicate to de-ionised water looks like a good method of increasing bond strength. However, changing the concentration and volume of bonding solution could increase the thickness of the bond created, which would cause extra mechanical loss in the system. The difference in bond thickness must be investigated before these changes to the used bonding solution would be considered for the purpose of joining elements of the suspensions for gravitational wave detectors.

Other parameters were varied to observe any effect on bond strength such as holding the bonds under vacuum and bonding samples which were rough on the sides that were in contact with the 4 point bend tester. These were found to have no influence on the bond strength measured.

A summary of all the strength values obtained for the samples undergoing the treatments assessed here is given in table 3.14 and table 3.15 for the shorter and longer samples respectively.

Tested Parameter		Strength (MPa)	Standard deviation
Reference		11.5 ± 1.7	4.8
Heat treatments	3 minutes at 400°C	12.3 ± 2.0	6.0
	3 minutes at 800°C	3.3 ± 2.7	3.8
	3 minutes at 1000°C	14.1 ± 2.3	4.6
	48 hours at 150°C	22.2 ± 1.1	3.2
Ground surfaces (except bonding surface)		14.0 ± 1.6	4.6
Polished surfaces		10.9 ± 0.9	2.5

Table 3.14: Strength test results of tests carried out using the shorter blocks, average taken of bonds which have no optical defects over more than 90% of the bond area

Tested Parameter		Strength (MPa)	Standard deviation
Reference, Corning 7890 0.4µl/cm^2 1:6 sodium silicate		14.8 ± 0.8	2.3
Using 1:4 concentration of sodium silicate solution		16.9 ± 1.4	3.5
Heating	12 minutes at 350°C	16.5 ± 2.0	5.4
Vacuum	1×10^{-4} mbar for 63 hours	15.2 ± 0.6	2.0
	4×10^{-3} mbar for 48 hours	14.5 ± 0.4	1.3
	4×10^{-3} mbar for 48 hours and heated at 150°C	18.4 ± 0.4	1.2
Loaded	10g	14.5 ± 1.1	2.7
	20g	14.5 ± 0.8	1.7
	40g	13.1 ± 0.6	1.8
Amount of solution	0.1µl/cm^2	15.7 ± 1.5	3.1
	0.2µl/cm^2	14.1 ± 0.9	2.7
	0.8µl/cm^2	17.6 ± 1.2	2.8
	4.0µl/cm^2	10.5 ± 1.2	3.1
Type of material	Suprasil 312	16.9 ± 0.8	2.1
Bulk silica	Corning 7980	67.9 ± 10.9	24.4
	Suprasil 312	66.6 ± 1.6	3.6
Chamfered bulk silica	Corning 7980	32.7 ± 2.0	4.4
	Suprasil 312	34.9 ± 1.3	2.9

Table 3.15: Strength test results of tests carried out using the longer blocks, average taken of bonds which have no optical defects over 90% of the bond area

Chapter 4

Mechanical Loss of Fused Silica for use as a Test Mass Material

4.1 Introduction

As discussed in chapters 1 and 2, the thermal noise of the suspension and mirror material is an important limiting factor in the sensitivity of gravitational wave detectors. To obtain a low level of thermal noise, the materials for the suspension must have a low mechanical loss. Also, the mirror material must be obtainable in the size (40 kg) and geometries required, be suitable for hydroxy-catalysis bonding and meet the specifications required for the opto-mechanical properties. These properties include a low thermal expansion coefficient and a high thermal conductivity to ensure the mirrors have minimum distortion due to the heat from the laser beam, and a refractive index which has a low dependency on temperature to ensure minimum thermal lensing effects [120]. Transmissive optics also require a low optical loss and high transparency at the wavelength of laser light being used, which is currently 1064 nm [120]. This is important as it ensures that the heat absorbed by the mirrors is minimised thus minimising thermal lensing and distortion.

The material which has been chosen for the mirrors and suspensions in advanced gravitational wave detectors is fused silica. There are many different types of fused silica, in which the mechanical and optical properties can vary as

they are dependent on the purity, manufacturing and polishing process. The manufacturing process can alter the loss of the bulk of the material as this is dependent on the micro-structure of the material, and certain treatments can alter the measured loss, such as heat treatments [121–123]. The polishing process can affect the mechanical loss of the surface layer of a sample as the loss can depend on the roughness of the surface. This will be discussed further in section 4.3. Heraeus and Corning both manufacture silica using flame hydrolysis [115, 116]. $SiCl_4$ is hydrolysed using a flame, this turns the silicon into a gas which is then oxidised to form SiO_2 and thermal fusion of the resulting dust forms the fused silica. However, there are proprietary differences between these companies' manufacturing processes which can lead to slightly different optical and mechanical properties within the fused silica produced. Corning 7980 and Suprasil 312 are the types of fused silica which have been chosen for the mirrors in the detector suspensions as they have been demonstrated to have a relatively low mechanical loss at room temperature[123], can be obtained and polished in the size and geometries required and are suitable for hydroxy-catalysis bonding. Despite having a low linear coefficient of thermal expansion, the low thermal conductivity of fused silica requires gravitational wave detectors with these mirrors to have active control in order to compensate for thermally induced distortions [89].

This Chapter describes measurements of the mechanical loss of Suprasil 3001. This type of fused silica has a lower optical absorption than Suprasil 312 at 1064 nm and has been chosen for use for the input mirrors of gravitational wave detectors to reduce thermal lensing effects. The mechanical loss has to be quantified in order to calculate the thermal noise of this substrate and hence determine if it is suitable for use in advanced gravitational wave detectors. The mechanical loss of hydroxy-catalysis bonds created between fused silica is also studied here. Possible methods of reducing the mechanical loss further through heat treatments and removal of the outer lossy surface layer through chemical etching are explored.

4.1.1 Measuring Mechanical Loss

The mechanical loss of a substrate can be obtained from measurements of the free decay of the amplitude of motion of an excited resonant mode. The amplitude of the resonant motion, $A(t)$, will decay in a form described by the behaviour of a damped harmonic oscillator. This decay may be expressed in the form:

$$A(t) = A_o e^{-\frac{\omega_o t}{2/\phi(\omega_o)}}, \tag{4.1}$$

where A_o is the amplitude at time $t = 0$, ω_o is the angular frequency of the resonant mode and $\phi(\omega_o)$ is the mechanical loss [124] of the material. From this it can be seen that by monitoring the amplitude over the decay time the mechanical loss can be calculated.

4.2 Experimental Set-Up

A photograph of a typical suspension for loss measurements of bulk material is shown in figure 4.1.

The samples studied here were cylindrical, each having a diameter of 65 mm and with lengths of 50, 70 or 120 mm. Each sample was suspended in turn as a pendulum using a single loop of silk which was placed around the centre of the barrel. Silk is selected as the suspension material as it has been shown to provide low mechanical loss pendulums compared to that of wire loops [125]. In order to study the intrinsic dissipation of the sample material, all external sources of dissipation must be minimised. The single loop suspension provides minimal contact with the sample surface in an attempt to minimise contact friction. Friction at the points of contact of the silk and the sample are further reduced by applying a very small quantity of grease to the thread. The suspension is placed under vacuum at a pressure $\sim 10^{-6}$ mbar to reduce the effects of gas damping on the system [126]. Short suspension lengths are used to increase the frequency separation of the violin modes [127]. By increasing the separation, the number of modes which reside in the frequency range of

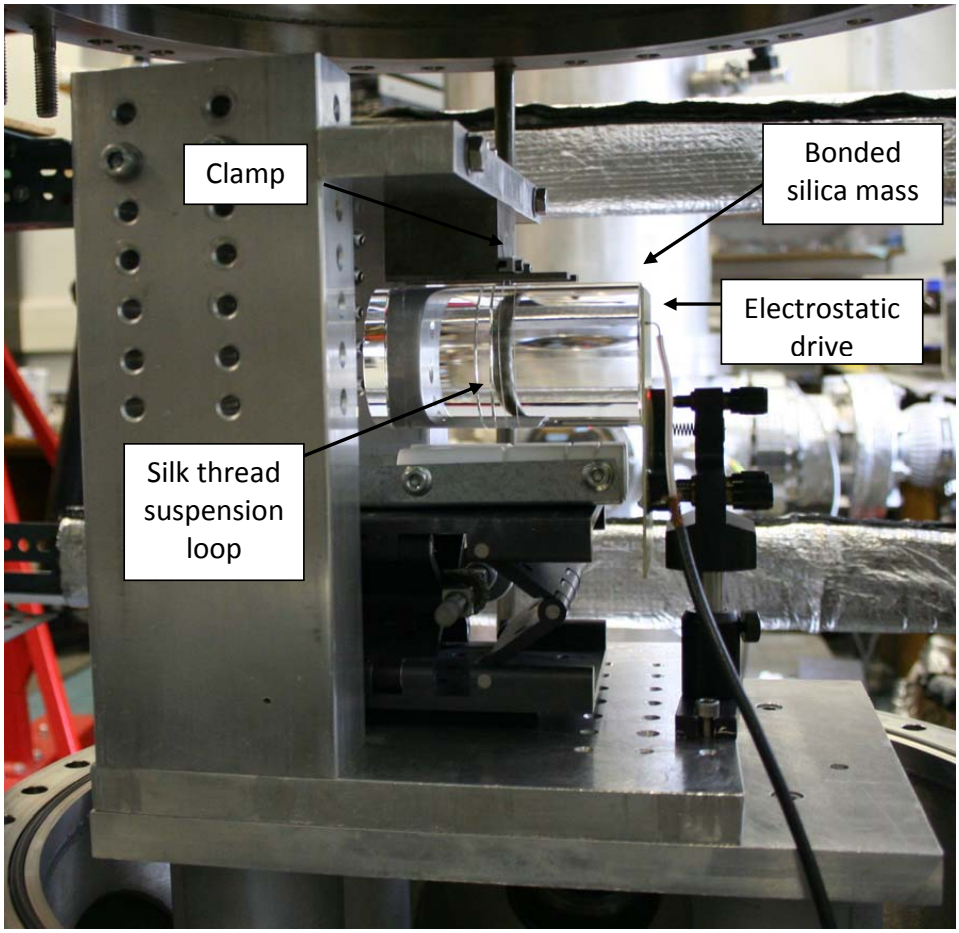

Figure 4.1: A bonded silica mass suspended as a pendulum using silk thread in order to measure mechanical loss.

interest can be decreased. The samples being measured are suspended multiple times changing the length of suspension each time. This changes the frequency of the violin modes present in the range of interest and also alters the position of the break-off points very slightly. This is an attempt to ensure that excessive loss is not present due to an accidental coupling to the violin modes or excess friction at the contact area of the mass and the break-off point of the suspension material [128]. The motion of the sample is excited using an electrostatic drive plate which is placed $\sim$ 1 mm behind the back surface of the sample. The drive plate has a DC voltage of 750 V which polarises the sample and an AC voltage of up to 360 V (peak-to-peak) which drives the resonant motion of the sample

at a frequency of interest. The motion of the front surface of the sample is then sensed using a table top interferometer. The interferometer has actuators on mirrors within a folded arm 4.3 which provide a low frequency feedback system. This is required to reduce noise caused by the pendulum motion of the suspended mass which can be excited by external seismic vibrations. The actuators include a piezoelectric transducer which filters out frequencies under 100 Hz and a pair of loudspeakers which filter out the large amplitude pendulum motion which is typically below 30 Hz. By subtracting the DC offset of the output signal the interference fringes are centred around 0 V and the feedback signal is taken from half way up a fringe. This allows a positive or negative voltage to be supplied to the actuators for feedback and the response to be approximately linear to movement of the mass along its arm axis. This feedback system allows the interferometer to be 'locked' on the point half way up a fringe.

A method used here for increasing the accuracy of the mechanical loss measurement is the placement of a normalised reference signal in the interferometer through the loudspeaker mounted behind one of the mirrors [127]. This can be used as a correction signal to remove effects of any random vibrations or fluctuations in laser power from the sample signal. A schematic diagram of the complete set-up is shown in figure 4.3.

4.2.1 Procedure

The amplitude decays are recorded and an exponential fit to each decay (or 'ringdown') is generated using a LabVIEW data acquisition program written by A. Cumming [127]. An example of a ringdown and of the reference correction signal is shown in figure 4.4 with amplitude expressed in arbitrary units shown to decay as readings are taken. 200 readings of amplitude are recorded every second. The program calculates the mechanical loss using the method explained in section 4.1.1 and outputs the value obtained.

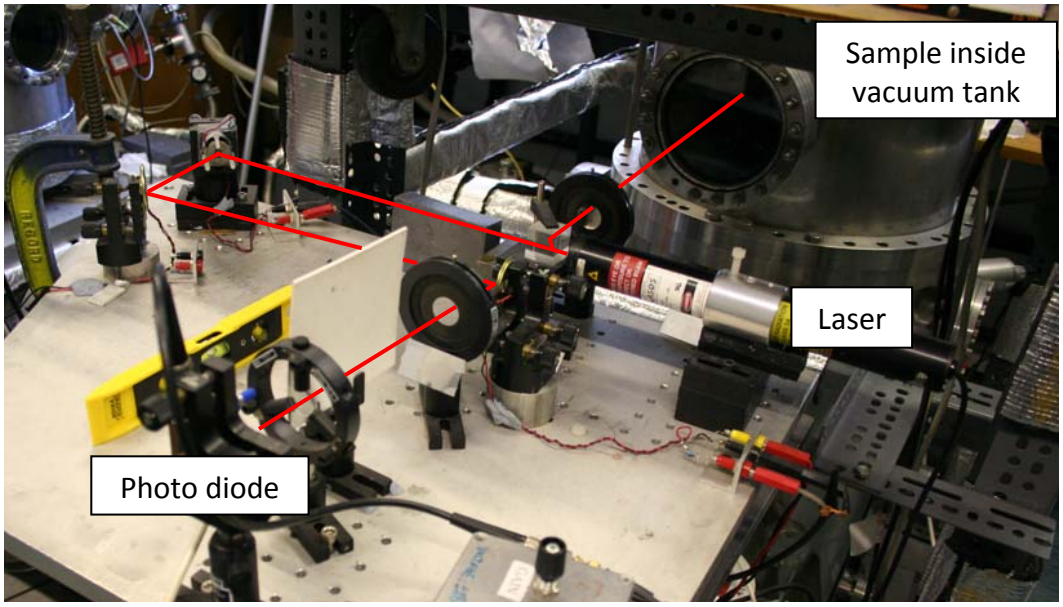

Figure 4.2: A table top interferometer used to sense the movement of the front surface of excited masses in order to measure mechanical loss.

External noise sources, such as fluctuations in the laser power, are shown in the correction signal and the computer program subtracts this from the measured ringdown in order to decrease the noise level.

4.2.2 Finite Element Analysis

Before measuring the mechanical loss, finite element analysis of each mass is carried out using ANSYS [129] modelling software to determine the internal mode shapes and frequencies of a sample. The shape of the resonant mode is important as the distribution of movement throughout the mass determines if the particular mode can be sensed using the interferometric set-up. In order for the movement induced by a resonant mode to be measurable there must be movement of the front face of the sample along the direction of the sensing beam. The shape of the resonant mode also indicates the probability of the measured dissipation being affected by residual frictional losses at the suspension points. A low level of motion around the centre of the barrel, minimises the loss introduced through frictional contact with the suspension material.

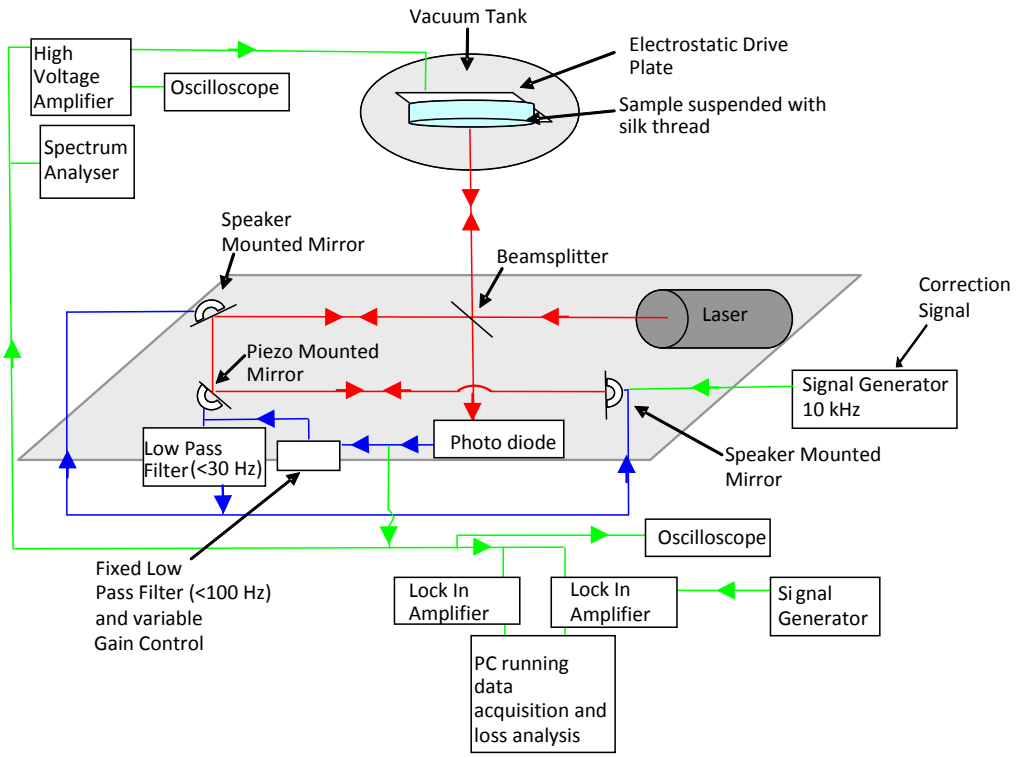

Figure 4.3: Schematic diagram of the experimental set-up for measuring the mechanical loss of bulk materials. Red lines indicate the path of the laser beam, blue lines show the locking system and the green lines show the detection and correction system.

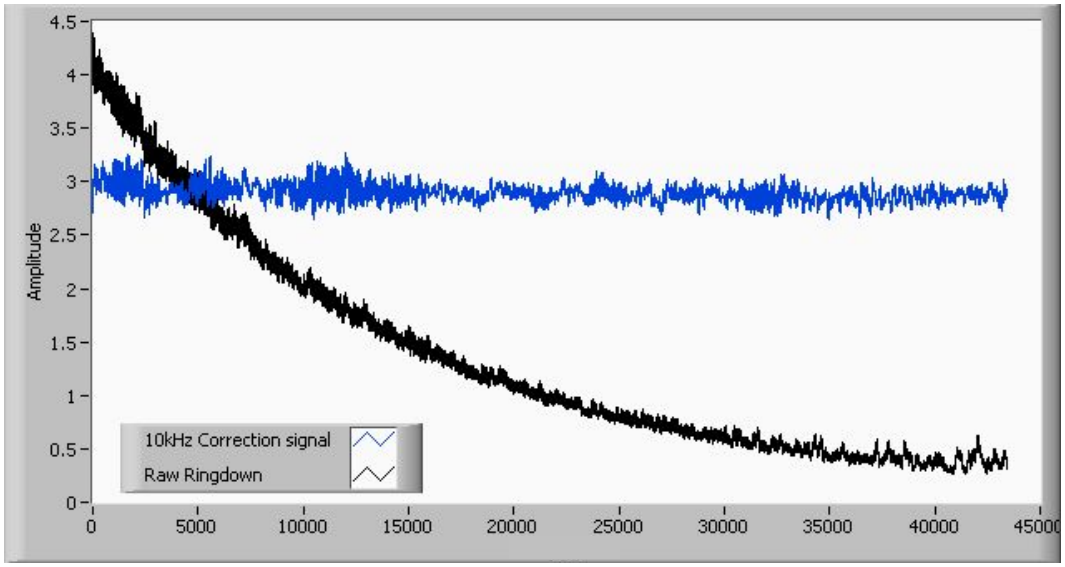

Figure 4.4: Ringdown of a silica sample shown in black. The 10 kHz correction signal is shown in blue.

Two typical mode shapes for a fused silica sample are shown in figure 4.5. The relative levels of motion of the sample surfaces are indicated using colour. Red denotes the portions of the surface with the largest displacement and blue denotes portions with the smallest displacement.

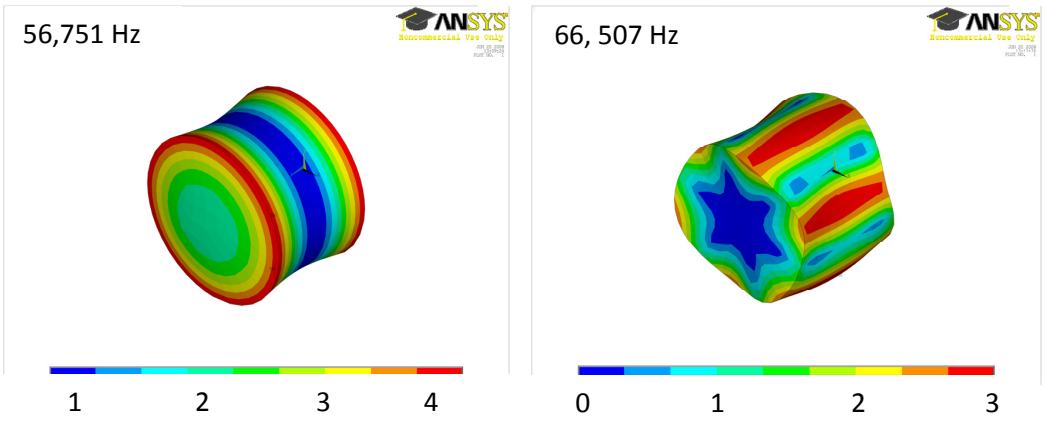

Figure 4.5: Two mode shapes for a Suprasil 3001 cylinder, 65 mm in diameter and 50 mm in length. The amplitude of motion is relative and indicated using colour where blue indicates the smallest amplitude of motion and red indicates the largest amplitude of motion.

The mode shape on the left of figure 4.5 has motion of the front face and no motion around the centre of the barrel. This makes it a good candidate for minimising effects related to the suspension. In contrast, the mode shape on the right has less motion across a large portion of the front surface, making the amplitude of motion lower and thus harder to sense. It also has a higher level of motion around the centre of the barrel and hence, is more likely to provide a loss value which is limited by additional loss from the suspension.

4.3 A Model for the Mechanical Loss of Fused Silica

There are two main vendors which are able to supply fused silica in the size required for advanced gravitational wave detectors (40 kg) with the appropriate optical and mechanical properties. Corning [117] supplied the end mirrors and the recycling mirror for Advanced LIGO, Heraeus [118] supplied the optics for the GEO600 and Virgo detectors and it also supplies the beamsplitter and input mirrors for Advanced LIGO. There are many different types of fused silica produced by each vendor in which the optical properties and homogeneity can vary greatly. Numata et al [130] measured the mechanical loss of different grades of silica from each vendor and their results suggest that fused silica produced by Heraeus has a lower mechanical loss than fused silica produced by Corning. Measurements suggest that Suprasil 312 has the lowest mechanical loss of all grades of Heraeus fused silica [130]. It is not fully understood which aspects of the manufacturing process optimise the mechanical performance - a better understanding may identify possible methods by which the thermal noise can be reduced further.

As discussed in section 4.1, the optical and mechanical properties of the fused silica masses are of great importance for gravitational wave detectors. Due to this, various investigations of these properties have been carried out to evaluate the use of different silicas for this application [123, 131–138]. A semi-

empirical model to describe the mechanical loss of different grades of fused silica was formulated by Penn et al. [139]. The model contains the mechanical loss arising from the surface of the sample, ϕ_{surf}, the bulk of the sample, ϕ_{bulk}, and the thermoelastic loss, ϕ_{th}, and then combines these to achieve the overall loss value. The loss given by this model is expressed as,

$$\begin{aligned}\phi(f, \frac{S}{V}) &= \phi_{\text{surf}} + \phi_{\text{bulk}} + \phi_{\text{th}} \\ &= C_1 \frac{S}{V} + C_2 f^{C_3} + C_4 \phi_{\text{th}}(f),\end{aligned} \tag{4.2}$$

where f is the frequency in Hz, S is the surface area of the sample in mm^2 and V is the volume in mm^3. C_1, C_2, C_3 and C_4 are constants which are empirically determined and are specific to the type of fused silica being studied.

The sources of dissipation associated with the surface of silica are not completely understood, however surface treatments such as the polishing technique used in sample production, which could be a mechanical, chemical or flame polish may affect the level of surface dissipation [140]. For example, a mechanical polishing technique could leave micro-cracks [140] on the surface and contaminants could be incorporated into the surface during flame polishing of a surface [125].

The bulk dissipation in high quality pure fused silica is believed to be associated with the relaxation of strained Si - O - Si bonds. An asymmetric double well potential exists where the energy of the bond has minima at two bond angles. If a strain is applied the distribution of the bond angle alters and this causes mechanical dissipation [141]. There are various models for the specific loss mechanism. The first is that oxygen atoms linking the ring like formations in the silica can flip between two possible bond angles [142]. A second is that some Si - O - Si can be naturally elongated. There are then two possible potential minima in which the oxygen would want to sit. The vibration of the oxygen atom between these potential wells would provide the loss mechanism [143]. The third model is that two neighbouring SiO_4 tetrahedrons can rotate between two possible stable states [144].

The magnitude of the thermoelastic dissipation is dependent on the thermo-mechanical properties of the material. For the majority of the measurements presented in this thesis, samples are used that have a geometry for which thermoelastic loss is negligible in comparison to the surface and bulk loss and C_4 is therefore given a value of zero [145].

For Suprasil 312 the empirical model of equation 4.2 yielded the coefficients [139]:

$C_1 = (6.5 \pm 0.2) \times 10^{-9}\,\mathrm{mm}$

$C_2 = (7.54 \pm 0.02) \times 10^{-12}\,\mathrm{Hz}^{-0.77}$

$C_3 = (0.77 \pm 0.02)$

$C_4 =$ (negligible in the samples measured)

By using these parameters it is possible to obtain a value for the expected mechanical loss of a sample of Suprasil 312 of particular geometry at different frequencies and therefore calculate the predicted thermal noise [139].

4.4 Suprasil 3001 Results

Until recently the materials Suprasil 311SV and 312SV brands of fused silica were selected for the optics in Advanced LIGO. Suprasil 311SV was selected for the beam splitter and Suprasil 312SV was selected for the input test masses [146]. They were chosen as they have a very low mechanical loss [123], the highest level of optical homogeneity and lowest optical absorption of all types of fused silica [116]. 311SV is made with the same manufacturing process as Suprasil 311 except for a proprietary extra drying stage which decreases its OH content giving lower optical absorption [147, 148]. Suprasil 312SV has the same properties as Suprasil 311SV but its homogeneity is only specified in one direction while 311 is specified in all directions. Recently it was decided to change to a different type of fused silica, Suprasil 3001, for the input and end optics as it has better optical properties; it has an even lower OH content so therefore has a lower optical absorption [149].

However, the mechanical loss of this type of fused silica was not characterised and previously the loss was assumed to be that calculated using the empirical model 4.2 [150] with previous measurements of the drier 311SV exhibiting an increase in bulk loss of a factor of ~ 2 [145]. Here the mechanical loss of two samples of Suprasil 3001 was measured, both samples were 65 mm in diameter, one was 50 mm in length and the other was 70 mm in length. The results are shown in figure 4.6. The mechanical loss was measured to evaluate the effect that this material would have on the thermal noise level in the suspension system of interferometric gravitational wave detectors. The samples were suspended in turn. Approximately 10 suspensions were used for each mass and the ringdown for each resonant mode was measured 5 times. The loss measured for each of the 5 ringdowns was averaged. The lowest average loss measured for each resonant mode was taken as the loss of the sample as higher measured losses are assumed to be limited by suspension losses. The model of equation 4.2 for fused silica was used to evaluate the results. The coefficient for surface loss, which Penn obtained for Suprasil 312, was used as the surface loss coefficient for Suprasil 3001. Penn obtained this value by measuring samples which had been mechanically polished and samples which had been flame polished. Therefore this value is for a mixture of polishing techniques and not specific to one type. The C_3 coefficient was also kept at the value given by Penn as research has shown this value does not alter significantly [139, 141]. This allowed for the change in the manufacturing technique from Suprasil 312 to Suprasil 3001 to be quantified as a purely bulk effect.

The mechanical loss values measured for Suprasil 3001 are shown in figure 4.6. The pattern of the majority of the loss values corresponds broadly to the pattern of loss which we would expect from inspection of the resonant mode shapes found using finite element analysis. For example, the highest loss was measured for the resonant mode at 46.466 kHz. This mode had significant motion around the centre of the barrel which is likely to create extra dissipation through friction. Other modes in which high losses were measured also had

motion around the barrel while the lowest measured losses were measured for mode shapes with minimal motion of the barrel.

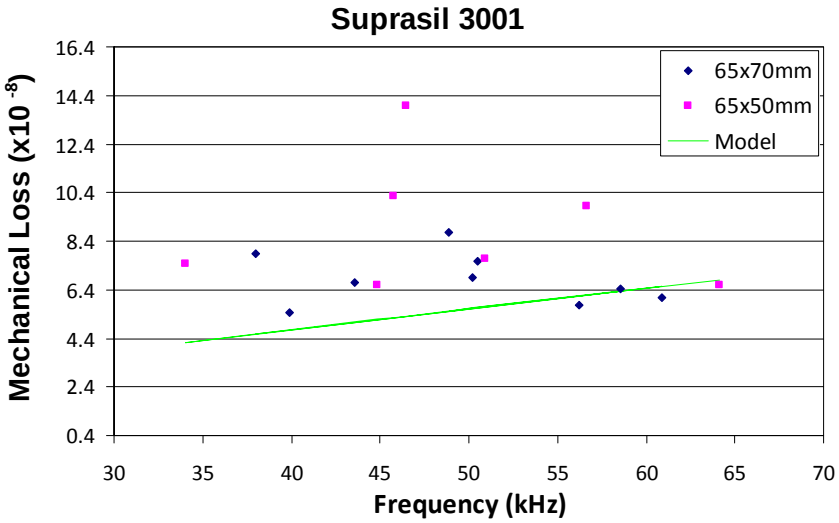

Figure 4.6: Mechanical loss measurements of two cylinders of Suprasil 3001, 65×50 mm and 65×70 mm, and fitted to the semi-empirical model for fused silica.

The frequency dependence of mechanical loss is well understood and so the empirical model was fitted to the lowest grouping of loss values which would lie on this curve. The empirical model was fitted to the loss values obtained for four resonant modes. These modes were the 56, 58 and 60 kHz modes for the 70 mm sample and the 64 kHz mode for the 50 mm sample. The shape of the resonant modes used for the fit are shown in figure 4.7.

This model is also presented in figure 4.6. Fitting the empirical model to these values gives an approximation for the loss of Suprasil 3001. The model was fitted to each of the selected modes in turn and the bulk coefficient required for the fit was recorded. The bulk coefficients were then averaged to obtain the best fit of the model to all of the selected modes.

Fitting the mechanical loss of Suprasil 3001 using Penn's model gave a coefficient of bulk loss, C_2, which was a factor of 1.70 ± 0.03 higher than the bulk loss coefficient of Suprasil 312. This increase in loss causes the thermal

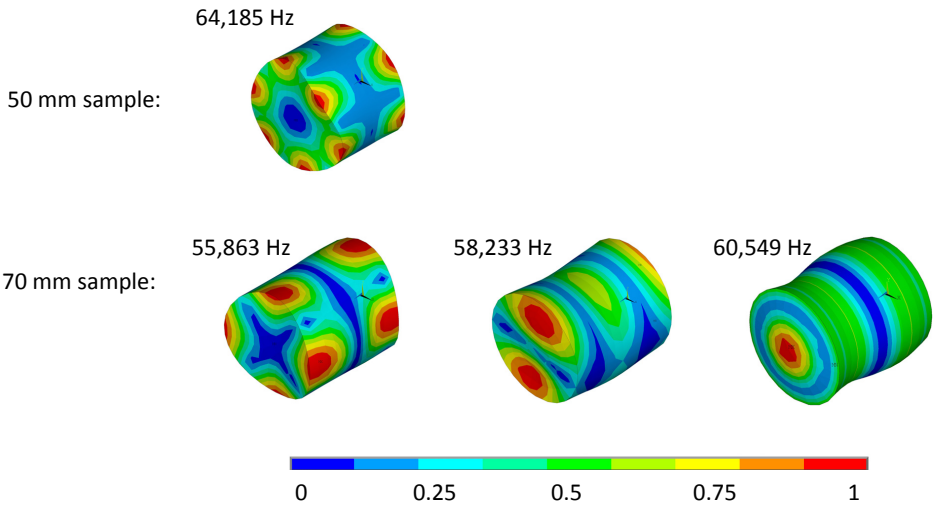

Figure 4.7: Resonant mode shapes of the frequencies for which the empirical model was fitted. The amplitude of motion is relative and colour coded. Red signifies maximum motion and blue signifies minimum motion.

noise contribution of the substrate to increase from 1.3×10^{-21} m per $\sqrt{\text{Hz}}$ to 1.6×10^{-21} m per $\sqrt{\text{Hz}}$ at 100 Hz. The thermal noise arising from the substrate is still considerably less than the thermal noise arising from the coating which is 8.8×10^{-21} m per $\sqrt{\text{Hz}}$ at 100 Hz and so should not affect the sensitivity of the advanced gravitational wave detectors. The thermal noise contribution from a Suprasil 312 test mass, a Suprasil 3001 test mass and for a coating over a range of frequencies is presented in figure 4.8.

Ongoing research at reducing coating thermal noise and methods of removing the need for coatings [97] is being carried out. As this research progresses it becomes increasingly important to reduce substrate thermal noise. Figure 4.9 shows the expected contribution to substrate loss which is provided by the surface and the bulk of the material calculated using the empirical model 4.2.

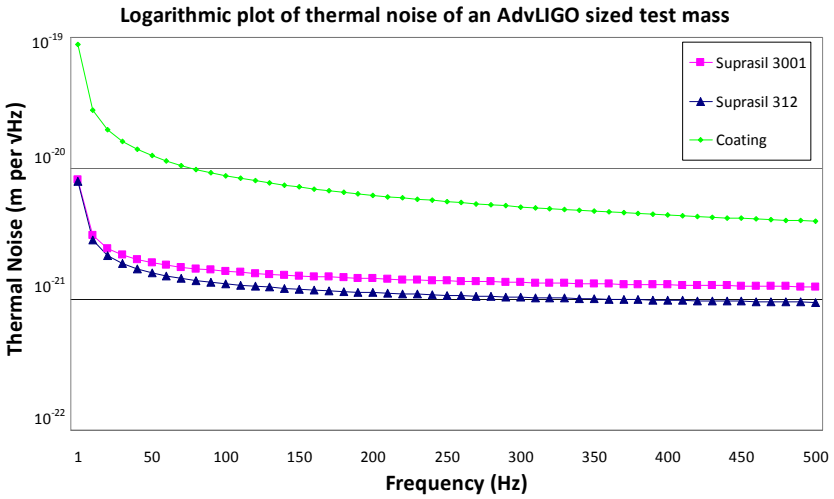

Figure 4.8: Comparison of the expected thermal noise as a function of frequency for an Advanced LIGO sized mass made from Suprasil 312 and Suprasil 3001 and the expected thermal noise of a coating.

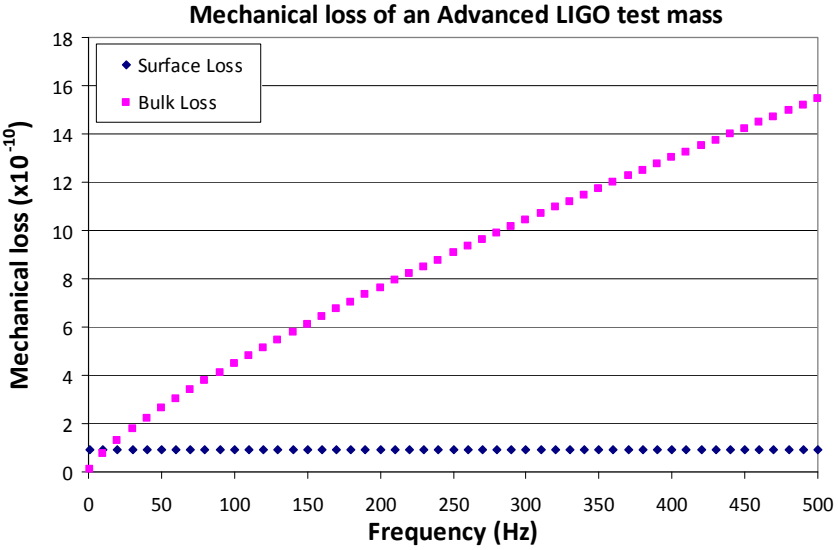

Figure 4.9: Loss contribution from surface and bulk of an Advanced LIGO size test mass of Suprasil 3001. It should be noted that the surface loss in the empirical model is weighted heavily towards flame pulled and flame polished surfaces and this may be higher in the case of a mechanically polished optic.

It can be observed from figure 4.9 that surface loss is dominant at low

frequencies. Thus, in order for the gravitational wave detectors to become more sensitive at low frequencies surface loss has to be reduced. Experiments were carried out here in order to investigate the possibility of removing the lossy surface layer through chemical etching.

4.5 Chemical Etching

As part of collaborative research between the Institute for Gravitational Research at the University of Glasgow and scientists at Moscow State University, the effects of chemical etching on the mechanical loss of fused silica were investigated. Scientists at Moscow State had previously seen that it is possible to reduce the mechanical loss of a silica sample which had been mechanically polished by removing the lossy surface layer [140]. The depth of the surface layer is dependent on the polish technique used on the sample. Evidence suggests that the damaged layer can be twice as deep as the diameter of the final abrasive used in the polishing process [151]. Final-stage polishing abrasives generally have a particle size of the order of a μm. Thus, methods of removing a surface layer of order 1μm is of interest.

The use of chemical etching to remove the surface layer of flame pulled samples has not been well investigated, with no evidence of improvements. It is known that the mechanical loss of flame polished samples is significantly less than that of mechanically polished samples [139]. This is likely to be due to the silica being melted and fusing back together, filling any micro-cracks that could have been present. Thus, we would expect the thickness of the surface layer to be smaller for flame polished sample than for mechanically polished samples. The effect of chemical etching on the loss of a flame-pulled fibre is studied here to investigate any possible reduction in the loss associated with surface effects [152] and to quantify any potential improvements which could be made to the flame polished fibres which are used to suspend the test masses in gravitational wave detectors. Thin fibres have an ideal geometry for carrying

out surface studies due to having a large surface-to-volume ratio, which help maximise surface effects.

The steps of the chemical etching process which was developed at Moscow State University are as follows [140]:

1. Place the sample in etching reagent (ammonium bifluoride, $NH_4HF_2 <$ 10% and 1-2 milligrams per 500 cm ^{3} of surfactant, $C_8F_{17}COOH$) for one and a half minutes.

2. Submerge in pure distilled water for 1-2 minutes.

3. Submerge in cleaning reagent (sulphuric acid, H_2SO_4 30% and 1-2 milligrams per 500 cm^3 of surfactant, $C_8F_{17}COOH$) for one and a half minutes to remove the products of the reaction.

4. Submerge in pure distilled water for 1-2 minutes.

5. Repeat steps 1 to 4 three times.

6. Boil the sample in pure distilled water for 10 minutes.

7. Place in an oven at 200 °C for 20 minutes.

The surfactant lowers the surface tension of the solution and the hydrofluoric acid etches the surface. The product of this reaction are 'silica salts' and these can remain on the sample surface. In the experience of scientists at Moscow State University and as discussed in section 4.7, placing a sample of fused silica in an oven, removes moisture from the surface and thus the mechanical loss of the sample decreases. If the steps of this etching process are followed exactly, the surface layer, with a depth of approximately 1 to 2 μm should be removed.

4.6 Suprasil 2 Fibre Before and After Etching

In order to investigate the possibility of reducing the surface loss of a silica sample with a large surface to volume ratio, a fibre was measured and then

chemically etched and remeasured. By choosing a sample with a large surface to volume ratio the effect of the etching process would be more easily observed and quantified. The mechanical loss of a fused silica fibre of length $\sim$ 1 cm, pulled from Suprasil 2 stock material, was measured before and after chemical etching. The stock was heated with a hydrogen-oxygen flame and pulled into a fibre. The dimensions of the fibre were recorded with an optical profiler which employs LED illumination and camera imaging as detailed in [153]. The dimensions are shown in figure 4.10. Suprasil 2 was used as it is nominally identical to Suprasil 312 but has a lower optical homogeneity. The homogeneity of the stock material is altered during the fibre fabrication process and so is not an important parameter.

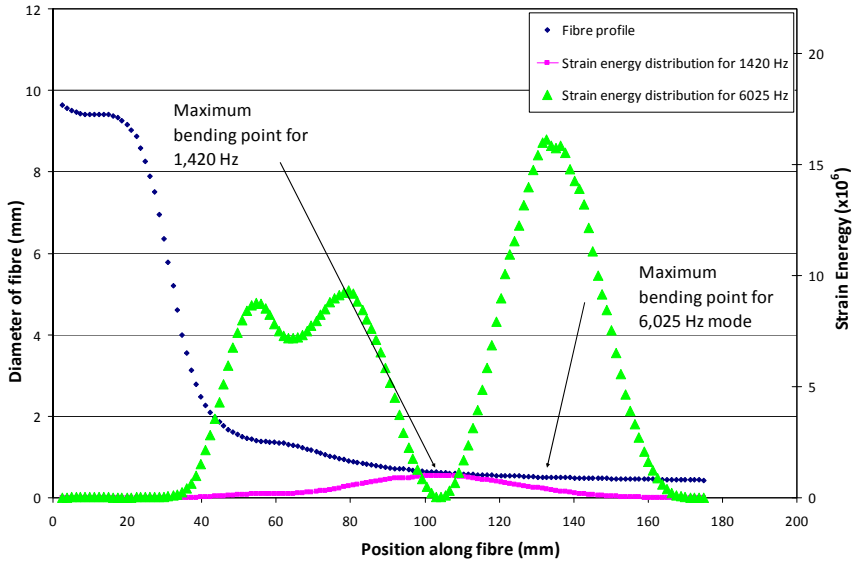

Figure 4.10: Profile of a flame pulled fibre from Suprasil 2 stock welded to a 1 cm silica post. Distributions of energy for two measured resonant modes.

The neck of the fibre was welded onto a machined silica post which was bonded onto a large silica cylinder of $\sim$ 0.5 kg. The large cylinder was suspended. Figure 4.11 shows a diagram of the suspension and a photograph of the fibre, where the stock is welded to the cylindrical mass.

A laser beam is reflected off the surface of the fibre and monitored using a

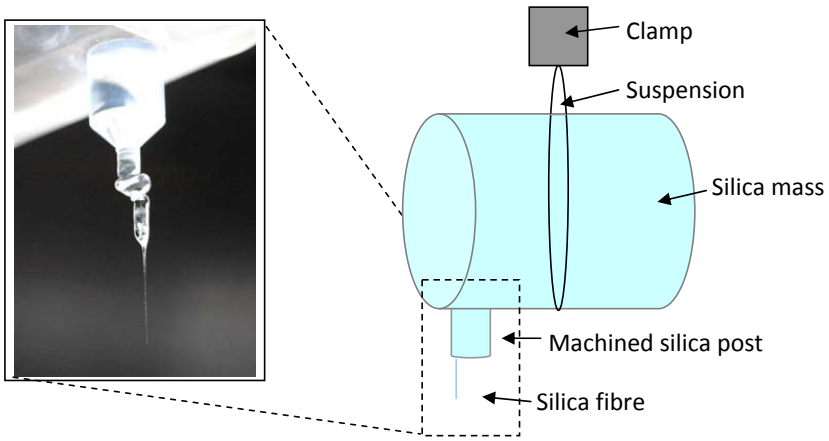

Figure 4.11: Diagram of the suspension set-up with a photograph of the fibre of material Suprasil 2 after it was chemically etched.

split-photodiode. A diagram of the readout system is shown in figure 4.12.

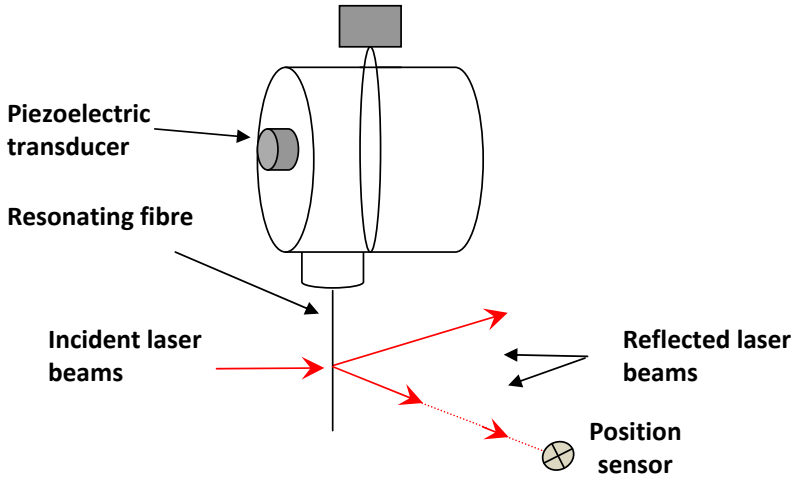

Figure 4.12: Optical readout system for monitoring the resonant motion of the free resonant bending modes of a fibre.

The fibre is excited at its resonant frequencies by a piezoelectric transducer which is attached to the cylindrical mass to which the fibre is attached. The decay of the motion after excitation is recorded by the split-photodiode and thus the mechanical loss can be determined by the method described in section 4.1.1. The mechanical loss of two resonant modes of the fibre were measured

at frequencies of 1,420 Hz and 6,025 Hz. The fibre was modelled using the ANSYS finite modelling package and the shape of the measured resonant modes obtained are shown in figure 4.13.

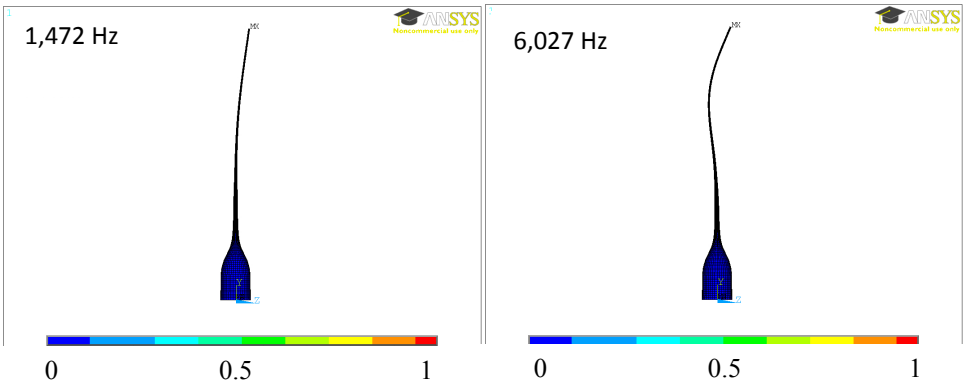

Figure 4.13: Mode shapes of the two measured frequencies, 1,472 Hz and 6,027 Hz of the fibre. Colours denote the relative amplitude of the motion where blue indicates a minimal amount of motion and red indicates a maximum amount of motion of the resonating sample.

The measured values of mechanical loss before and after the chemical etch are shown in figure 4.14.

It was found that the loss of the fibre decreased after the fibre was etched using the same technique that was described in section 4.5. The sample was then kept under vacuum for 2 months and remeasured without being exposed to air. After this period the loss had decreased further. The further decrease in loss after being held in vacuum for 2 months was likely to be caused by water being removed from the fibre surface [140]. A layer of water molecules can be adsorbed onto the surface of silica when it is exposed to air. These molecules can attach through weak hydrogen bonds which can break and reform causing excess loss of the surface. Thus, the removal of this hydrated layer reduces the mechanical loss of the sample [140].

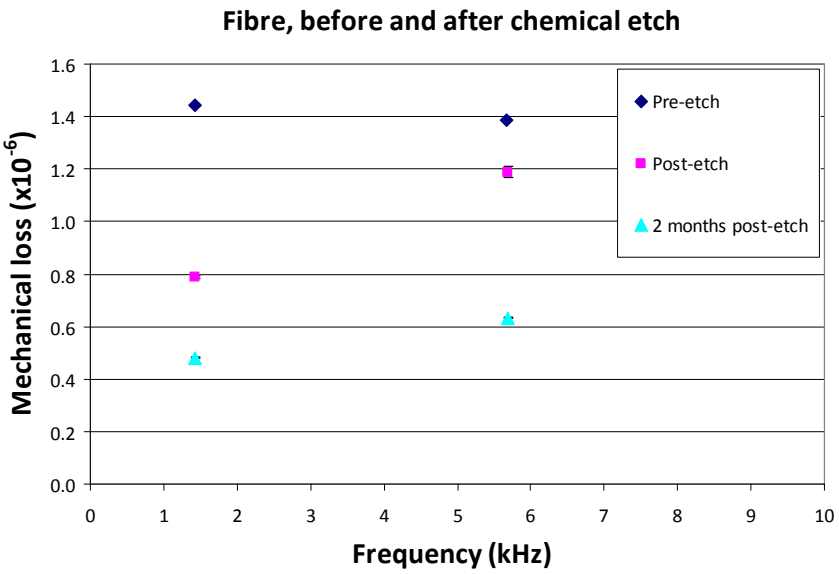

Figure 4.14: Mechanical loss of a $\sim$ 1 cm long fibre before etch, a few hours after a chemical etch and 2 months after a chemical etch held in vacuum.

4.6.1 Analysis of Loss Measurements

For this geometry of sample, thermoelastic loss is at a level which is significant compared to other losses in the system and bulk loss is negligible. Thus, the measured loss values consists of a combination of the surface loss and thermoelastic loss. The thermoelastic loss of the fibre was calculated using the equations [79, 98],

$$\phi_{\text{thermoelastic}} = \triangle \frac{\omega\tau}{1+\omega^2\tau^2}, \tag{4.3}$$

with

$$\triangle = \frac{Y\alpha^2 T}{\rho C} \tag{4.4}$$

and

$$\tau = \frac{1}{4.32\pi}\frac{\rho C d}{\kappa} \tag{4.5}$$

ω is the angular resonant frequency, τ is the characteristic time for the heat to cross the fibre, Y is the Young's modulus of the material, α is the linear coefficient of thermal expansion of the material, T is the temperature, ρ is the density, C is the specific heat capacity, κ is the thermal conductivity and

Parameter	
Y	7.2×10^{10} Nm^{-2}
α	$(3.7 \pm 0.7) \times 10^{-7}$ K^{-1}
ρ	2202 kg/m^3
C	746 Jkg^{-1}K^{-1}
κ	1.38 Wm^{-1}K^{-1}

Table 4.1: Material properties of silica. [154, 155]

d is the diameter of the fibre. The values of the parameters used for fused silica are shown in table 4.1 [154, 155]. A range of possible values of the linear coefficient of thermal expansion of silica is given. Measurements suggest that this parameter can vary due to the thermal history of the sample [155]. The range shown is that of the range of measured values of the thermal expansion coefficient of silica which had undergone similar heat treatment to the fibre studied here, such as being pulled in a hydrogen-oxygen flame [155]. Some other parameters may also vary for the surface and bulk material such as the Young's modulus [152]. It is kept the same here for simplicity.

As the diameter of the fibre varied through the sample the value of the thermoelastic loss and surface loss also varied depending on which area of the fibre for which it was calculated. The loss values were calculated for 138 segments of the fibre. The strain energy within each element of the model was obtained using ANSYS. Thus the loss values calculated for each diameter of the fibre could be scaled accordingly and integrated over the fibre length to give the total loss. This was carried out for both of the measured resonant modes and the results are shown in figure 4.15.

The total loss of the sample is the sum of the surface loss and the thermoelastic loss. The total loss values of the fibre are shown in table 4.3. The errors given for these values arise from the range of possible values for the linear coefficient of thermal expansion which is discussed above. If we assume that a surface layer of a certain thickness exists and it has a higher loss than the

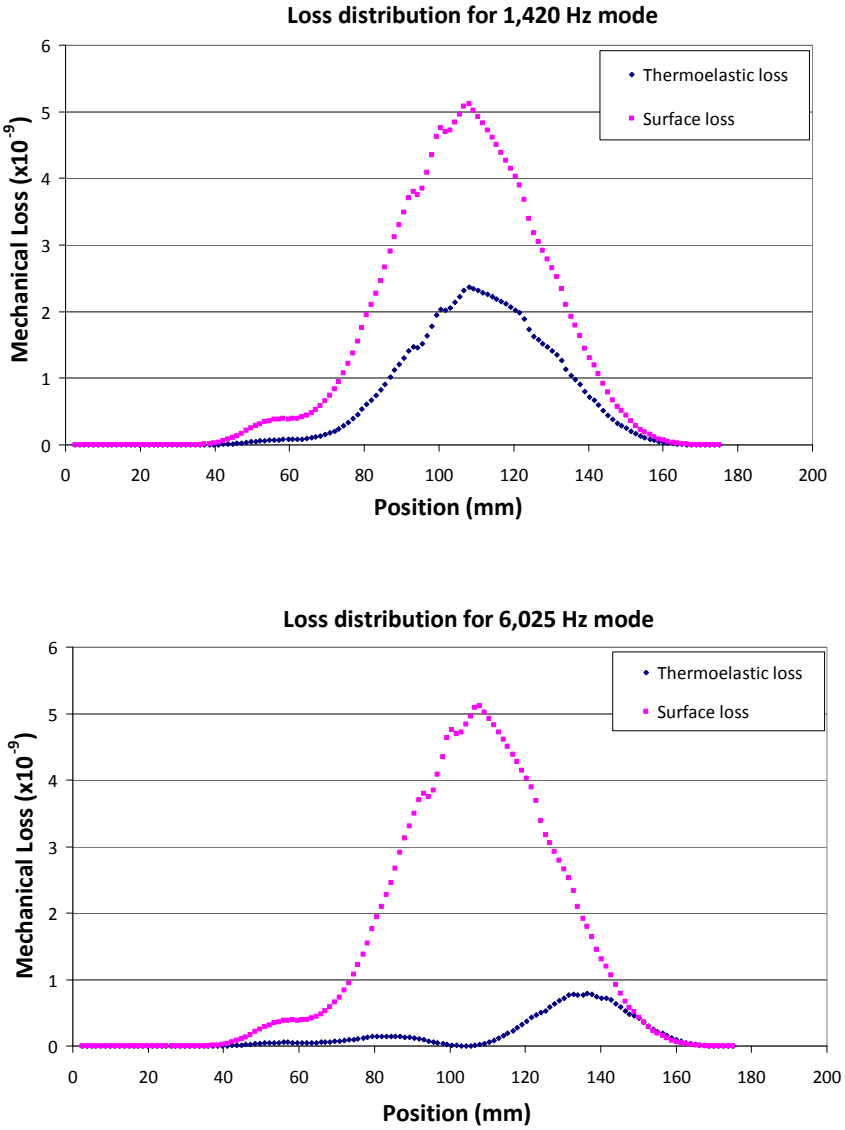

Figure 4.15: Thermoelastic and surface loss calculated for 138 positions on the fibre.

bulk of the material then we can relate the measured surface loss, $\phi_{\text{surf measured}}$ with the actual surface loss, ϕ_{surface}:

$$\phi_{\text{surf measured}} = \frac{E_{\text{surface}}}{E_{\text{bulk}}}\phi_{\text{surface}} \tag{4.6}$$

where E_{surface} is the energy stored in the surface layer and E_{bulk} is the energy stored in the bulk of the sample. The energy ratio is given by [156],

$$\phi_{\text{surface}} = \frac{d}{8h}\phi_{\text{surf measured}} \tag{4.7}$$

where d is the diameter of the fibre and h is the thickness of the surface layer, taken to be $\sim 1\mu$m. Using this equation and the strain energy within each element of the model the surface loss values could be calculated for each diameter of the fibre and scaled accordingly then integrated over the fibre length to give the total loss as above. The surface loss values are given in table 4.4.

The lowest mechanical loss values ever measured for a fibre surface have been measured by Gretarsson to be $\sim 10^{-5}$ [138] and Heptonstall to be $\sim 4 \times 10^{-6}$ [157]. Heptonstall obtained the lowest ever measured value published in the literature of a thin silica surface, 3×10^{-6} which was measured for a silica ribbon [152]. Here, we find the value of surface loss to be $(6.2 \pm 1.0) \times10^{-6}$. Thus, this process of chemical etching can be used as a method to reduce the mechanical loss of a fibre surface to a value lower than that previously measured by Gretarsson and to bring the measured loss of a fibre close to the lowest ever measured values of surface loss. Thus, this method can not yet be used to reduce the thermal noise of a fibre to a level which is lower than that of the best possible fibres but can be used to improve non-optimised fibres to a level a factor of ~ 2 away from the level of that of state of the art fibres.

	1,472 Hz	6,027 Hz
ϕ_{TE} modelled	$(1.4 \pm 0.5) \times10^{-7}$	$(3.6 \pm 1.3) \times10^{-8}$
ϕ_{surf} modelled	$(2.0 \pm 0.2) \times10^{-7}$	$(2.0 \pm 0.2)\times10^{-7}$

Table 4.2: Modelled mechanical loss values of the fibre.

	1,472 Hz	6,027 Hz
$\phi_{\text{total}} = \phi_{\text{TE}} + \phi_{\text{surf}}$ modelled	$(3.4 \pm 0.5) \times10^{-7}$	$(2.3 \pm 0.1) \times10^{-7}$
ϕ measured	$(4.87 \pm 0.03) \times10^{-7}$	$(6.33 \pm 0.01) \times10^{-7}$

Table 4.3: Modelled and measured mechanical loss values of the fibre after it was chemically etched and kept under vacuum for 2 months for comparison.

1,472 Hz	6,027 Hz
$(6.2 \pm 1.0) \times 10^{-6}$	$(1.2 \pm 0.1) \times 10^{-5}$

Table 4.4: Actual surface loss assuming a surface layer of thickness 1 μm after the fibre was chemically etched and kept under vacuum for 2 months.

4.7 Suprasil 311 Before and After Etching

The current dominant noise source of the detector suspension systems is that of coating thermal noise. Significant efforts are underway to identify and reduce the sources of the loss associated with standard dielectric multilayer coatings and efforts are aimed at developing novel technologies which require minimal or no deposited coating materials, for example, monolithic structured surfaces [97]. If coating thermal noise is suitably reduced then the thermal noise of the mechanically polished substrates could become an increasingly significant noise source. As the chemical etching method has been shown to reduce the loss of flame pulled fibres it is of interest to quantify any effect it may have on mechanically polished surfaces. The loss associated with mechanically polished surfaces is known to be greater than the loss associated with a flame pulled, flame polished or CO_2 pulled fibre [139]. Measurements have been made of the loss of a mechanically polished surface and given to be $\sim 3 \times 10^{-5}$ [158]. As the surface loss after chemical etching which is presented here is lower than this value for mechanically polished surface loss then it is interesting to investigate the possibility of using the chemical etching process to reduce the loss of the silica optics in gravitational wave detectors. Previously, only methods such as flame polishing have been able to significantly reduce the loss of the surface and this method could induce undesirable thermal stresses in the material [156]. Thus, a method which does not use heat is of much interest.

The effect which the chemical etching process has on samples which are more similar to the geometry of the test masses and have been manufactured and polished by a similar method was investigated. Three silica rods of material

Suprasil 311 with diameter 20 mm and lengths of 109 mm, 109 mm and 102 mm were measured in Glasgow and again in Moscow. This material was used as it was chosen to be used in the gravitational wave detector suspensions. Using the empirical model 4.2 to describe the total loss of the samples, it is found that the expected surface loss contributes between $\sim 4\%$ and 18% of the expected total loss across the resonant frequencies measured for this geometry of sample. Thus, we do not expect to see a large difference in loss due to etching off the surface layer.

In the experimental set-up in Glasgow several resonant modes of each sample were measured. The set-up and procedure in Moscow varied slightly from that used in the Glasgow experiments. Figure 4.16 shows a photograph of the Moscow set-up and a schematic of the sample suspension.

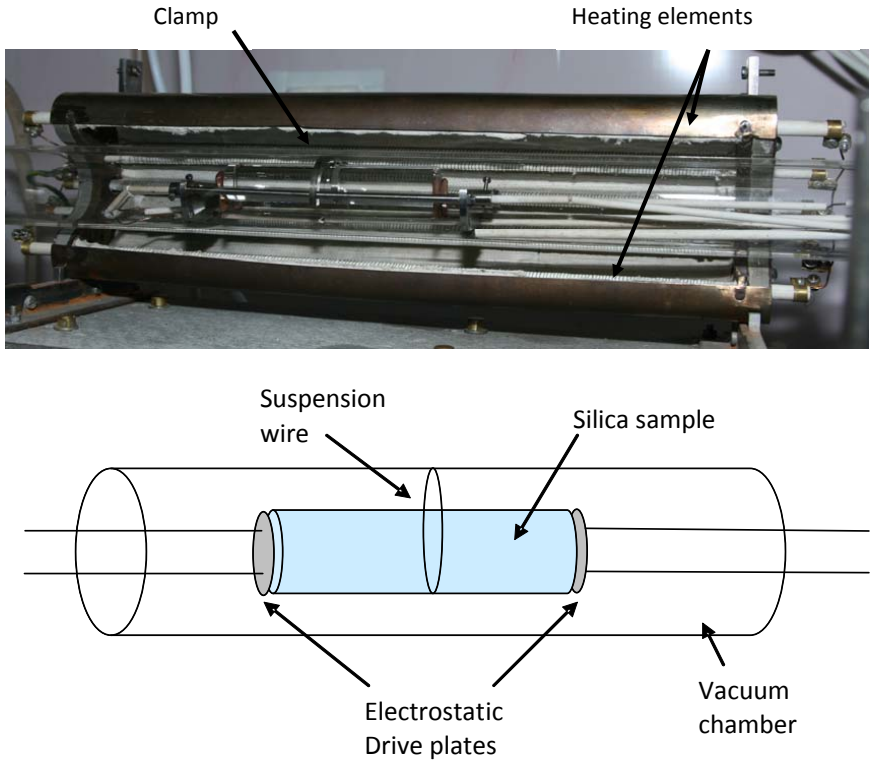

Figure 4.16: Top: experimental set-up for measuring the mechanical loss for bulk materials in Moscow State University, Bottom: a schematic of the suspended mass.

In Moscow, samples are boiled in a solution which is 15% hydrogen peroxide, (H_2O_2), and 85% distilled water for 10 minutes and then dried in an oven at 180°C for 20 minutes to clean the surface as the scientists have observed that this procedure removes contaminants from the surface. This is used as a cleaning process and not as a replacement to the etching process described in section 4.5. The sample is then suspended using 50 μm tungsten wire as a suspension material. Using a rough material to suspend the masses can add additional friction into the system, therefore the surface quality and cleanliness of the suspension wire is important. The wire used for this experiment was unpolished and cleaned using acetone. Once the sample is suspended under a vacuum of 2×10^{-4} mbar, heating elements and insulation are placed around the vacuum chamber to heat the sample to 200°C for 1 hour. This has been shown to remove the hydrated layer from the surface of the sample. This hydrated layer has been seen to cause an increase in the mechanical loss of silica substrates by a factor of ~ 2 [140]. A resonant circuit is used to excite the sample and to sense the motion as it decays. For this set-up only the longitudinal modes of the samples were measured. The results of the initial mechanical loss measurements for all three samples in Glasgow are shown in figure 4.17.

A comparison of the mechanical loss values measured for samples 1 and 2 in both the Glasgow and Moscow set-ups is also shown in figure 4.17. The first two resonant modes, located at ~ 7 kHz and the first bending modes. They deform the sample so that it bends directly in the middle of the sample where the suspension material is located. Thus, a high mechanical loss is expected to be measured here as is shown in figure 4.17. From this figure we can see that both set-ups give approximately the same value for the lowest measurable loss allowing us to be confident that no significant extra loss is being measured due to coupling in the set-up.

The chemical etching described in section 4.5 was then carried out on sample 1. The resulting mechanical loss values measured are presented in figure 4.18.

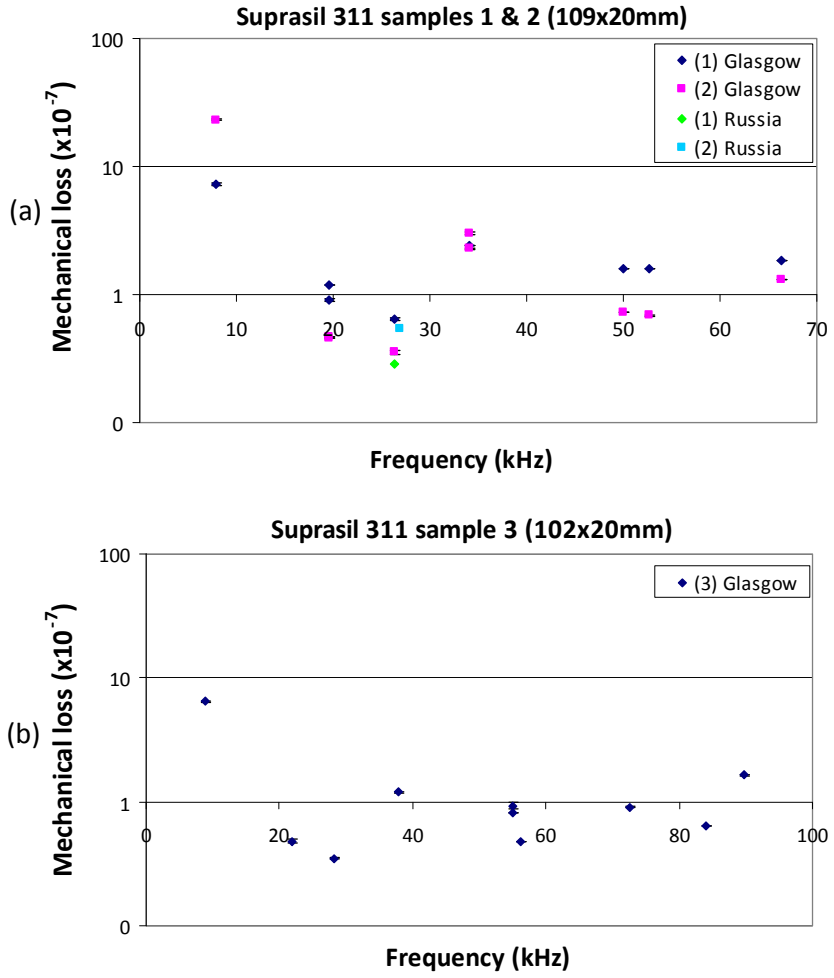

Figure 4.17: (a) Mechanical loss values measured in Glasgow and Moscow of two identical samples of Suprasil 311. (b) Mechanical loss values measured in Glasgow of sample 3, a slightly shorter rod of Suprasil 311.

The mechanical loss increased for the majority of the measured resonant modes. Possible reasons for this increase could include increased friction between the wire suspension and the barrel due to an increased surface roughness caused by the chemical etch or alternatively dissipation arising from micro-cracks on the surfaces. Roughness measurements for samples 1 and 2, taken using a VEECO optical interferometer, before and after the chemical etch are shown in table 4.5. It is seen that the surface roughness was increased, in particularly on the barrel, due to the chemical etching process.

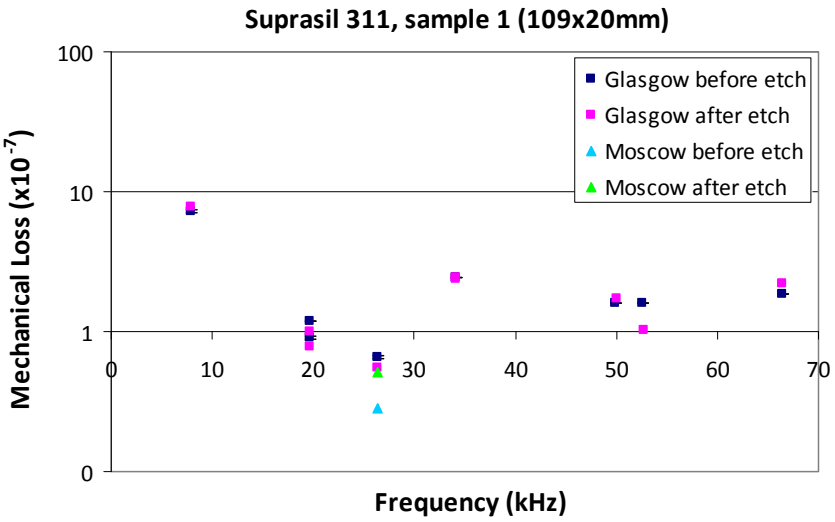

Figure 4.18: Mechanical loss of sample 1 before and after being chemically etched, measured in both Glasgow and Moscow.

		Before Etch	After Etch
Sample 1	Face A	4.73	4.88
	Face B	3.84	6.51
	Barrel	11.87	18.21
Sample 2	Face A	4.24	4.88
	Face B	4.22	5.35
	Barrel	16.32	35.30

Table 4.5: Summary of roughness (nm) of Suprasil 311, samples 1 and 2 before and after they had been chemically etched. These results were averaged over several areas of the samples. Sample 1 and 2 both have a diameter of 20 mm and a length of 109 mm.

However, in some areas of the surface images would not be obtained - see figure 4.19. The "blacked out" areas represent peaks or troughs which are too high or too low for the VEECO to measure. In calculating the roughness the VEECO does not take these areas into account thereby underestimating the actual roughness. Images taken of the sample after it was etched have more of these un-imaged areas than the images taken before etching suggesting that

the change in roughness could be larger than the values estimated here.

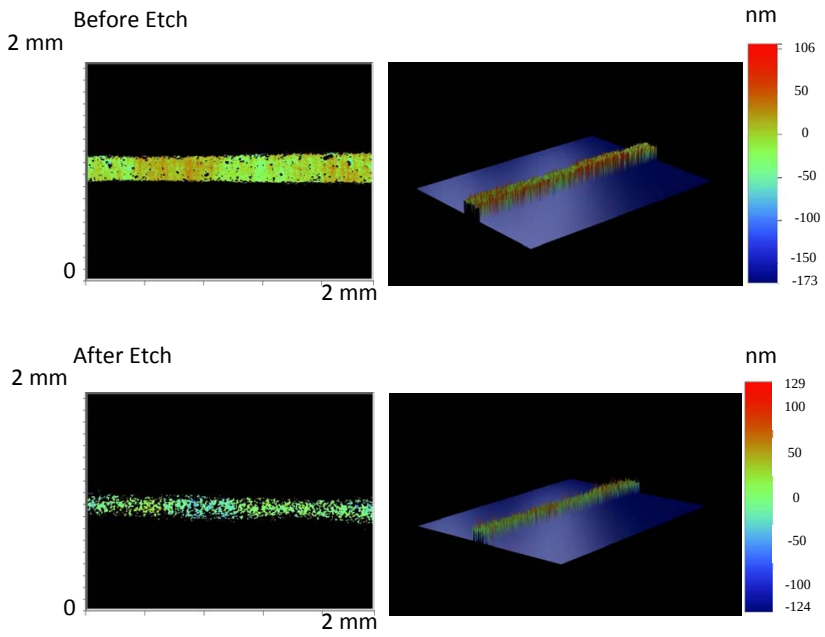

Figure 4.19: Roughness measurements using a VEECO interferometer of the barrel of the sample before (top) and after (bottom) it had been chemically etched. Black areas indicate peaks or troughs which are too high or low for the dynamic range of the VEECO.

Table 4.5 and figure 4.19 show that the chemical etch increases the roughness of the sample surface. To investigate whether the etching of sample 1 had caused increased suspension losses due to friction at the contact points between the wire suspension and the roughened surface of the mass, sample 2 was etched with the centre of the barrel covered with teflon to avoid etching the area where the suspension material is in contact with the sample. However, the chemicals managed to seep under the teflon and the barrel was etched. The mechanical loss value obtained is shown in figure 4.20. For the majority of the resonant modes, the loss increased due to the etching process on a similar scale to the loss values of sample 1.

The chemical etching process caused an increase in the measured mechanical loss of the silica rods. However, this may be caused by excess dissipation

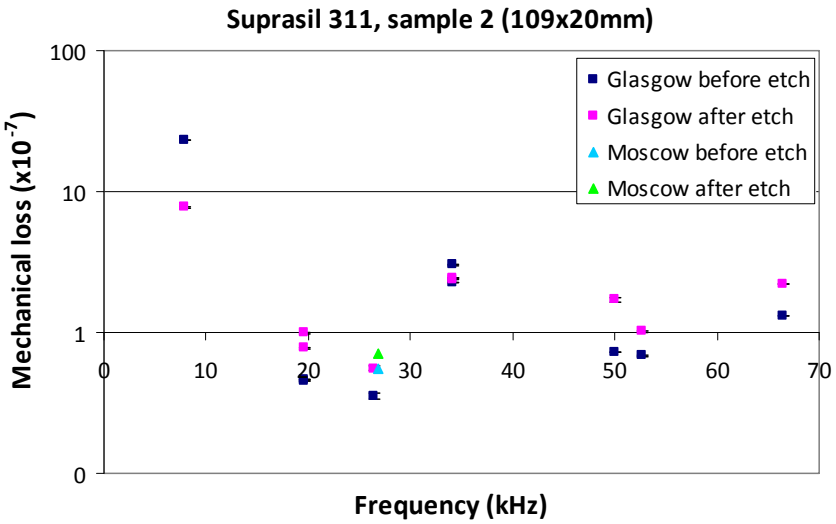

Figure 4.20: Mechanical loss of sample 2 before and after being chemically etched, measured in both Glasgow and Moscow.

at the suspension points due to the increased surface roughness. Chemical etching looks a highly promising technique for reducing the mechanical loss associated with silica components, however, the final surface condition needs to be further improved in order to use this for fabricating precision optical components, where optical scatter and absorption set stringent requirements on surface micro-roughness.

4.8 Effect of Time on the Mechanical Loss of a Bond

As part of previous research in the IGR, experiments were carried out to determine the mechanical loss associated with a hydroxy-catalysis bond formed between fused silica. Two Suprasil 311 fused silica cylinders were jointed using hydroxy-catalysis bonding in December 2007 and the mechanical loss of the bonded samples was measured by Murray *et al* using the technique described in section 4.2 [106]. Both cylinders had a diameter of 65 mm, one was 50 mm in length and the other was 70 mm in length. A reference sample of

65 mm diameter and 120 mm long was also measured to observe wether any changes that occur in the loss are due to the bulk of the material or due to the bond layer. The lowest mechanical loss obtained for the bonded cylinder was $9.9 \pm 0.5 \times 10^{-8}$ and the bond loss was calculated to be 0.11 ± 0.02 on average across all the measured resonant frequencies. Bond loss is defined in equation 5.3. The lowest mechanical loss measured for the reference cylinder was $3.2 \times 10^{-8} \pm 0.9 \times 10^{-9}$. Three years later the samples were re-measured here using the same method and suspension material as was used three years previously to quantify the effect of time on the mechanical loss of a hydroxy-catalysis bond. The measured loss values are shown in figure 4.21.

4.8.1 Analysis

The mechanical loss of the hydroxy-catalysis bond can be obtained from the measured loss of the bonded sample, ϕ_{bonded}, the loss predicted by Penn's model for a sample of this geometry, $\phi_{\text{substrate}}$, (Penn's model was used to predict the substrate loss value to enable an upper limit of the bond loss to be calculated) the amount of energy stored in the substrate divided by the total energy in the sample, $\frac{E_{\text{substrate}}}{E_{\text{total}}}$, and the amount of energy stored in the bond divided by the total energy in the sample, $\frac{E_{\text{bond}}}{E_{\text{total}}}$ through use of the equation,

$$\phi_{\text{bonded}} \simeq \frac{E_{\text{substrate}}}{E_{\text{total}}}\phi_{\text{substrate}} + \frac{E_{\text{bond}}}{E_{\text{total}}}\phi_{\text{bond}} \tag{4.8}$$

As the substrate is much larger than the bond, $\mathrm{E_{total}} \simeq \mathrm{E_{substrate}}$. Therefore $\frac{E_{\text{substrate}}}{E_{\text{total}}}$ is ~ 1 and can be removed from the calculation. The equation can be rearranged to give the mechanical loss of the hydroxy-catalysis bond, ϕ_{bond},

$$\phi_{\text{bond}} \simeq \frac{\phi_{\text{bonded}} - \phi_{\text{substrate}}}{\frac{E_{\text{bond}}}{E_{\text{total}}}} \tag{4.9}$$

The energy ratio obtained for each resonant mode was obtained using ANSYS [106, 129] and the mechanical loss of the bond at each mode frequency found.

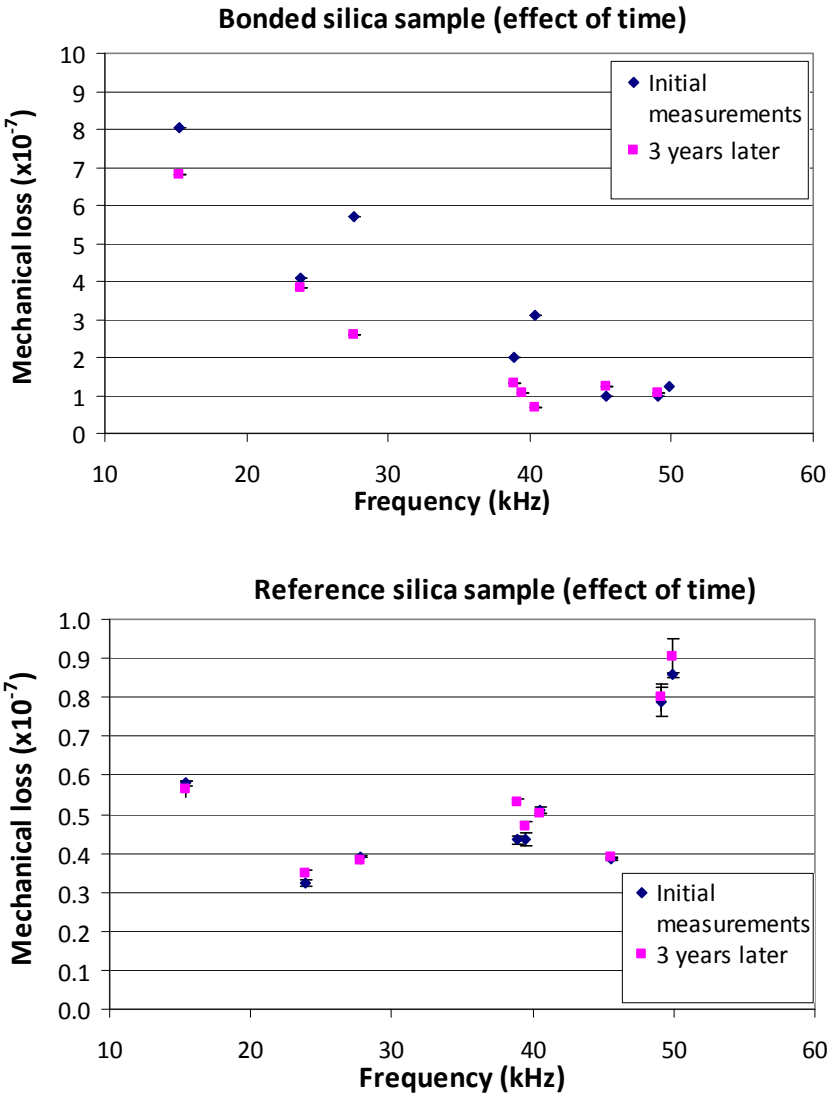

Figure 4.21: The mechanical loss of a bonded silica 311 substrate and a reference silica 311 substrate measured three years apart.

4.8.2 Results

It was seen that the mechanical loss of the reference mass remained at the same value within error after 3 years curing time. The lowest loss of the bonded mass decreased slightly to 6.9×10^{-8}. Thus, we know that it is the loss of the hydroxy-catalysis bond which is changing with time. The bond loss values for each resonant mode are shown in table 4.6 and figure 4.22. The bond loss was averaged over all the resonant modes using the same technique

Frequency (Hz)	Bond Loss	Error
15,351	0.088	0.007
23,822	0.048	0.004
27,674	0.028	0.004
38,889	0.092	0.016
40,464	0.022	0.007
45,463	0.030	0.004
49,043	0.185	0.012
49,896	0.167	0.010

Table 4.6: Bond loss value obtained for each of the resonant modes measured

described in [106] and a value of 0.08 ± 0.02 was obtained.

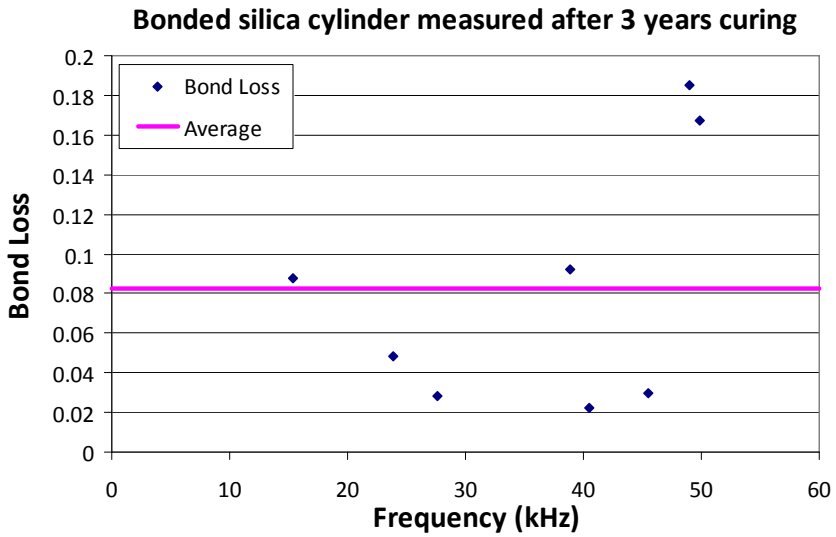

Figure 4.22: Bond loss measured for each resonant mode after 3 years curing time.

This decrease in the average bond loss shows that the bond is changing over time. This could be due to an increase in rigidity as the bond cures for a longer time and hence an increase in the Young's modulus of the bond. Another possible explanation is that the bond could be becoming thinner over time as water evaporates from the edges and migrates out of the bond.

4.9 Effect of Heat Treatment on the Mechanical Loss of a Bond

It has been shown in Chapter 3 that heat treating samples can improve the strength of a hydroxy-catalysis bond. The effect this treatment has on the mechanical loss of a sample was then investigated as it is an important factor for the suspensions in gravitational wave detectors as a high loss material is very noisy and this can reduce the sensitivity of the detector as discussed in section 4.1. The bonded and reference samples discussed in section 4.8 were subsequently heat treated to a temperature of 150°C for 48 hours to imitate the bake out conditions which were seen to increase bond strength in section 3.5.3. After the heat treatment the mechanical loss of each sample was remeasured to observe the effect. Figure 4.23 shows the values of mechanical loss obtained both before and after the heat treatment.

4.9.1 Analysis

The bond loss values for each resonant mode, calculated by the same method shown in section 4.8, are shown in table 4.7. As in section 4.8, the empirical model 4.2 was used to predict the value of the substrate loss to enable an upper limit of the bond loss to be calculated.

4.9.2 Results

There was no systematic change in the loss of the modes of the reference sample while the minimum loss of the bonded sample decreased slightly to a value of $6.29 \times 10^{-8} \pm 1.65 \times 10^{-7}$. This shows that the reduction in loss of the bonded sample is not a bulk material effect but a reduction of loss of the bond. The heat treatment process reduced the average mechanical loss of the bond over all the measured resonant modes to 0.06 ± 0.01. The change could be due to water being evaporated from the bond due to the heat.

As the model 4.2 was used to calculate the loss of the substrate material, this value is an upper limit to the mechanical loss of the bond. If the measured

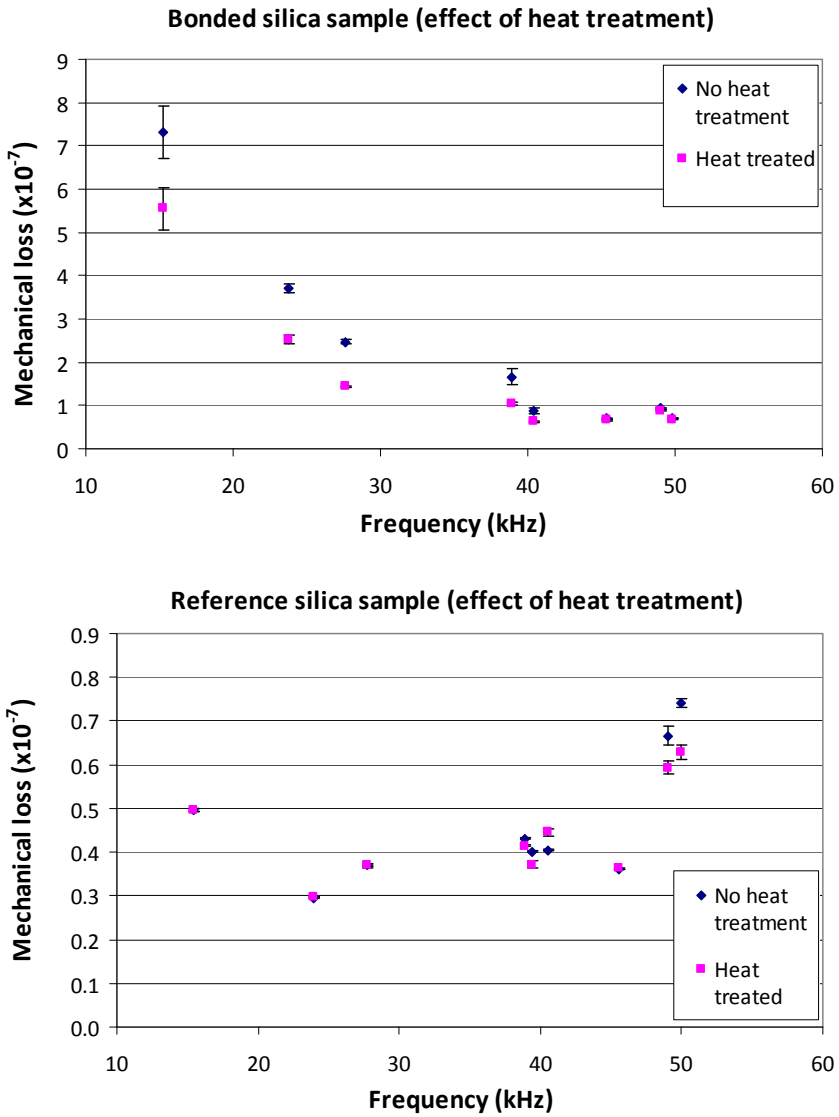

Figure 4.23: The mechanical loss of a bonded silica 311 substrate and a reference silica 311 substrate measured before and after a heat treatment of 48 hours at 150°C.

mechanical loss values of the reference sample was used as the substrate loss a slightly lower value for the bond loss is obtained, 0.032 ± 0.008.

Frequency (Hz)	Bond Loss	Error
15,351	0.072	0.007
23,822	0.031	0.004
27,674	0.014	0.004
38,889	0.070	0.016
40,464	0.011	0.007
45,463	0.028	0.004
49,043	0.121	0.012
49,896	0.091	0.010

Table 4.7: Bond loss value obtained for each of the resonant modes measured after the sample was heat treated

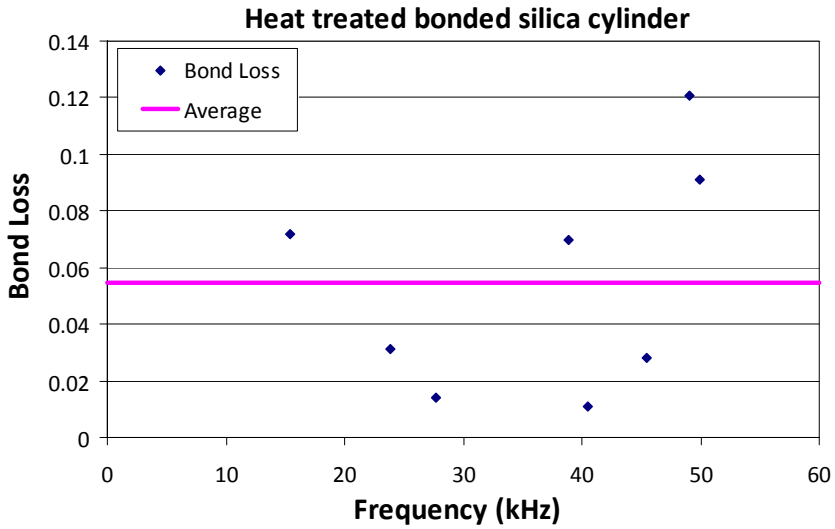

Figure 4.24: Bond loss measured for each resonant mode after heat treatment.

4.10 Conclusions

The results presented in this chapter show that the change in the chosen grade of fused silica for the mirrors in advanced LIGO from 311SV to 3001 is not expected to affect the overall expected sensitivity as the substrate thermal noise is still at a level which is considerably below the coating thermal noise.

Methods of further reducing the thermal noise of the test masses that were investigated and evidence was found that heat treating the suspension to 150°C

for 48 hours could further decrease the expected loss. This could possibly be due to heat treatment acting as a method of removing stresses and evaporating water from the surface and within the hydroxy-catalysis bonds. It is also possible to further reduce surface loss by chemically etching away the lossy surface layer of the suspension fibres. These methods should be investigated further as it was found that masses used in this thesis reveal suspension limited loss. Further studies of fibres and other sample geometries such as cantilevers which were mechanically polished could provide a more accurate measurement of the etching affect.

There are other methods currently being considered to reduce noise in advanced detectors by further developing expertise in silica technology, for example by altering the fibre geometry [159]. Further research is necessary to fully understand and quantify the impact and benefit of different techniques but it is predicted that by implementing all of the enhancements which are currently being researched the predicted loss of Advanced LIGO could be improved by a factor of $\sim$8 [159].

Chapter 5

Mechanical Loss of Silicon as a Test Mass Material: Bond Loss of Hydroxy-Catalysis Bonds between Silicon Substrates

5.1 Introduction

As discussed in chapter 1, the designs under consideration for third generation interferometric gravitational wave detectors may use cooling of the suspensions and mirrors to cryogenic temperatures in order to reduce thermal noise and thus increase detector sensitivity. Fused silica, the current suspension material for gravitational wave detectors, has a broad dissipation peak centred around ~ 40 K which would make it unsuitable for use at cryogenic temperatures [160, 161]. Thus different materials are being investigated as potential candidates for the suspension and test mass material in future detectors. At present, the two most likely candidates are silicon and sapphire as they can have low mechanical losses at low temperatures [131, 162–164]. Cooled sapphire substrates and suspension elements are currently being studied in several laboratories and universities in Japan [49]. In Europe and the US research is ongoing on the use of silicon as a material for substrates and suspension elements [48, 165–168]. This chapter describes some investigations into the mechanical loss of silicon

substrates and of hydroxy-catalysis bonds created between silicon samples.

At frequencies, greater than a few 100 Hz, thermal noise is no longer the limiting factor to detector sensitivity. Instead photoelectron shot noise is the dominant noise source. The effect of photoelectron shot noise can be reduced by increasing the power of the laser beam. However any laser power absorbed by the mirrors causes thermally induced deformations of the front face of the masses which introduces excess noise to the system. This deformation is proportional to $\frac{\alpha}{\kappa}$, where α is the linear coefficient of thermal expansion of the substrate material and κ is the thermal conductivity of the mirror substrate [120]. Thus, minimisation of $\frac{\alpha}{\kappa}$ would allow for an increase in the laser power used, improving the sensitivity in this frequency range. Power handling can also be improved by using an all-reflective topology as this topology reduces the effect of thermal distortion caused by laser light passing through the input mirrors of the cavities. Silicon is opaque to the 1.064 μm of the Nd:YAG laser light currently used for gravitational wave detection and has a $\frac{\alpha}{\kappa}$ ratio which is approximately 22 times lower than fused silica and 7 times lower than sapphire [165]. This makes silicon a good candidate for the suspension mirror and fibre material in an all-reflective interferometer as it is able to withstand a substantially larger increase of power than silica or sapphire before it would become thermally distorted [165].

Thermo-elastic loss would be expected to be a source of significant noise in the current operating frequency band of gravitational wave detectors if crystalline optics were utilised and the detector operated at room temperature [162]. The intrinsic internal friction in a substrate material arising from defects in the material, dislocations of the crystal structure or impurities etc is also a source of thermal noise. Both the thermo-elastic loss [56] and the intrinsic mechanical dissipation [121, 165] of silicon are comparable to that of sapphire at room temperature. However, the thermal expansion coefficient of silicon is reduced to zero at two temperatures, $\sim$ 18 K and $\sim$ 120 K [169]. Silicon has also been seen to exhibit two loss peaks at $\sim$ 13 K and $\sim$ 115 K [163].

The origin of these loss peaks are currently not fully understood. If investigations show it is possible to shift the temperature at which these peaks occur, operating a silicon interferometer at $\sim$ 18 K or $\sim$ 120 K would provide an interferometer with a higher sensitivity than that of a sapphire interferometer operated at cryogenic temperatures.

As there are plans to increase the laser power, the test mass mirrors must be increased (to $\sim$ 200 kg [170]) so that sensitivity at low frequencies is not decreased due to the effect of radiation pressure on the mirrors. Silicon is available in these large sizes.

Silicon samples can be cut with different crystal orientations and can be grown using different methods. These factors may effect the intrinsic mechanical loss of the sample and therefore should be investigated to ensure the lowest mechanical loss material is selected for use in future detectors. Experiments were carried out here to measure the mechanical loss of two orientations of bulk silicon, <100> and <111>, grown using the Czochralski method [171]. The samples were manufactured by Prolog Semicor Ltd [172] and polished by Spanoptic Ltd [173]. The results are shown in section 5.4.2. It has been shown in Chapter 3 that hydroxy-catalysis bonds can be used as a low mechanical loss technique of joining silica elements of the detector suspension. Initial investigations were carried out here of the mechanical loss of hydroxy-catalysis bonds between silicon substrates, to ensure this bonding process could still be used as a low loss technique for joining the detector suspension elements for future generation detectors which use silicon substrates.

5.2 Silicon Crystal Structure

5.2.1 Crystal Orientation of Silicon

The silicon structure is cubic and has 3-fold rotational symmetry and 2 axes of mirror symmetry [174]. The properties of a material with a crystal structure are defined relative to the (100) plane. For the cylinders of single crystalline

silicon studied, the orientation of these samples indicates how the cylindrical axis lies with respect to the crystal axes. The samples investigated in this thesis have been manufactured such that their cylindrical axis is perpendicular to either the (100) or (111) planes of the crystal structure giving them the direction notation <100> and <111> respectively. Figure 5.1 shows the planes of these cuts [174].

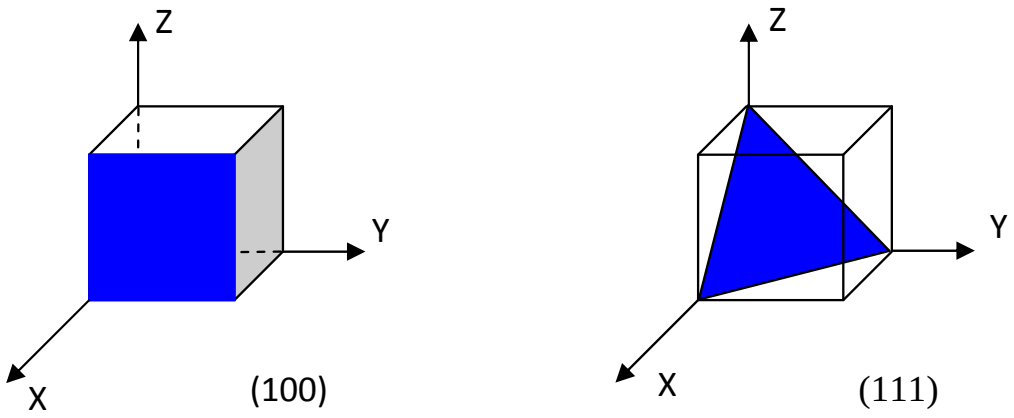

Figure 5.1: Planes of a cubic crystal such as silicon.

5.2.2 Elastic Constants of Silicon

When carrying out finite element analysis of a material it is necessary to include appropriate information on the elastic properties of the material as these properties denote how the material can distort. As the structure of silicon is anisotropic the Young's modulus is dependent on the orientation of the material. Thus, a single number cannot denote the Young's modulus. Instead it is represented by a stiffness matrix. The elastic modulus for a material with a cubic crystal structure such as silicon is represented by a 6×6 stiffness matrix. The elastic constants for <100> silicon are [175],

$$|c_{<100>}| = \begin{vmatrix} 1.657 & 0.639 & 0.639 & 0 & 0 & 0 \\ 0.639 & 1.657 & 0.639 & 0 & 0 & 0 \\ 0.639 & 0.639 & 1.657 & 0 & 0 & 0 \\ 0 & 0 & 0 & 0.796 & 0 & 0 \\ 0 & 0 & 0 & 0 & 0.796 & 0 \\ 0 & 0 & 0 & 0 & 0 & 0.796 \end{vmatrix} \times 10^{11}\ \mathrm{kg/ms^2}$$

The <111> elastic constants can be calculated from the <100> elastic constants by performing a coordinate transformation technique created by W. L. Bond [176]. Figure 5.2 shows the rotations required to change from a <100> orientation to a <111> orientation. The matrix representing the elastic constants of <100> silicon is rotated 45° around the z-axis to give the elastic constants for the <110> and then rotated by an angle of -$\cos^{-1}1/\sqrt{3}$ around the y axis to give the elastic constants for the <111> oriented silicon.

The stiffness matrix representing the elastic modulus of <111> silicon is [177],

$$|c_{<111>}| = \begin{vmatrix} 1.940 & 0.543 & 0.448 & 0 & 0 & 0.135 \\ 0.543 & 1.940 & 0.448 & 0 & 0 & -0.135 \\ 0.448 & 0.448 & 2.040 & 0 & 0 & 0 \\ 0 & 0 & 0 & 0.700 & -0.135 & 0 \\ 0 & 0 & 0 & -0.135 & 0.700 & 0 \\ 0.135 & -0.135 & 0 & 0 & 0 & 0.700 \end{vmatrix} \times 10^{11}\ \mathrm{kg/ms^2}$$

As the stiffness matrix is different for <100> and <111> silicon the different oriented samples will distort in different ways when they are excited at their resonant frequencies. As discussed in section 2.3.2 the mechanical loss of a material is related to the imaginary part of the stiffness, the phase lag between

a stress being formed in the material and the resultant strain being formed. Thus, the difference in the Young's modulus for the different orientations of silicon may suggest that the mechanical loss of the material is also different. Thus, the mechanical loss of samples of both of these orientations of silicon are measured in order to aid the selection of the orientation of silicon with the lowest mechanical loss, and therefore lowest thermal noise, for use in gravitational wave detectors.

It is also noted that the distribution of motion can differ in the samples of different crystal orientations. Thus, for the experimental set-up used here the losses measured could be limited by the position of the sample with respect to the break-off points of the suspension material.

5.3 Experimental Measurements

The mechanical loss measurements were made using the experimental set-up described in Chapter 4. As silicon has a definite crystal structure, and silica is amorphous, additional factors have to be considered when measuring the mechanical loss of the silicon compared to silica. The first is that the properties of the suspension which allow for the lowest loss of the material to be measured may differ, such as the suspension material, or that the orientation of a resonant mode shape with respect to the suspension may become significant as for crystal structures the resonant mode shape is related to the positioning of the crystal axes. If areas with a high amplitude of motion are positioned near to the break-off points of the suspension material then excess loss can be added to the system through frictional forces. Thus, there may be an optimum rotation of the sample with respect to the suspension which allows for the lowest loss to be measured. Different suspension materials and orientations of the sample with respect to the suspension were investigated in order to find the optimum material and method which would allow for the most accurate measurement of mechanical loss of the material.

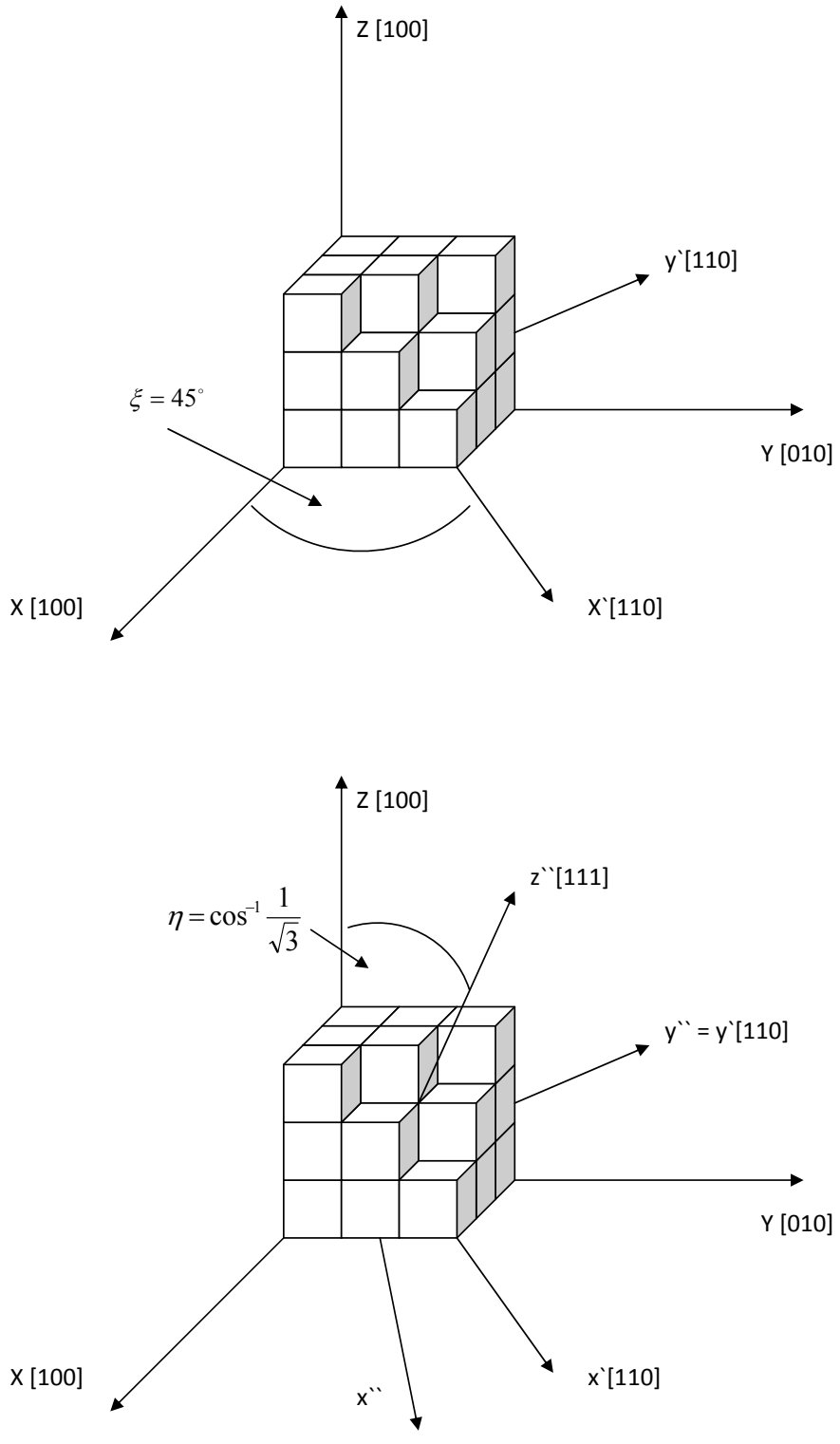

Figure 5.2: Rotated coordinate system for cubic crystals.

5.3.1 Suspension Material

The mechanical loss of a silicon sample with the <100> axis perpendicular to the cylindrical axis of the sample, with 65 mm diameter and 120 mm length, was measured when suspended using different types of suspension materials in turn. Silk thread, Nichrome wire and Tungsten wire [178] were used. The thickness of the wire was selected so that its breaking stress was just greater than the stress formed in the wire by suspending the mass of the sample, to allow for the smallest contact area with the sample possible. Tungsten has been traditionally used in experiments due to its high strength. Nichrome was investigated as it is a softer material than tungsten so has a possibility of providing a smaller damping effect as it could be more forgiving to some movement therefore causing less friction. The mechanical loss values measured are shown in figure 5.3.

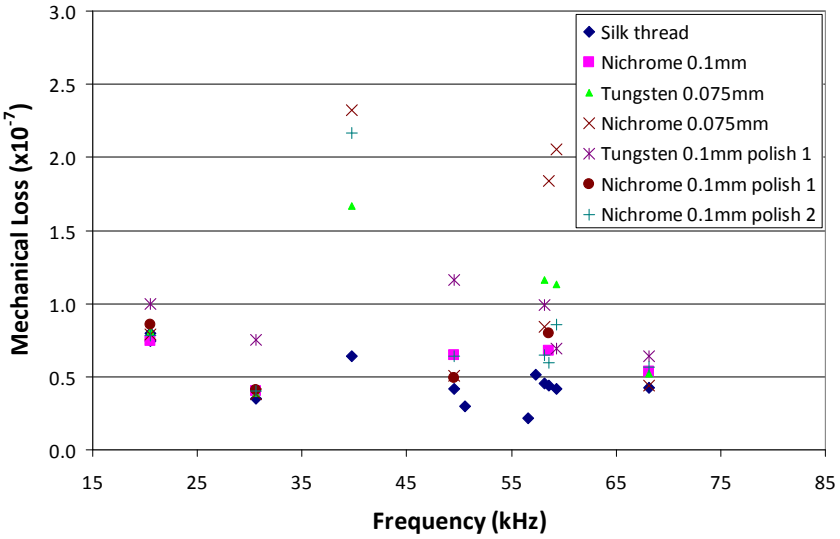

Figure 5.3: Mechanical loss values of silicon <100>, 65x120 mm sample, measured using silk thread, Nichrome wire and Tungsten wire. The results were obtained using different thicknesses of wire for the suspension, treated using different polishing techniques.

From figure 5.3 it can be seen that using silk thread as a suspension material allows for the measurement of lower mechanical loss values. There was no

overall benefit seen when using Nichrome wire rather than tungsten wire or vice versa as whilst the different materials gave lower losses on different mode shapes the majority of the values were within a few percent of each other.

The Tungsten and Nichrome wire of 0.1 mm thickness were polished. Two polishing techniques were used: polish 1 used decreasing grades of diamond paste for 15 minutes and then a commercial brand of metal polish, Brasso, for 20 minutes. For polish 2, the same polishing materials were used but the polishing times were doubled. The polished wire was imaged using an Olympic Nomarski Microscope [179] and it could be seen that the polishing technique was reducing the diameter of the wire. A series of images of the wire, taken after polishing steps each of 5 minutes duration is shown in figure 5.4. For small

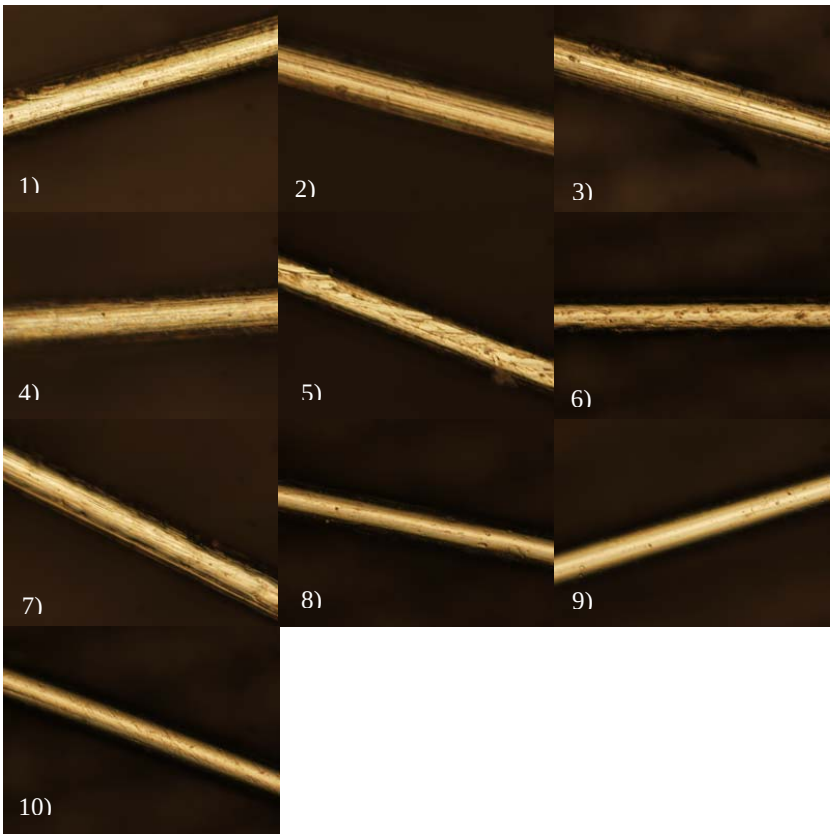

Figure 5.4: A series of images of a 100 μm Nichrome wire after 5 minute intervals of polishing with diamond paste. Dark specks show peaks and troughs in the material.

polishing times the roughness of the wire was observed to increase. Image (1) in figure 5.4 shows the wire before it was polished. Darker regions or 'specks' can be seen on the wire. These indicate peaks or troughs in the material and thus, the amount of specks is related to the roughness of the wire. It can be seen that the roughness of the wire increases up to image (6), which relates to 30 minutes of polishing time. For longer polishing times the roughness begins to decrease, as shown in image (7)-(10). An increase in roughness could cause an increase in the amount of friction with the sample when it is suspended and contribute extra loss to the measurement. Figure 5.3 shows that the measured mechanical loss increases for some resonant modes after polishing which could be associated with increased roughness of the suspension material. Longer polishing times were investigated to explore the possibility of eventually obtaining a smoother surface area on the wire and hence possibly reducing the associated loss by decreasing excess friction. After the longer polishing times (up to 50 minutes) the loss did not decrease significantly. It is thought that it may be possible to reduce the loss by increasing the polishing time by a much larger amount, however, it is difficult to polish the wire evenly for great lengths of time and it is easy to cause kinks in the wire during polishing. For these reasons it is thought that polishing wire for long periods of time for the use in suspensions is not as effective as using silk thread as a suspension material. Silk thread is a good suspension material as it is soft, and therefore has minimal resistance to the natural motion of the resonating sample. However, loose fibres from the material can cause excess loss through friction. To compensate for this, a very small amount of grease is put onto the thread. This reduces the amount of loose fibres and reduces friction with the sample.

5.3.2 Orientation of Silicon Test Masses to the Suspension

Silicon is an anisotropic material; the atoms have positions in specific places in a crystalline structure. Therefore, the position at which the suspension thread

leaves the sides of a sample, the 'break-off' points, with respect to the resonant mode shape of a sample could be an important factor for measuring mechanical loss. An arbitrary point was marked using a water based pen, on the sample of <111> orientation and length 70 mm to indicate 0° rotation. The loss at this position was measured and then the sample was rotated in increments of 15° in order to find the position which has minimum motion at the location of the break off points and hence allows for the measurement of the lowest mechanical loss. The thinnest silk thread which was able to suspend the mass was used and was found to become weaker as the sample was rotated, causing it at times to snap and thus a complete 360° rotation could not always be completed. A slightly thicker silk thread was thus used which contributes a slightly larger amount of excess loss but did not break. The complete mechanical loss results are shown in figure 5.5. Patterns in the loss values against frequency can be seen which correlate with some of the resonant mode shapes, for example, one peak can be clearly seen for the 47 kHz mode which has one red region on the mode shape picture which indicates the maximum amount of movement. Thus, it is observed that the loss measurable at each resonant mode can be dependent on the orientation of the sample to the break-off points. However, the optimum positioning of the sample in the suspension with respect to the resonant mode shape which allows for the lowest loss value to be measured is different for each resonant mode.

The sample was re-suspended using the thinner thread and the two lowest loss resonant modes were measured through the range of rotation which previously obtained the lowest loss values. The results are shown in figure 5.6.

It was found that positioning the sample at a rotation of 180° from the arbitrary start mark allowed for the lowest loss to be measured. The sample was then re-suspended at this position several times to measure the lowest loss value of $(1.6 \pm 0.2) \times 10^{-8}$.

As the optimum rotation for measuring the lowest loss of the material is different for each resonant mode and a thicker thread would have to be used

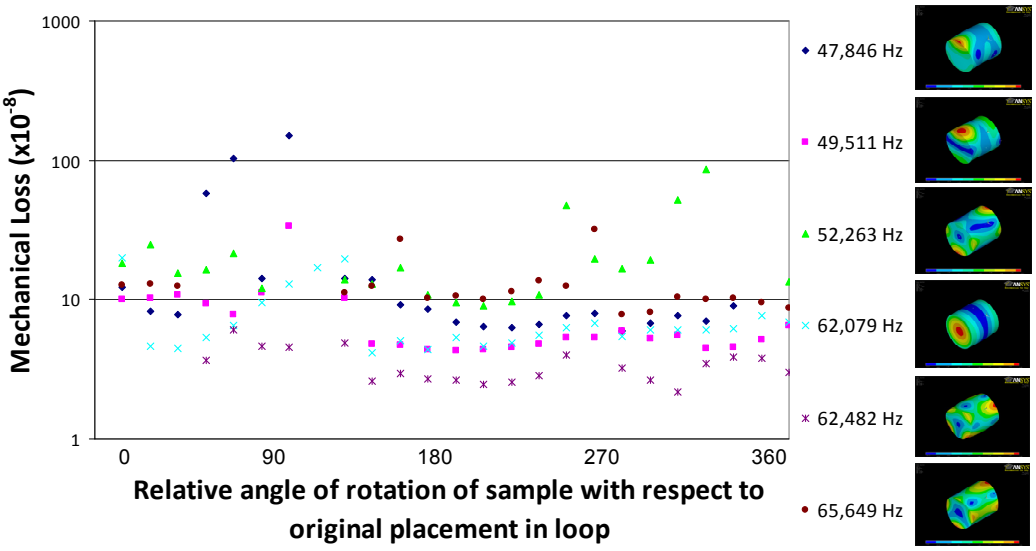

Figure 5.5: Mechanical loss of a sample of <111> oriented silicon with 65 mm diameter and 70 mm length as it is rotated in its suspension loop.

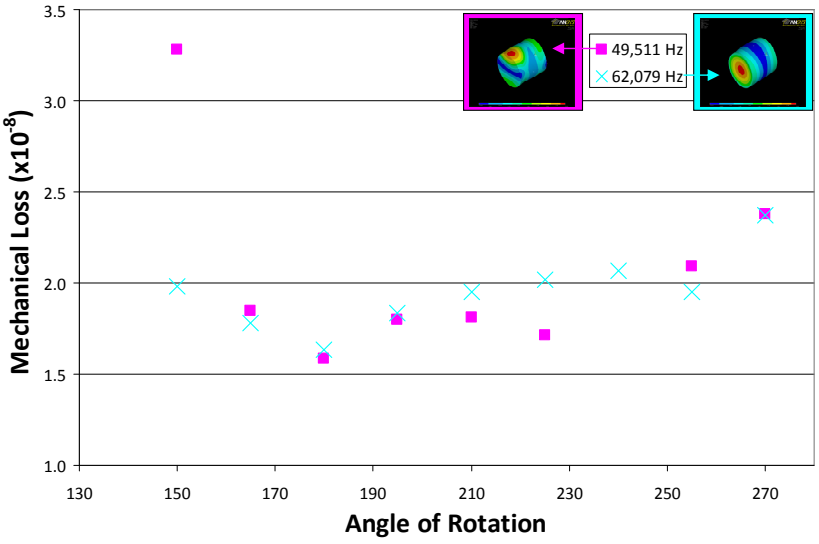

Figure 5.6: Mechanical loss of silicon <111> as it is rotated by smaller increments over a peak region of its suspension.

for rotating the mass it was decided that suspending the mass several times at arbitrary rotations using the thinner thread was the most practical compromise to enable measurement of low mechanical losses.

5.4 Bulk Silicon Results

5.4.1 <111> Oriented Silicon

The mechanical loss of three samples of silicon <111> were measured at room temperature in the experimental set-up described in Chapter 4. The dimensions of the three samples are listed in table 5.1.

Parameter	Sample 1	Sample 2	Sample 3
Diameter	65 ± 0.05 mm	65 ± 0.05 mm	65 ± 0.05 mm
Length	50 ± 0.05 mm	70 ± 0.05 mm	120 ± 0.05 mm

Table 5.1: Summary of silicon <111> sample parameters

Silk thread was used as the suspension material as it had been found to allow for lower losses to be measured in section 5.3.1. The sample was suspended several times at arbitrary rotations. The resonant mode shapes measured for the 50 mm, 70 mm and 120 mm samples are shown in figures 5.7, 5.8 and 5.9 respectively.

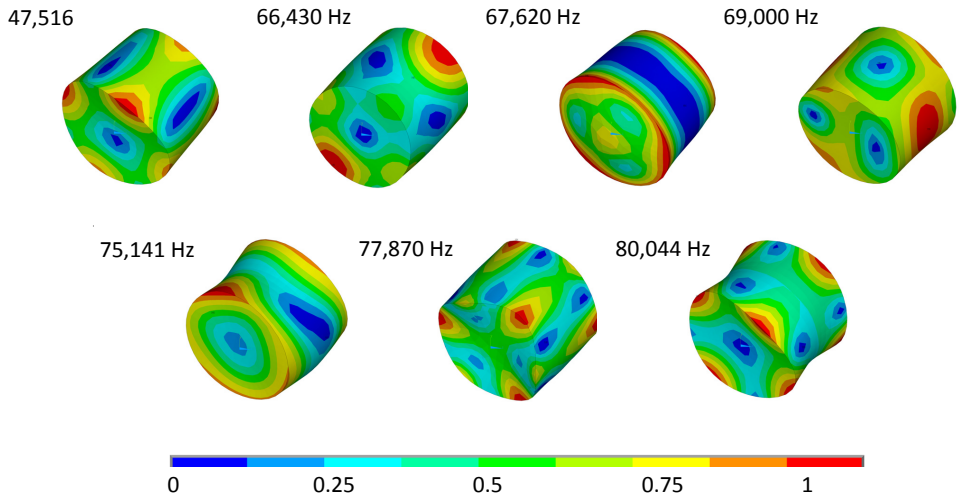

Figure 5.7: Resonant mode shapes of the measured frequencies of a silicon <111> sample, 65 mm in diameter and 50 mm in length. The amplitude of motion is relative and indicated using colour. Blue indicates the smallest amplitude and red indicates the largest amplitude.

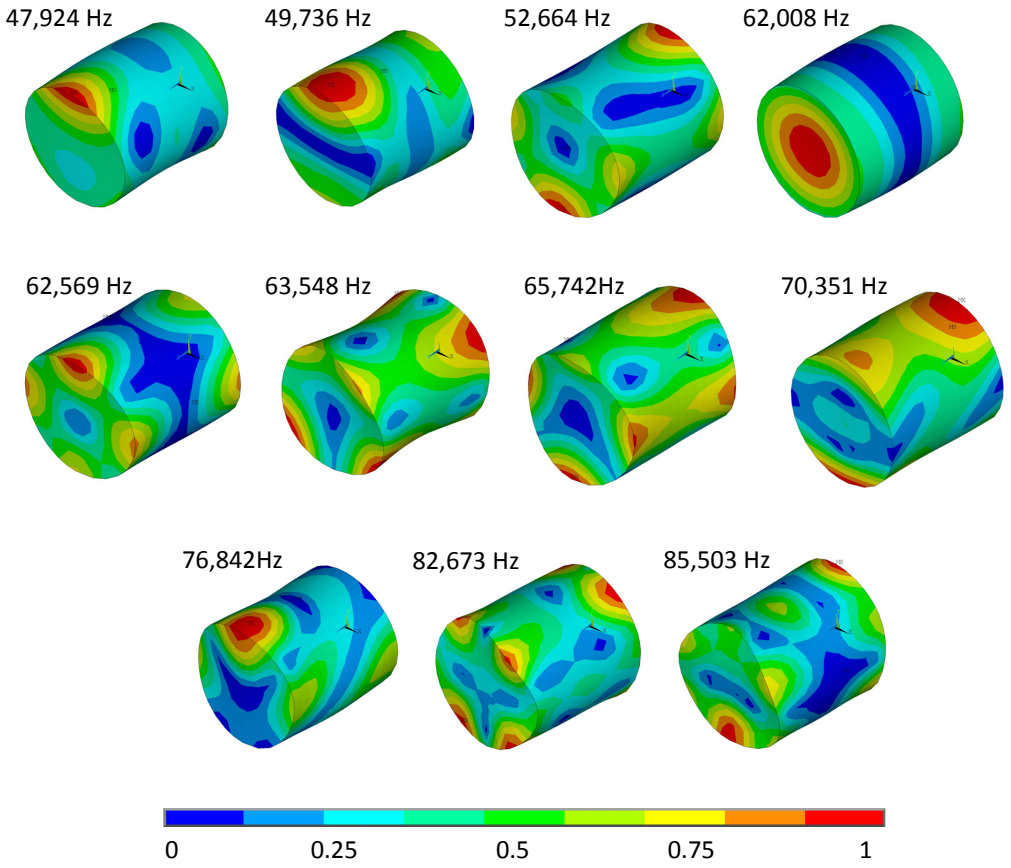

Figure 5.8: Resonant mode shapes of the measured frequencies of a silicon <111> sample, 65 mm in diameter and 70 mm in length. The amplitude of motion is relative and indicated using colour where blue indicates the smallest amplitude of motion and red indicates the largest amplitude of motion.

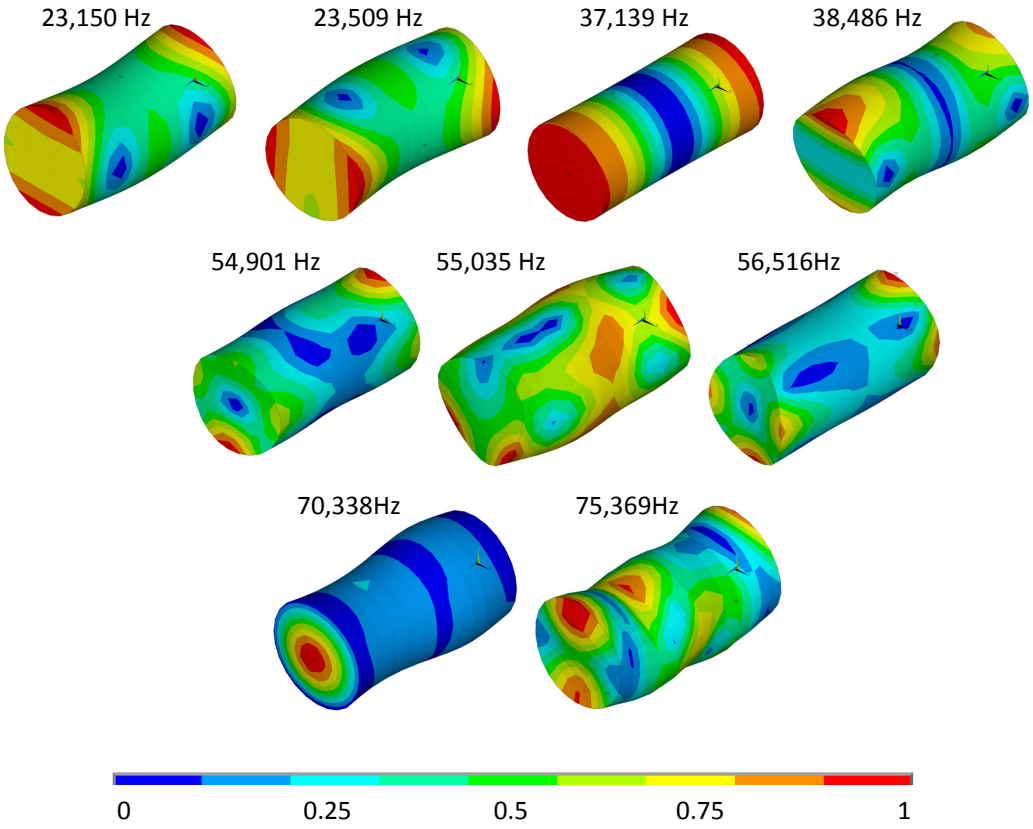

Figure 5.9: Resonant mode shapes of the measured frequencies of a silicon <111> sample, 65 mm in diameter and 120 mm in length. The amplitude of motion is relative and indicated using colour where blue indicates the smallest amplitude of motion and red indicates the largest amplitude of motion.

The mechanical loss values obtained were larger than expected as silicon <111> samples from the same vendor, grown using the same technique, have previously been measured with lower losses [166]. In an attempt to check whether the losses measured were being limited by properties of the suspension set-up used in Glasgow the mechanical loss of the three samples was re-measured in a set-up at the Friedrich Schiller University in Jena, Germany. The mechanical loss values measured are shown in 5.10, 5.11 and 5.12.

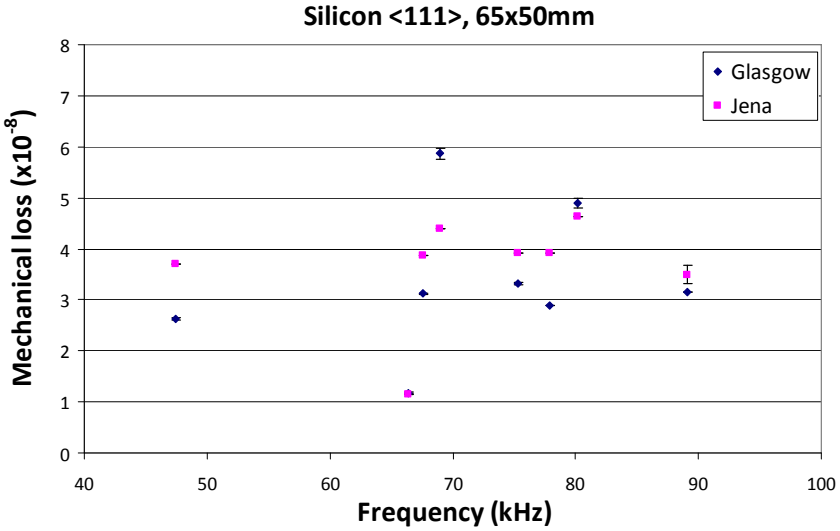

Figure 5.10: The mechanical loss as a function of frequency of a silicon <111> sample, 65 mm in diameter and 50 mm in length with results obtained in both Glasgow and Jena shown.

The set-up in Jena operates by the same principle as the set-up in Glasgow. The main difference between the two experimental set-ups is that the movement of the front face of the sample was recorded using a SIOS interferometer, manufactured by Meßtechnik GmbH [180]. The majority of the lowest mechanical loss values measured in Jena of the 70 mm and 120 mm long samples and the lowest measured loss of the 50 mm long sample agreed within error with the loss values measured in Glasgow. Thus, the lowest value measured of the mechanical loss for each sample was taken as the intrinsic material loss value of the sample.

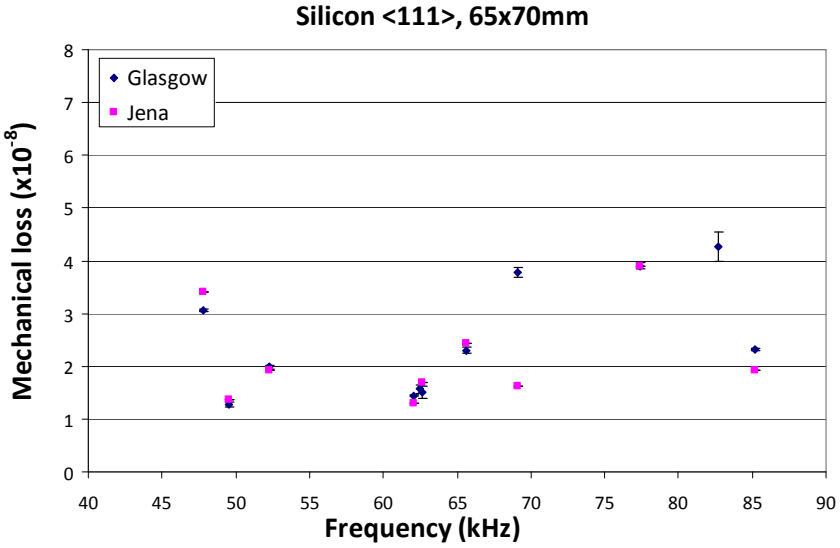

Figure 5.11: The mechanical loss as a function of frequency of a silicon <111> sample, 65 mm in diameter and 70 mm in length with results obtained in both Glasgow and Jena shown.

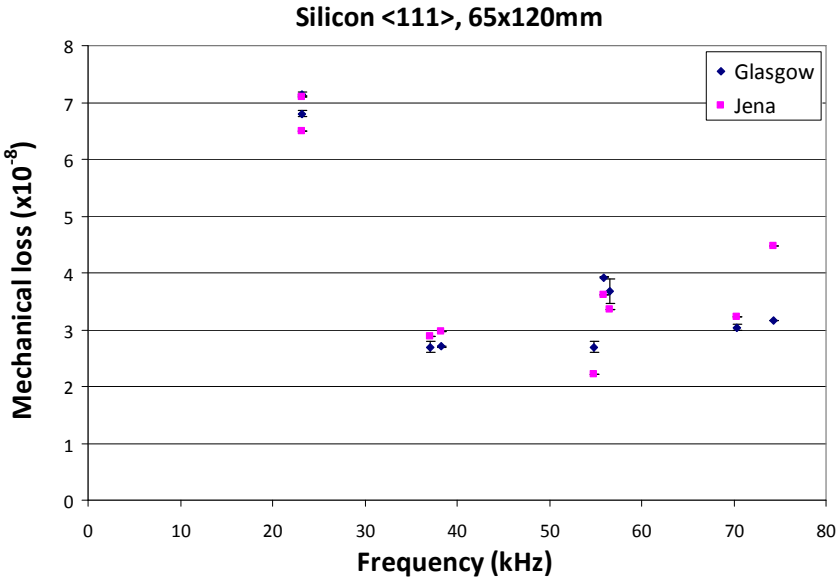

Figure 5.12: The mechanical loss as a function of frequency of a silicon <111> sample, 65 mm in diameter and 120 mm in length with results obtained in both Glasgow and Jena shown.

5.4.2 <100> Oriented Silicon

In order to make a comparison of the mechanical loss of different orientations of silicon, three samples of silicon, cut such that the cylindrical axis of the samples was perpendicular to the (100) plane of the crystal were measured using the same technique as described in section 4.2. A photograph of the samples is shown in figure 5.13 and the dimensions of the samples are listed in table 5.2.

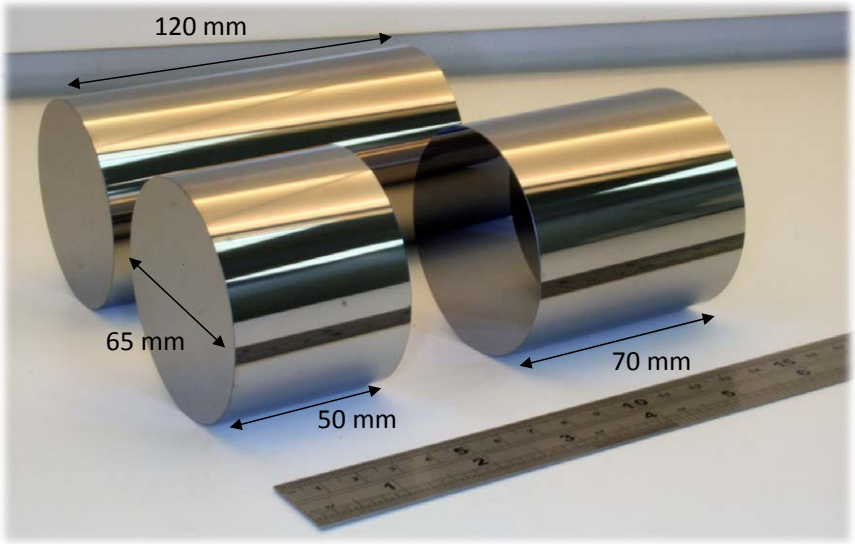

Figure 5.13: <100> silicon samples, all 65mm diameter, one 50mm in length, one 70mm in length and one 120mm in length.

Parameter	Sample 1	Sample 2	Sample 3
Diameter	65 ± 0.5 mm	65 ± 0.5 mm	65 ± 0.5 mm
Length	50 ± 0.5 mm	70 ± 0.5 mm	120 ± 0.5 mm

Table 5.2: Summary of silicon <100> sample parameters

Samples 1 and 2 were to be hydroxy-catalysis bonded together. Similar to the bonded silica cylinders discussed in section 4.8, the lengths were chosen to ensure that the bond would be offset from the centre of mass when the sample was bonded. This offset is required to ensure that the suspension thread does

not lie on the bond which would cause an increase in friction between the thread and sample and therefore increase the measured mechanical loss. The third sample was measured as a reference sample. It had the same geometry as the bonded sample but without the bond layer. This allowed an estimate of the value of mechanical loss of a sample of the same total size as the substrate but without the bond.

The resonant mode shapes measured for the 50 mm, 70 mm and 120 mm samples are shown in figures 5.14, 5.15 and 5.16 respectively.

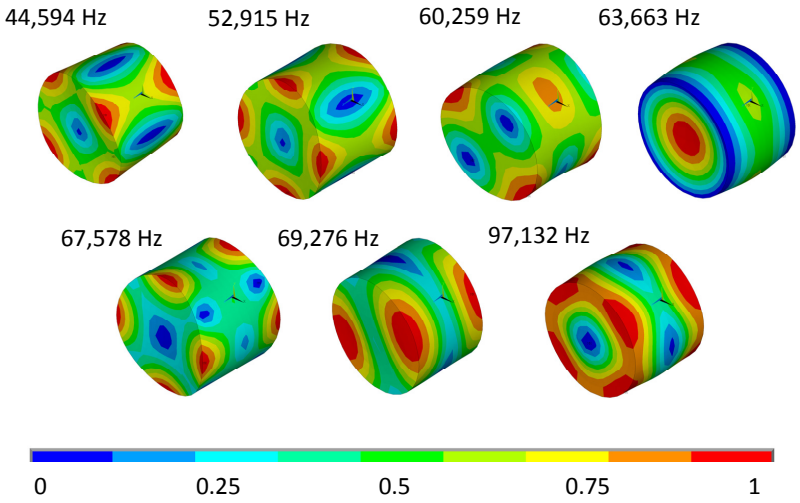

Figure 5.14: Resonant mode shapes of the measured frequencies of a silicon <100> sample, 65 mm in diameter and 50 mm in length. The amplitude of motion is relative and indicated using colour where blue indicates the smallest amplitude of motion and red indicates the largest amplitude of motion.

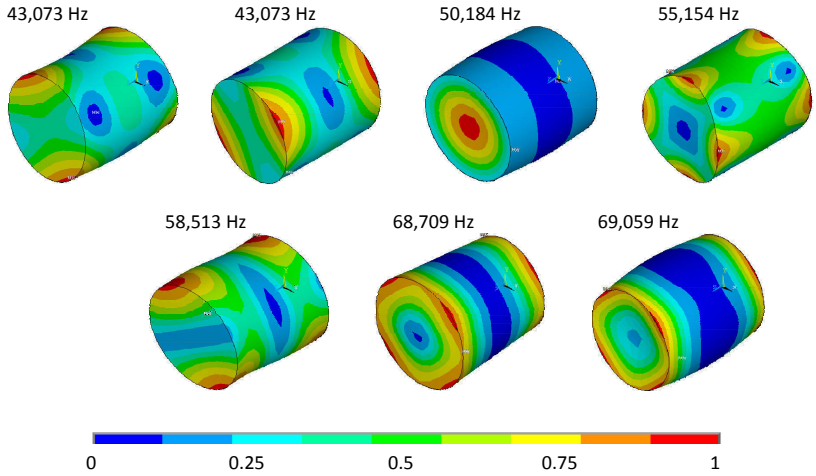

Figure 5.15: Resonant mode shapes of the measured frequencies of a silicon <100> sample, 65 mm in diameter and 70 mm in length. The amplitude of motion is relative and indicated using colour where blue indicates the smallest amplitude of motion and red indicates the largest amplitude of motion.

In order for a bond to be formed between silicon substrates, a silicon oxide layer has to be present on the bond surfaces as this allows the etching step of the bonding process described in Chapter 3 to be performed. It has been found that the oxide layer should be a minimum of 50 nm as bonding with thinner oxide layers have been shown to detrimental to the strength of the bond [168]. One method of producing the necessary oxide layers is using wet thermal oxidation. In this procedure the samples are placed in an oven, with water vapour being carried through the oven by nitrogen gas, at 1000°C. The water vapour diffuses into the silicon surface and reacts with it to produce SiO_2 and H_2. The oxide layer grows both downwards into the silicon and upwards on the surface [181].

Before the samples are placed in the oven they are acid cleaned using piranha solution, which is a mixture of 7 parts sulphuric acid and 1 part 30% hydrogen peroxide solution to remove any organic substances from the sample surface which could inhibit the oxide layer growth. The samples were then

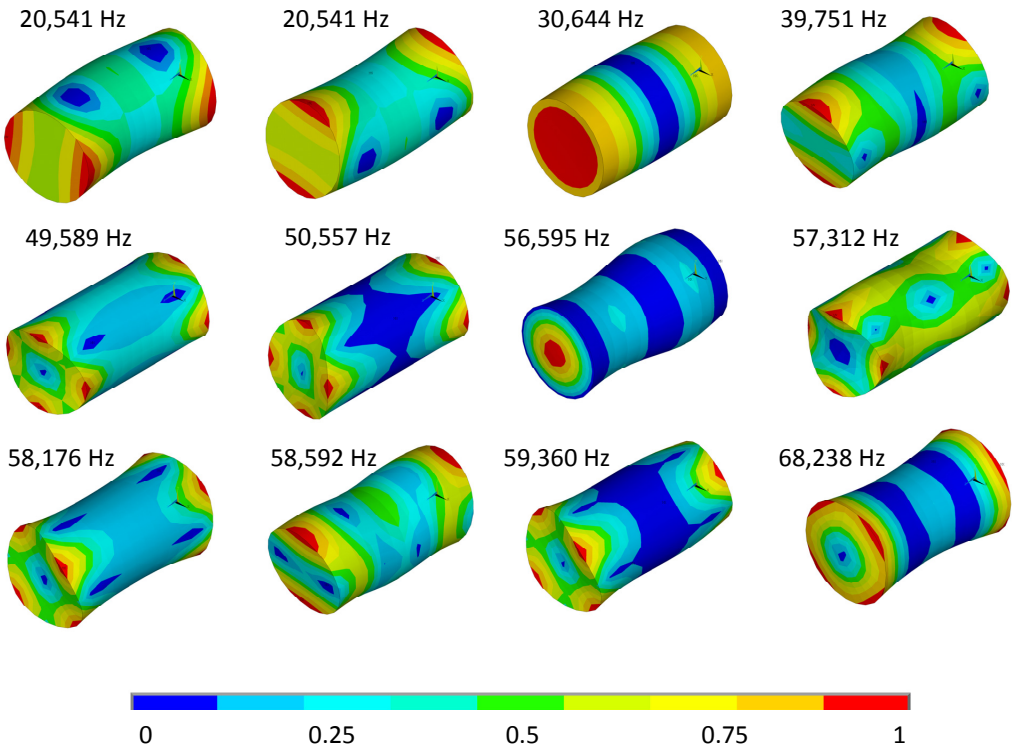

Figure 5.16: Resonant mode shapes of the measured frequencies of a silicon <100> sample, 65 mm in diameter and 120 mm in length. The amplitude of motion is relative and indicated using colour where blue indicates the smallest amplitude of motion and red indicates the largest amplitude of motion.

placed on a silica holder, known as a silica boat, and slid into the pre-heated oven. Photographs of a silicon sample being put into the oven and brought out of the oven are shown in figure 5.17.

Figure 5.17: (a) A silicon mass going into the oven at 1000°C to be oxidised. (b) Silicon mass after being oxidised in the oven (still glowing hot).

The samples were oxidised for 45 minutes. Figure 5.18 shows samples 1 and 2 after they were oxidised. The colour of the sample is indicative of the thickness of the oxide layer, however the thickness was measured more accurately using a Sentech 850 laser ellipsometer [182]. The 50 mm sample has an oxide layer thickness of 170 $\pm$ 0.5 nm and the thickness of the oxide layer on the 70 mm sample is 170 $\pm$ 0.5 nm. These measurements are averages of two measurements taken on the face of the samples.

After the oxidisation processes small raised areas were identified on the edge of the bonding surface of both the 50 mm and 70 mm samples. At first this was thought to be some silica deposited on the surface from the silica boat on which they sit in the oven. A ZYGO GPI XP/D interferometer [110] was used to measure the height of the raised area on both samples optically with the heights found to be $\sim$ 1000 nm. The heights measured were confirmed by measurements using a Taylor Hobson Talysurf [183]. The raised areas had diameters of $\sim$ 1 mm. As this would be detrimental to successful bonding, the samples were etched in hydrofluoric acid in an attempt to remove the oxide layer and thus the raised area. After etching, the raised area remained,

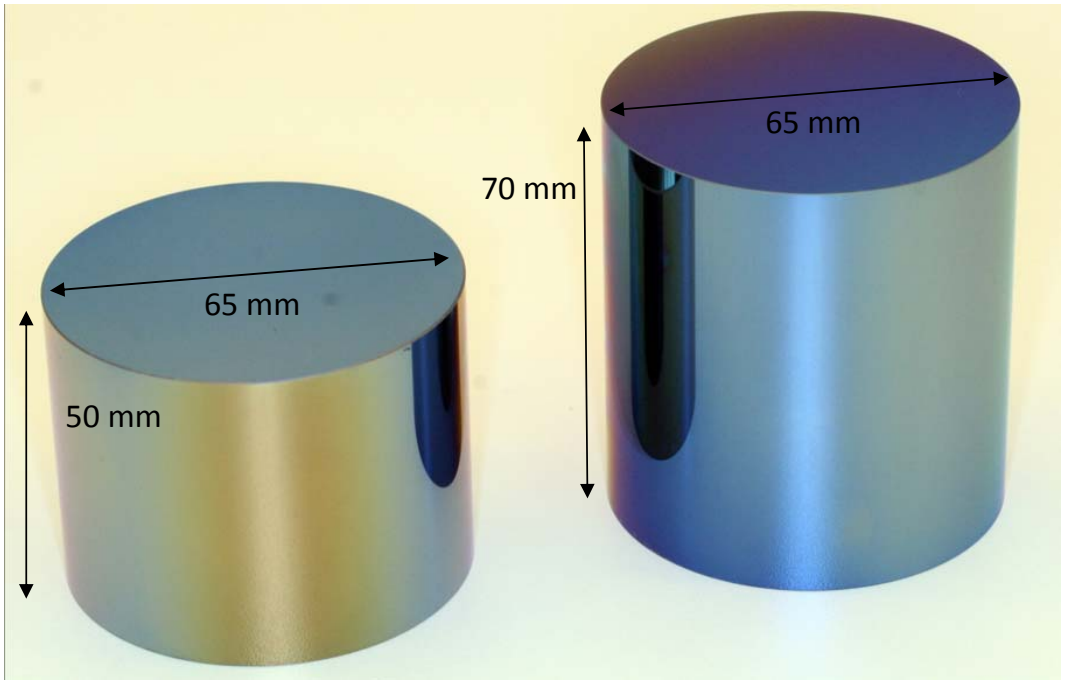

Figure 5.18: Silicon <100> samples with oxide layers.

suggesting that it is made from silicon and not silica. A possible explanation could be that the raised area occurred due to the samples being bumped against the silica boat when it was being taken out of the oven. As silicon becomes increasingly ductile from 850°C it is more susceptible to damage [184]. The raised areas were removed by the action of placing a silica disc, which was polished to a flatness of $\lambda/10$ by General Optics [119], and moving it across the raised area. This caused the raised part to be chipped off. The raised part on the 70 mm sample was completely removed, however the height of the raised area on the 50 mm sample was not completely removed. It was greatly reduced to a height of $\sim$ 300 nm while the diameter remained at $\sim$ 1 mm. The presence of the remainder of the raised area can be seen from the fringe pattern visible in figure 5.19. It was thus decided to offset the samples by 2 mm when bonding in order to have the remaining raised area outside the bond as the remaining raised area would still have been detrimental to the creation of a successful bond. If the raised area had been within the bond it could

potentially be a source of additional friction and hence increase the loss of the sample and affect the overall reliability and strength of the bond.

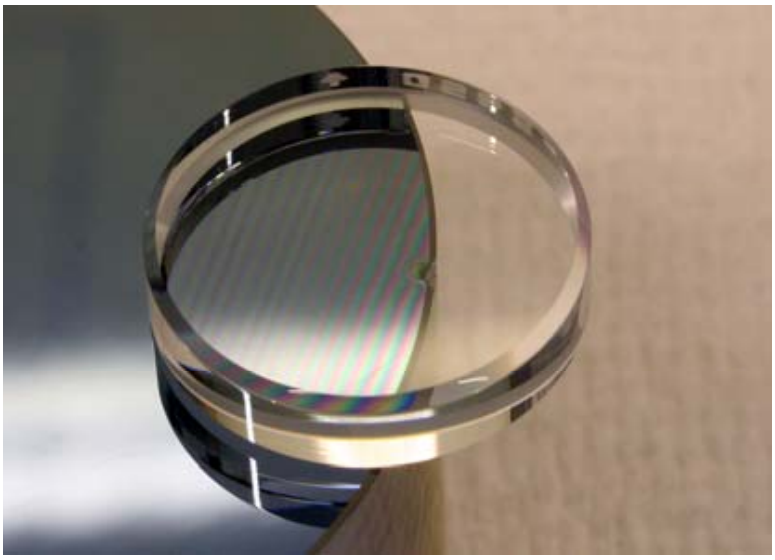

Figure 5.19: Silicon <100> , 65 mm diameter and 50 mm long mass with a raised area removed, a flat polished to $> \lambda/10$ on top of chip to show fringes. The fringes go around the chip in a bow, indicating part of the raised area is still present.

The mechanical loss of the samples after the raised areas were removed was measured. The samples were re-oxidised ensuring that the surfaces to be bonded were not touching the silica boat, and the boat was slid into and removed from the oven at a very slow rate. This process did not result in any additional raised areas on the surfaces to be bonded. After the second oxidisation the oxide thickness of the 50 mm sample was measured to be 171 $\pm$ 0.5 nm and the oxide thickness of the 70 mm sample was 317 $\pm$ 0.5 nm using a Sentech 850 laser ellipsometer [182]. Two measurements were taken of a face of the sample and these were averaged. The difference in thickness could be due to the higher saturation level of the nitrogen with water vapour in the oven during the oxidation of the 70 mm sample. This may induce a faster growth rate as the water is the oxidising agent [181].

The measured mechanical losses of a set of resonant modes the 50 mm and

70 mm samples before and after the oxidisation process are shown in figures 5.20 and 5.21 respectively. After the second oxidisation the mechanical loss of each resonant mode of silicon decreased. This could be due to the effect of the heat treatment associated with the growth of the oxide reducing any internal stresses [125]. Another possible explanation is that the chemical cleaning and etching process had removed a lossy surface layer. The 120 mm sample was oxidised and then chemically etched. The mechanical loss was measured after the chemical etch. The resultant mechanical loss values obtained are shown in figure 5.22.

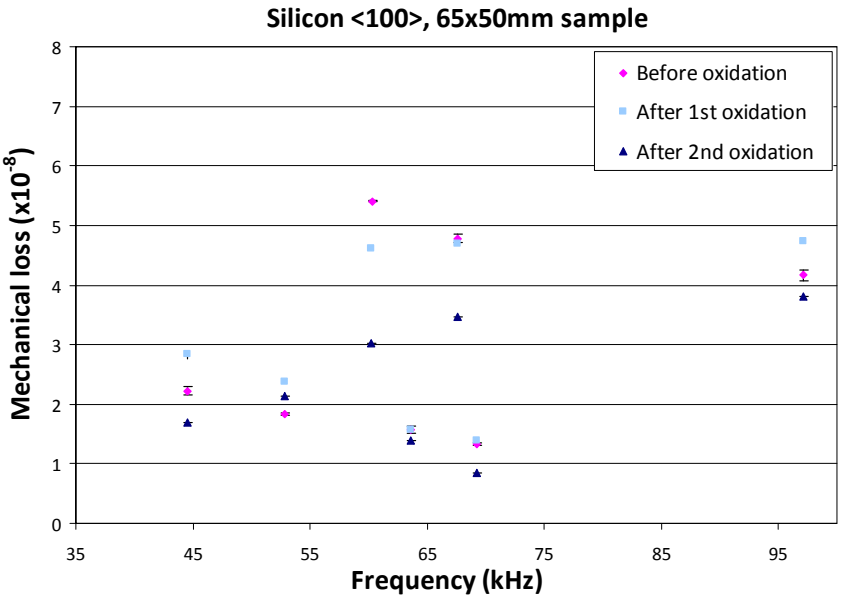

Figure 5.20: Mechanical loss of silicon <100> 50 mm sample before and after oxide layers were grown on all surfaces.

It can be seen that as previously, the effect of the first oxidisation step was to decrease the measured loss. The mechanical loss then increased after the etching process and then decreased again after re-oxidisation. This is consistent with the results reported earlier of the effect of a hydrofluoric acid etch the measured loss of fused silica. The results are suggestive of the increased loss due to etching being a result of an associated increase in contact friction at the

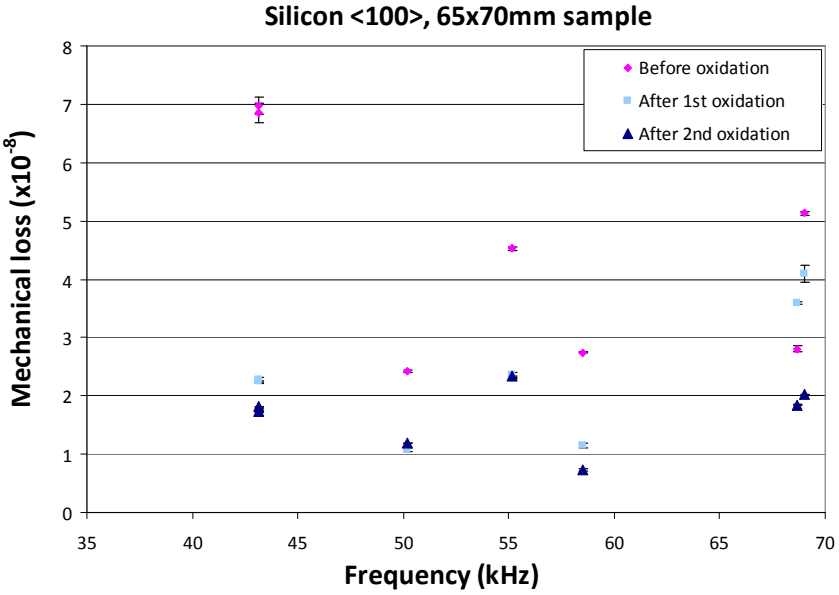

Figure 5.21: Mechanical loss of silicon <100> 70 mm sample before and after oxide layers were grown on all surfaces.

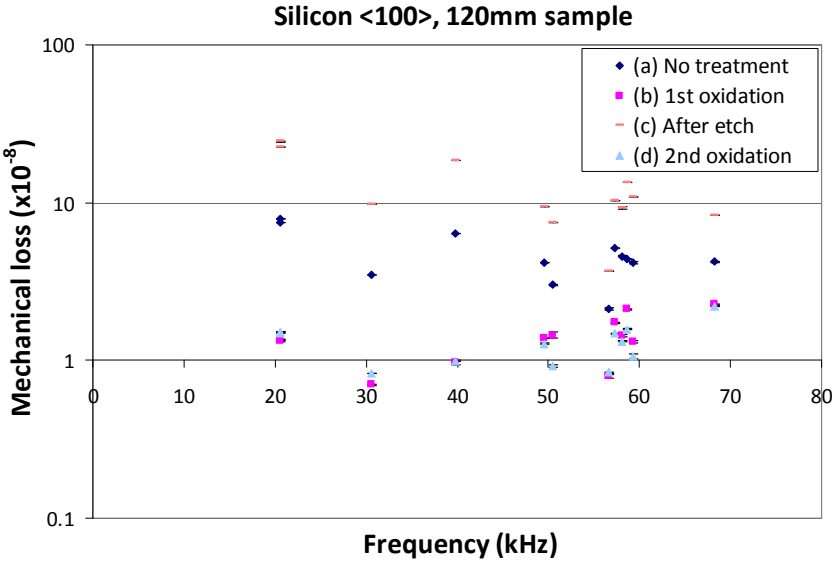

Figure 5.22: Mechanical loss of silicon <100> 120 mm sample before and after oxide layers were grown and after etch.

surfaces of the samples. Research carried out by Lunin [140] suggests that the reactant products of the etching process are left on the surface of the sample

as 'silica salts', which may be removed using sulphuric acid.

5.5 Effect of Bonding on the Mechanical Loss

5.5.1 Introduction

In order to measure the mechanical loss of a hydroxy-catalysis bond formed between silicon substrates, the 50 mm long and 70 mm long <100> samples which are discussed in section 5.4.2 were to be bonded together and the loss of the bonded sample measured. The 120 mm long sample discussed in section 5.4.2 can be used as a reference sample to provide the mechanical loss of a single substrate without the bond. As discussed in section 5.3.2, the resonant mode shapes of silicon have specific orientations with respect to the crystal axes. Thus, it is desirable to orient the crystal axes of the two samples to be bonded together such that they are co-aligned to allow the resultant resonant mode shapes of the bonded sample to match that of the reference sample. Only by comparing the loss measured for the same resonant mode will an accurate value of the loss of the bond be provided.

The loss of the bonded sample, ϕ_{bonded} can be considered to be the sum of three loss components [185],

$$\phi_{\text{bonded}} \simeq \frac{E_{\text{substrate}}}{E_{\text{total}}}\phi_{\text{substrate}} + \frac{E_{\text{bond}}}{E_{\text{total}}}\phi_{\text{bond}} + \frac{E_{\text{oxide}}}{E_{\text{total}}}\phi_{\text{oxide}} \tag{5.1}$$

where $\phi_{\text{substrate}}$ is the mechanical loss measured for the reference sample, ϕ_{bond} is the mechanical loss of the hydroxy-catalysis bond, ϕ_{oxide} is the loss of the oxide layer, $\text{E}_{\text{substrate}}/\text{E}_{\text{total}}$ is the ratio of strain energy stored in the substrate to the total strain energy in the system and $\text{E}_{\text{bond}}/\text{E}_{\text{total}}$ is the ratio of strain energy stored in the bond to the energy stored in the whole system. As the substrate is much larger than the bond and oxide layers $\text{E}_{\text{total}} \simeq \text{E}_{\text{substrate}}$, thus $\frac{E_{\text{substrate}}}{E_{\text{total}}} \sim 1$. Equation 5.1 can then be rearranged to express the mechanical loss of the hydroxy-catalysis bond, ϕ_{bond}, as:

$$\phi_{\text{bond}} \simeq \frac{\phi_{\text{bonded}} - \phi_{\text{substrate}} - \frac{E_{\text{oxide}}}{E_{\text{total}}}\phi_{\text{oxide}}}{\frac{E_{\text{bond}}}{E_{\text{total}}}} \tag{5.2}$$

Thus, to calculate ϕ_{bond}, finite element analysis must be carried out to obtain values for $\frac{E_{\text{bond}}}{E_{\text{total}}}$ and $\frac{E_{\text{oxide}}}{E_{\text{total}}}$, and a value for ϕ_{oxide} must be obtained. This will be discussed further in sections 5.5.4 and 5.5.6.

5.5.2 Crystal Axis Alignment and Hydroxy-Catalysis Bonding

The relative orientations of the crystal axes of both samples were determined using the following experimental set-up shown in figure 5.23. The motion of each sample was excited with a piezoelectric transducer which was driven at a frequency corresponding to each resonant frequency of the sample in turn. Lycopodium (pollen) was sprinkled on the top surface of the sample. When the sample was excited at a resonant frequency the pollen would move away from the places on the surface which had the largest amplitude of motion to the places with least motion, showing the shape of the resonant mode. The mode shape known as a "clover 4" (16, n=2) following the numbering classification of McMahon [186] to denote the symmetry classification of the mode was used to align the 70 mm and 50 mm samples of <100> silicon which are to be bonded together for the bond loss experiment. These mode shapes are shown in figure 5.24. All other mode shapes found were used to improve the accuracy of the relative alignment of the crystal axes of both samples with respect to each other to $\pm 3°$.

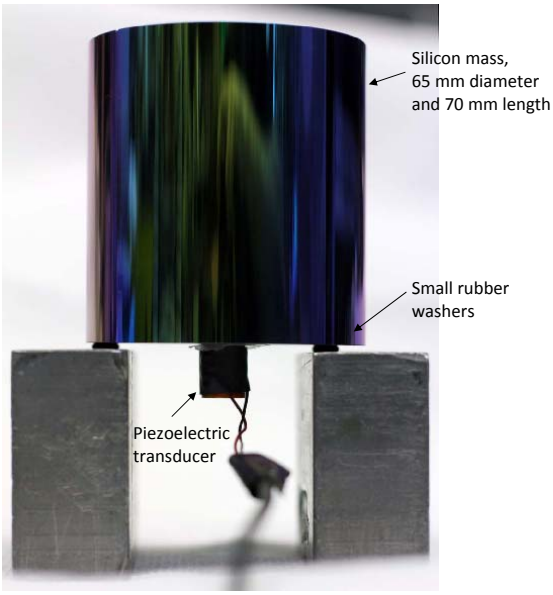

Figure 5.23: A silicon mass with a piezoelectric transducer attached to excite the mass at its resonant frequencies. Lycopodium is sprinkled on the top surface and as the sample is excited the lycopodium moves to reveal the mode shape.

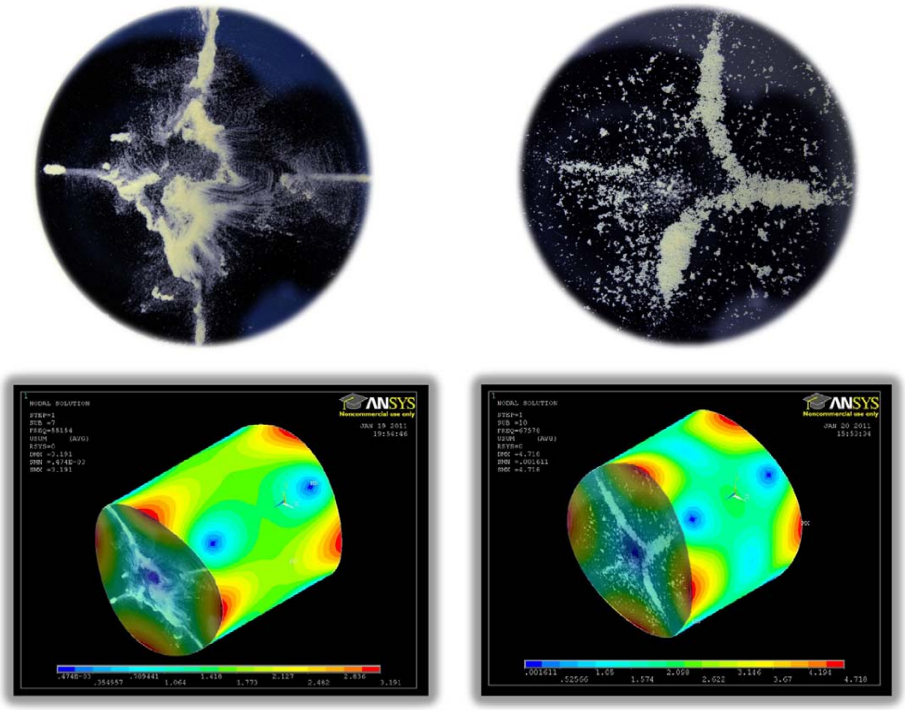

Figure 5.24: Resonant modes at 55.154 kHz and 67.578 kHz, observed on the two bonding surfaces that were positioned using lycopodium in order to align the relative crystal axes for bonding.

5.5.3 Bonding Process

Each of the two samples had an SiO_2 layer applied to their surfaces to enable the creation of a reliable bond as discussed previously in detail in section 5.4.2. After the oxidisation process the flatness of the two surfaces which were to be bonded was measured using a ZYGO GPI XP/D interferometer [110]. The global flatness of the bonding surface of the 50 mm long sample was 118.6 ± 0.05 nm and the flatness of the bonding surface of the 70 mm long sample was 118.4 ± 0.05 nm. This is an important parameter as it can aid the calculation of possible bond thickness.

Both surfaces which were to be bonded were cleaned using the method described in section 3.3. The faces of the sample, with diameter 65 mm, were jointed using hydroxy-catalysis bonding using 12.2 µl of bonding solution to allow 0.4µl of solution per cm^2 of bonding area of 1:6 sodium silicate solution as has been determined to be appropriate for use in the construction of suspensions for the Advanced LIGO mirrors. This was then left for a minimum of 4 weeks to allow the bond to cure.

Figure 5.25 shows the 50 mm and 70 mm silicon <100> samples after they were hydroxy-catalysis bonded.

5.5.4 Finite Element Analysis of Bonded Silicon Sample

The strain energy ratio of the bond to the whole sample is required for calculating bond loss as is shown in equations 5.1 and 5.3. The energy ratios are calculated by performing finite element analysis of the sample using ANSYS which calculates the strain energy in each element of a model. The elements making up each component can then be summed to allow the relevant energy ratios to be calculated. In order to model the bonded sample an estimate of the bond thickness was obtained by adding the flatness values of the two bonding surfaces and dividing by two. The flatness of the two bond surfaces were 118.39 ± 0.05 nm and 118.57 ± 0.05 nm. This was measured using a ZYGO GPI XP/D interferometer [110]. This gives a maximum possible bond

Figure 5.25: Bonded silicon <100> samples.

thickness of $\sim$ 236.96 nm and a minimum possible bond thickness of $\sim$ 118.48 nm. As this is a very thin layer the CFX mesh in ANSYS workbench was used for modelling [187]. This type of mesh overrides the shape checking in the model to allow for very thin layers to be modelled as solid elements. This allows for the thin (of order 100 nm) bond and oxide layers to be modelled as solids. Solid185 elements were used. This method of using a CFX mesh has been shown to agree with an extrapolation method [187] which has previously been used for calculating bond loss and is discussed in [188]. The extrapolation method involves models being generated with different bond thicknesses between $\sim$ 0.5 and 1 mm. The energy ratio for each thickness is obtained and plotted against bond thickness. This graph can be extrapolated to obtain the energy ratio for the small bond thickness required. Figure 5.26 shows a picture of the model with the isolated bond region.

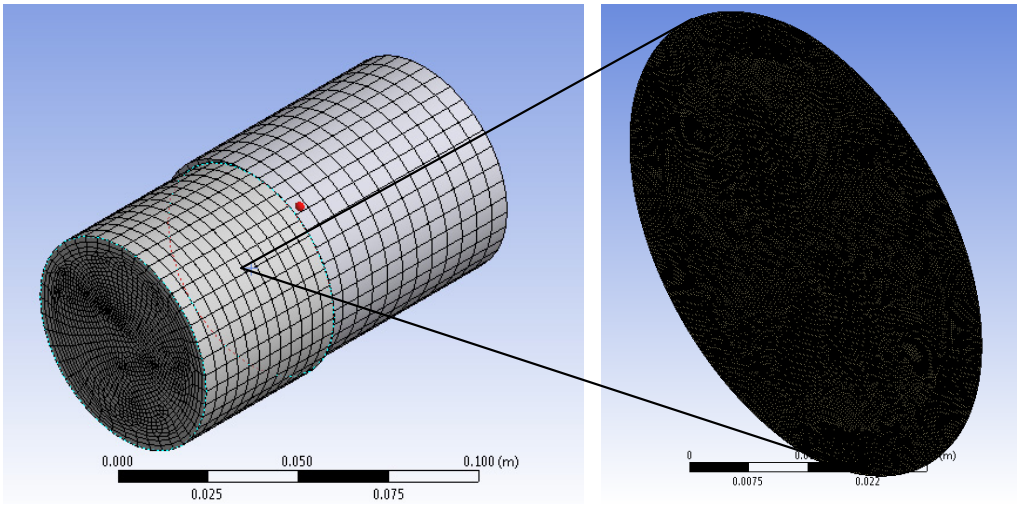

Figure 5.26: Finite element model of the 65 mm diameter by 120 mm long (offset) bonded silicon <100> mass, and isolated bond region.

The strain energy in each component of the bonded mass was calculated. The strain energy ratios, $\frac{E_{\text{bond}}}{E_{\text{total}}}$ and $\frac{E_{\text{oxide}}}{E_{\text{total}}}$ were calculated for the measured resonant modes. The energy ratios are shown in figure 5.3 and the mode shapes of the measured resonant frequencies are shown in figure 5.27.

5.5.5 Measurement of a Hydroxy-Catalysis Bonded Silicon Mass

Mechanical loss measurements were made for 6 resonant modes of the bonded silicon masses using the experimental set-up described in section 4.2. The measured resonant frequencies of the bonded sample are compared to the resonant frequencies predicted by model in table 5.4. The 120 mm long silicon <100> mass which is discussed in section 5.4.2 is the control mass and therefore provides the mechanical loss of the substrate material which is used to calculate the loss of the bond.

After the bond had cured for 14 weeks the mechanical loss of the bonded sample was measured using the same technique as described in section 4.2. The bonded sample was suspended 17 times at arbitrary rotations using silk

	If bond is $\sim$ 118 nm		If bond is $\sim$ 237 nm	
Frequency (Hz)	Bond Energy Ratio ($\times 10^{-5}$)	Oxide Energy Ratio($\times 10^{-5}$)	Bond Energy Ratio ($\times 10^{-5}$)	Oxide Energy Ratio($\times 10^{-5}$)
20,513	4.09	1.73	8.20	1.73
20,526	3.57	1.53	7.21	1.54
49,532	0.43	0.34	0.84	0.33
50,486	0.31	0.13	0.62	0.13
57,228	0.39	0.24	0.74	0.23
58,110	0.42	0.18	0.79	0.17

Table 5.3: Ratio of strain energy stored in the($\sim$ 180 nm) bond region of six resonant modes of the 65 mm diameter by 120 mm long bonded <100> silicon cylinder modelled using solid185 elements.

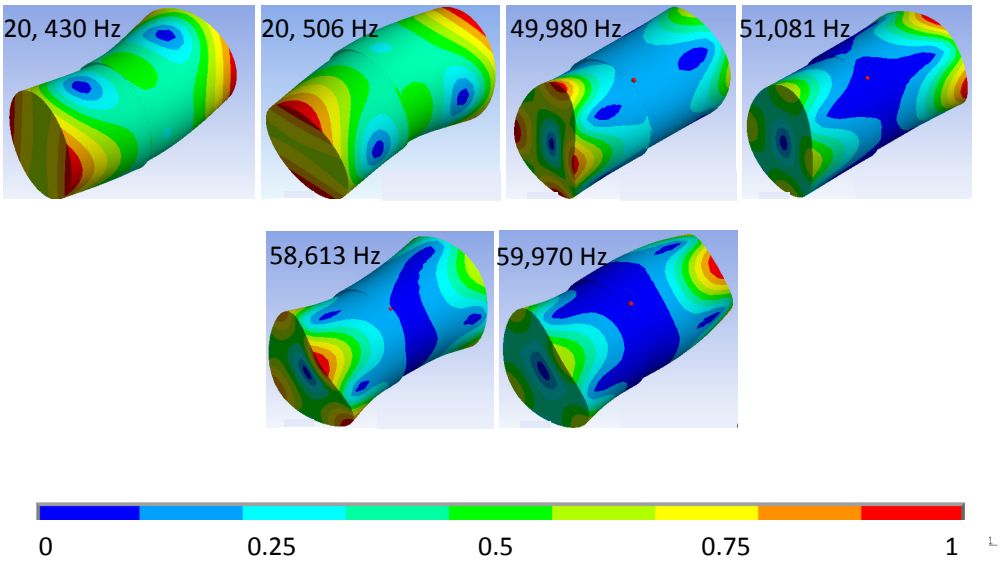

Figure 5.27: Resonant mode shapes of the measured frequencies of a bonded silicon sample of 120 mm in length (50 mm and 70 mm samples bonded together). The amplitude of motion is relative and indicated using colour where blue indicates the smallest amplitude of motion and red indicates the largest amplitude of motion.

Experimentally Measured Freq (Hz)	Modelled Freq (Hz)
20,513	20,430
20,526	20,506
49,532	49,980
50,486	51,081
57,228	58,613
58,110	59,970

Table 5.4: Comparison of experimentally measured resonant frequencies to those modelled in ANSYS of the 65 mm diameter by 120 mm long bonded silicon <100> cylinder.

thread as a suspension material. The length of the thread was altered for different suspensions to reduce excess suspension loss. Three ringdowns were recorded for each resonant frequency and the loss values were averaged to give the mechanical loss for the resonant mode. The lowest mechanical loss values obtained for each of the resonant modes of the bonded sample is shown in figure 5.28(a) and the lowest loss values measured for each resonant mode of the reference sample are shown in figure 5.28(b).

The lowest mechanical loss of the bonded sample is higher than that of the reference sample, suggesting additional loss from the hydroxy-catalysis bond is of a measurable level.

5.5.6 Calculation of Bond Loss

The mechanical loss values for each of the six measured resonant modes of the bonded silicon sample are shown in table 5.5 and the loss values for the equivalent modes for the reference sample are shown in table 5.6.

These loss values along with the strain energies obtained from ANSYS were substituted into,

$$\phi_{\text{bond}} \simeq \frac{\phi_{\text{bonded}} - \phi_{\text{substrate}} - \frac{E_{\text{oxide}}}{E_{\text{total}}}\phi_{\text{oxide}}}{\frac{E_{\text{bond}}}{E_{\text{total}}}} \tag{5.3}$$

to obtain the calculated value for the bond loss of each resonant mode. The parameters used for the bond loss calculation for each resonant mode are shown

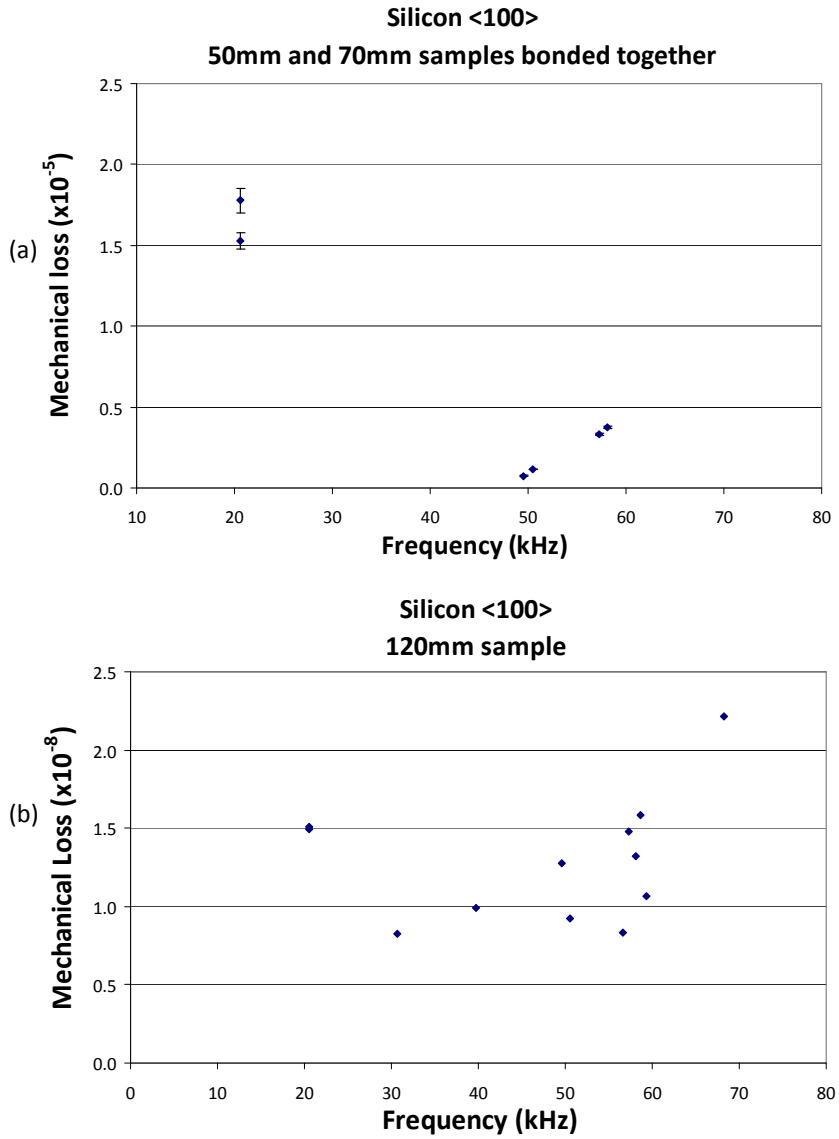

Figure 5.28: (a) Mechanical loss of the silicon <100> bonded sample (b) reference sample as a function of frequency.

in table 5.3 and table 5.7. The mechanical loss of the oxide layers was estimated to be $\sim 5.8 \pm 0.05 \times 10^{-5}$. This is the loss predicted using the empirical model which was discussed in section 4.3 for a silica layer with the measured oxide layer thickness. Oxide loss has never been quantified at room temperature however, at low temperatures the oxide loss has been shown to follow the loss-temperature curve of bulk silica [189]. Thus, it is reasonable to assume that

Frequency (Hz)	ϕ_{bonded} ($\times 10^{-5}$)
20,513	1.78 ± 0.07
20,526	1.53 ± 0.05
49,532	0.07 ± 0.01
50,486	0.11 ± 0.01
57,228	0.33 ± 0.01
58,110	0.37 ± 0.01

Table 5.5: Lowest measured mechanical losses of six resonant modes of the 65 mm diameter by 120 mm long bonded <100> silicon cylinder after oxidisation.

Frequency (Hz)	$\phi_{\text{substrate}}$ ($\times 10^{-8}$)
20,551	1.51 ± 0.01
20,552	1.49 ± 0.02
49,563	1.27 ± 0.01
50,526	0.92 ± 0.02
57,301	1.48 ± 0.01
58,155	1.32 ± 0.02

Table 5.6: Lowest measured mechanical losses of six resonant modes of the 65 mm diameter by 120 mm long reference <100> silicon cylinder after oxidisation.

the oxide loss will follow the empirical model at room temperature. A value for the overall bond loss is determined by averaging the bond loss values obtained for each of the resonant modes measured. These values are presented in table 5.8.

Using the equations 5.1 and 5.3 a range of possible values of bond loss is calculated to be 0.27 - 0.52. This value for the mechanical loss of a hydroxy-catalysis bond created between silicon substrates is below the upper limit which had previously been calculated as 1.39 ± 0.94 [190].

Frequency (Hz)	ϕ_{bonded} ($\times 10^{-5}$)	ϕ_{substate} ($\times 10^{-8}$)
20,479	1.78 ± 0.07	1.51 ± 0.01
20,510	1.53 ± 0.05	1.49 ± 0.02
49,558	0.07 ± 0.01	1.27 ± 0.01
50,485	0.12 ± 0.01	0.92 ± 0.02
57,228	0.33 ± 0.01	1.48 ± 0.01
58,084	0.37 ± 0.06	1.32 ± 0.02

Table 5.7: Lowest measured mechanical loss values for each of 6 resonant modes of the bonded and reference silicon <100> sample.

	If bond thickness is ∼ 118 nm	If bond thickness is ∼ 237 nm
Frequency (Hz)	Bond Loss	Bond Loss
20,512	0.435 ± 0.01	0.217 ± 0.01
20,536	0.428 ± 0.01	0.212 ± 0.01
49,530	0.169 ± 0.01	0.085 ± 0.01
50,486	0.370 ± 0.01	0.183 ± 0.01
57,229	0.846 ± 0.01	0.446 ± 0.01
58,084	0.891 ± 0.01	0.471 ± 0.01

Table 5.8: Bond losses of 6 resonant modes of the 65 mm diameter by 120 mm long bonded <100> silicon cylinder calculated using the two extremes of bond thickness, 118 nm and 237 nm and the measured mechanical losses of the 120 mm long substrate cylinder.

5.6 Conclusion

The mechanical loss of silicon is less than that of silica at room temperature. This makes silicon a promising candidate for future generation gravitational wave detectors.

The mechanical loss of <111> silicon has been seen to be lower than the mechanical loss of <100> silicon before heat treatment.

The mechanical loss of a hydroxy-catalysis bond between silicon substrates is found to be between 0.27 and 0.52. This is larger than the mechanical loss of hydroxy-catalysis bonds created between silica substrates, which was

calculated in chapter 4 to be 0.06 ± 0.01. However, the offset nature of the two samples introduced an undesirable geometry where excess losses at the overlapped edge of the bonded samples could occur. Excess loss could also be introduced at the interfaces of the bonds and the oxide layers. Further investigations into the effect of these additional layers would be of interest.

Thus the stated value for the mechanical loss of a hydroxy-catalysis bond between silicon substrates is an upper limit, and aspects of this experiment could in future be optimised. Techniques learned from this experiment, such as the best method of oxidising silicon, could be implemented in future experiments to obtain a more accurate bond loss value.

Chapter 6

Conclusions

The current network of gravitational wave detectors around the world is nearing design sensitivity and detection of gravitational waves from astrophysical sources becomes more likely than ever before. However, there is a lot of research and development still being carried out with the aim of upgrading the current and advanced detectors and designing more sensitive third generation instruments which should guarantee detection and will have an increased detection rate. This will provide more information on the sources and will allow for large scale astronomical observations.

Much of the current research is aimed at reducing the thermal noise of the mirror suspensions as this is one of the dominant noise sources in the current operating frequency band. The fluctuation-dissipation theorem [75, 76] is an extremely useful tool for predicting thermal noise levels and providing an insight into methods of thermal noise reduction.

One method of increasing the sensitivity of the longer base-line interferometric gravitational wave detectors is by the introduction of the monolithic suspensions created for the GEO600 detector. This suspension system makes use of fused silica, which has a low mechanical loss, and a low mechanical loss bonding method to join the components. This bonding technique, hydroxy-catalysis bonding, is a strong, reliable method of joining the elements of the suspension by creating chemical bonds between them.

In this thesis hydroxy-catalysis bonds created between silica substrates have

been shown to have an average strength of 14.8 ± 0.8 MPa. These bonds can withstand great amounts of heat without degrading and it is possible to create bonds which are optically clearer and stronger through different processes, such as loading and annealing. Bonds which are optically clearer generally have a smaller spread in the strength results obtained. Short heat treatments, $\sim$ 3 minutes, are seen to degrade the optical clarity of the bond. However heating the sample for longer periods does not. Heat treating to 150 °C for 48 hours increases the strength by a factor of $\sim$ 1.9. This heat treatment also has been shown to reduce the mechanical loss of the bonded silica sample making it a good treatment for the suspension on two counts. It is also shown that the mechanical loss of a hydroxy-catalysis bond can decrease over time.

For Advanced LIGO, the material chosen for the mirrors was changed from Suprasil 312 to Suprasil 3001 as it has better optical properties. Measurements were taken to show that this change in material slightly increases the bulk thermal noise of a mirror substrate from 1.3×10^{-21} to 1.6×10^{-21} m per $\sqrt{\text{Hz}}$ at 100 Hz. This level of thermal noise is still well below the coating thermal noise level, hence, the overall sensitivity of the detector is not affected.

A method of chemically etching the surface of silica fibres is shown to be a possible technique to reduce the mechanical loss of the sample by reducing the lossy surface layer. However, the technique has not yet been successful in the measurements on bulk silica samples. Etching causes an increased roughness of the surface of samples. When a bulk sample is suspended to allow the mechanical loss to be measured this increased roughness at the suspension points could contribute excess loss. Thus, further investigations are required to quantify this effect. The chemical etching process looks like a promising technique for reducing the loss of silica components. However, further development in the final surface condition of the samples must be improved before this chemical etching process can be used on the optics in advanced gravitational wave detectors for which the optical properties can depend on the roughness of the surface.

A possible technique considered for third generation gravitational wave detectors is to cool the mirrors and the suspensions to reduce thermal noise. Silicon is being studied as a possible material for these detectors and has been shown in this thesis to have a mechanical loss ~ 7 times less than that of fused silica at room temperature. Its mechanical loss decreases by a factor of ~ 4 as the temperature decreased to ~ 5 K [191]. Thus, it is a promising candidate for cryogenically run gravitational wave detectors. Research here suggests that heat treating silicon to 1000 °C for 45 minutes decreases the mechanical loss. This is thought to be due to the removal of surface defects or due to the sample being annealed and stresses being removed. Preliminary studies here suggest that different crystal orientations of silicon have different mechanical loss values. Silicon which is cut with a <100> orientation was found to have a measured mechanical loss which is a factor of ~ 1.33 times greater than <111> silicon at room temperature, however, it is yet to be determined whether this is due to suspension effects or effects intrinsic to the material.

The bonding process used to join the elements of the suspension also contributes loss to the system and this has to be quantified. In order to enable a hydroxy-catalysis bond to be created between silicon substrates a thermal oxide layer has to be grown on the bonding surfaces. A range of possible values of the mechanical loss of a hydroxy-catalysis bond between silicon substrates was measured and calculated to be 0.27 - 0.52. While the mechanical loss of hydroxy-catalysis bonds created between silica substrates is shown to be 0.06 ± 0.01. Further investigations should give a more accurate mechanical loss value and a better understanding of the loss difference in bonds created between silica substrates and silicon substrates will be gained.

The research presented in this thesis was an extension of experimental work carried out at the University of Glasgow and within the gravitational wave community.

The detection of gravitational waves grows closer as current detectors are upgraded to greater sensitivities and progress is made in designing third gen-

eration detectors. When gravitational waves are detected a new window into astronomy will be created.

Appendix A

Calculating the Thickness of the Hydroxy-Catalysis Bond

A calculated estimate of the thickness of a hydroxy-catalysis bond can be made using the properties of the bonding solution and its chemical components. The estimated bond thickness of a sodium silicate bond is calculated in this appendix. Some important densities, ρ, which are required for the calculation are:

- $\rho_{\text{silicate solution}} = 1.53\text{g/cm}^3 = 1530\text{kg/m}^3$
- $\rho_{\text{water}} = 1\text{g/cm}^3 = 1000\text{kg/m}^3$
- $\rho_{SiO_2} = 2202\text{kg/m}^3$

Table A.1 shows the chemical content of the sodium silicate bonding solution.

Chemical	%
NaOH	14
SiO_2	27
H_2O	59

Table A.1: Chemical composition of sodium silicate bonding solution

The mass of silica in the bond is calculated first:

To create a hydroxy-catalysis bond, sodium silicate is diluted with de-ionised water at a ratio of 1:6, so we can find the density of the bonding solution to be,

$$\rho_{\text{bonding solution}} = \frac{1 \times 1.53 + 6 \times 1}{7} = 1.0757\text{g/m}^3 = 1075.7\text{kg/m}^3, \quad \text{(A.1)}$$

From the density and volume of $0.4{\times}10^{-9}\text{m}^3$, ($0.4\mu l/cm^2$ for 1×1 cm) the mass can be calculated,

$$\text{Mass of the bonding solution} = \rho\text{V} = 1075.7 \times 0.4 \times 10^{-9} = 4.2308 \times 10^{-7}\text{kg}, \quad \text{(A.2)}$$

Only 1/7th of the bonding solution is sodium silicate,

$$\text{Mass of the sodium silicate} = \frac{4.2308 \times 10^{-7}}{7} = 6.044 \times 10^{-8}\text{kg}, \quad \text{(A.3)}$$

Sodium silicate is 27% SiO_2 therefore the mass of silica is calculated to be,

$$SiO_2 = 6.044 \times 10^{-8}\text{kg} \times 0.27 = 1.63188 \times 10^{-8}\text{kg} \quad \text{(A.4)}$$

Thickness of SiO_2:

The volume of SiO_2 can then be calculated using the mass and density,

$$V = \frac{m}{\rho} = \frac{1.63188 \times 10^{-8}}{2202} = 7.4109 \times 10^{-12}\text{m}^3, \quad \text{(A.5)}$$

The volume can then be divided by the bond area, which is 1 cm × 1 cm for the amount of solution entered in these equations and we find the thickness to be,

$$t_{SiO_2} = \frac{V}{A} = \frac{7.4109 \times 10^{-12}}{0.01 \times 0.01} = 7.4109 \times 10^{-8}\text{m} \approx 74\text{nm}, \quad \text{(A.6)}$$

The average thickness for a hydroxy-catalysis bond created using sodium silicate between silica substrates has been measured to be 61 ± 4 nm [106], which appears to be a relatively good match to the measured value. It is not clear if the starting volume determines the final thickness of the bond. However, this shows that $0.4\mu l/cm^2$ should certainly be about the right amount of solution to create a strong bond.

Appendix B

De-bonding

'Ears' have to be bonded to the silica masses for gravitational wave detector suspension systems to allow for a monolithic suspension to be created using silica fibres. It is possible to create a bond that does not fully connect the two surfaces. This could be caused by a bubble of hydrogen or air being trapped in the bond or a speck of dust for example. If an imperfect bond is created the ear will have to be de-bonded to allow for a perfect bond. However, as hydroxy-catalysis bonds are so strong and stable, de-bonding is extremely difficult once the bond has cured.

Different methods of de-bonding were investigated. Thermal shocking the bonds, soaking them in different chemicals such an alkaline detergeant, Micro90® and a paint stripper: Nitromors, which is manufactured in the UK by Henkel Consumer Adhesives at different temperatures, exposing the bond to ultra violet radiation and driving a razor blade using a piezoelectric transducer into the edge of the bond while submerged in boiling water were methods that were tested on several bonds of different ages. It was found that de-bonding is possible for up to 14 hour old bonds using de-ionised water. Adding micro90 to the de-ionised water and placing the sample in an ultrasonic bath speeds up the process by a few minutes. Samples which have been bonded for less than 14 hours should take $\sim$ 10 minutes to de-bond. After a bond has been curing for 14 hours the bond is stronger and more aggressive methods have to be investigated as techniques for de-bonding.

When trying to replace a bond there are more difficulties than just the removal. The original bond will have caused etching on the mass and this can affect the flatness of the surface. If the surface is not flat it could be difficult to create a proper bond or the bond created may have a reduced strength. Therefore this flatness is essential for the large interferometers. No correlation was found between the change in flatness and the age of the bond up to 14 hours old.

The procedure for debonding in Advanced LIGO now includes thorough inspection routines over the first 8 hours following the bonding procedure. This period is more than long enough to decide wether a bond is acceptable for use or not. Also, if a bond is found to be unacceptable in this time it is relatively easy to debond the ear and any damage to the mass is minimal allowing for another bond to be created on the surface.

Bibliography

[1] A. Einstein. *Die Grundlage der allgemeinen Relativitatstheorie. Annalen der Physik*, **49**:769, 1916.

[2] R.A. Hulse. *The discovery of the binary pulsar(PSR 1916 +13). Reviews of Modern Physics*, **66**:699, 1994.

[3] J.H. Taylor. *Binary pulsars and relativistic gravity. Reviews of Modern Physics*, **66**:711, 1994.

[4] J. Weber. *Evidence for discovery of gravitational radiation. Physical Review Letters*, **22**:1320–1324, 1969.

[5] P. R. Saulson. *Fundamentals of Interferometric Gravitational Wave Detectors*. World Scientific, Singapore, 1994.

[6] M. Gilfanov and Á. Bogdán. *An upper limit on the contribution of accreting white dwarfs to the typeIa supernova rate. Nature*, **463**:924–925, 2010.

[7] C. D. Ott. *The gravitational-wave signature of core-collapse supernovae. Classical and Quantum Gravity*, **26**(6), 2009.

[8] B. Schutz. *Determining the Hubble Constant from Gravitational Wave Observations. Nature*, **323**:310–311, 1986.

[9] A. Hewish, S. J. Bell, J. D. H. Pilkington, et al. *Observation of a Rapidly Pulsating Radio Source. Nature*, **217**:709–713, 1968.

[10] K. S. Thorne. *Proceedings of the Snowmass '94 Summer Study on Particle and Nuclear Astrophysics and Cosmology. World Scientific, Singapore*, 1995.

[11] J. L. Friedman and B. F. Schutz. *Secular instability of rotating Newtonian stars. Astrophysical Journal*, **222**:281–296, 1978.

[12] R. V. Wagoner. *Gravitational radiation from accreting neutron stars. Astrophysical Journal*, **278**:345–348, 1984.

[13] J. Hough, H. Walther, B. F. Schutz, et al. *Proposal for a joint German-British Interferometric gravitational wave detector. Max-Planck-Institut für Quantenopik Report*, **147**, 1989.

[14] B. P. Abbott, R Abbott, R Adhikari, et al. *LIGO: the Laser Interferometer Gravitational-Wave Observatory. Reports on Progress in Physics*, **72**(7), 2009.

[15] M. Cerdonio, L. Franceschini G., Fontana, et al. *Status of the AURIGA gravitational wave antenna and perspectives for the gravitational waves search with ultracryogenic resonant detectors.* In *Gravitational Wave Experiments*, pages 176–194, 1995.

[16] P. Astone, M. Bassan, P. Bonifazi, et al. *The gravitational wave detector NAUTILUS operating at T = 0.1 K. Astroparticle Physics*, **7**:231–243, 1997.

[17] A. Abramovici W. E. Althouse, R. W. P. Drever, et al. *LIGO - The Laser Interferometer Gravitational-Wave Observatory. Science*, **256**:325–333, 1992.

[18] C. Bradaschia, R. del Fabbro, A. di Virgilio, et al. *The VIRGO Project: A wide band antenna for gravitational wave detection. Nuclear Instruments and Methods in Physics Research A*, **289**:518–525, 1990.

[19] H. Lück and the GEO600 Team. *The GEO600 project. Classical and Quantum Gravity*, **14**:1471–1476, 1997.

[20] K. Tsubono and The TAMA Collaboration. *TAMA Project.* In *Gravitational Wave Detection*, page 183, 1997.

[21] G. Hobbs, A. Archibald, Z. Arzoumanian, et al. *The International Pulsar Timing Array project: using pulsars as a gravitational wave detector. Classical and Quantum Gravity*, **27**(8):084013, 2010.

[22] G. Hobbs, A. Archibald, Z. Arzoumanian, et al. *The International Pulsar Timing Array project: using pulsars as a gravitational wave detector. Classical and Quantum Gravity*, 27(8):084013, 2010.

[23] G. H. Janssen, B. W. Stappers, , M. Kramer, et al. European pulsar timing array. In *40 Years of Pulsars: Millisecond Pulsars, Magnetars and More*, volume **983** of *American Institute of Physics Conference Series*, pages 633–635, 2008.

[24] F. Jenet, L. S. Finn, J. Lazio, et al. *The North American Nanohertz Observatory for Gravitational Waves. arXiv:0909.1058v1 [astro-ph.IM]*, 2009.

[25] R. N. Manchester. *The Parkes Pulsar Timing Array Project.* In *40 Years of Pulsars: Millisecond Pulsars, Magnetars and More*, volume **983** of *American Institute of Physics Conference Series*, pages 584–592, 2008.

[26] J. Weber. *Gravitational-wave-detector events. Physical Review Letters*, **20**:1307–1308, 1968.

[27] J. Weber. *Anisotropy and polarization in the gravitational-radiation experiments. Physical Review Letters*, **22**:1320, 1969.

[28] J. Weber. *Evidence for discovery of gravitational radiation. Physical Review Letters*, **25**:180, 1970.

[29] J. A. Tyson and R. P. Giffard. *Gravitational-wave astronomy. Annual Review of Astronomy and Astrophysics*, **16**:521–554, 1978.

[30] M. P. McHugh, Z. Allen, W. O. Hamilton, et al. *The ALLEGRO gravitational wave detector.* In *The Ninth Marcel Grossmann Meeting*, pages 1904–1905, 2002.

[31] P. Astone, M. Bassan, P. Bonifazi, et al. *The EXPLORER gravitational wave antenna: recent improvements and performances. Classical and Quantum Gravity*, **19**:1905–1910, 2002.

[32] P. Astone, L. Baggio, M. Bassan, et al. *IGEC2: A 17-month search for gravitational wave bursts in 2005-2007. Physical Review Letters D*, **82** (2):022003, 2010.

[33] M. Pitkin, S. Reid, S. Rowan, et al. *Gravitational Wave Detection by Interferometry (Ground and Space). Living Reviews in Relativity*, **14**(5), 2011.

[34] S. M. Merkowitz and W. W. Johnson. *Spherical gravitational wave antennas and the truncated icosahedral arrangement. Physical Review Letters D*, **51**:2546–2558, 1995.

[35] L. Gottardi, A. de Waard, O. Usenko, et al. *Sensitivity of the spherical gravitational wave detector MiniGRAIL operating at 5K. Physical Review Letters D*, **76**(10):102005, 2007.

[36] O. D. Aguiar, L. A. Andrade, J. J. Barroso, et al. *The Brazilian gravitational wave detector Mario Schenberg: status report. Classical and Quantum Gravity*, **23**:239, 2006.

[37] M. Cerdonio, L. Conti, J. A. Lobo, et al. *Wideband Dual Sphere Detector of Gravitational Waves. Physical Review Letters*, **87**(3):031101, 2001.

[38] R. L. Forward. *Wideband laser-interferometer gravitational-radiation experiment. Physics Review D*, **17**:379–390, 1978.

[39] D. Dewey, P. S. Linsay, J. Livas, and othrs. *The MIT Prototype Gravitational Wave Detector: A Status Report.* In *Bulletin of the American Astronomical Society*, volume 16 of *Bulletin of the American Astronomical Society*, page 517, 1984.

[40] R. Weiss. *MIT Quarterly Progress Report (Research Laboratory of Electronics).* **105**(54), 1972.

[41] *Max-Planck-Institut für Quantenopik.* http://www.mpq.mpg.de/mpq.html.

[42] D. Shoemaker, R. Schilling, L. Schnupp, et al. *Noise behavior of the Garching 30-meter prototype gravitational wave detector. Physical Review Letters D*, **38**(2), 1988.

[43] R. Drever, G. Ford, J. Hough, et al. *A gravity-wave detector using optical cavity sensing, Proceedings of the 9th international conference on general relativity and gravitation, edited by E. Schmutzer. Cambridge Press*, **306**, 1983.

[44] B. J. Meers. *Recycling in laser-interferometric gravitational-wave detectors. Physical Review D*, **38**(8):2317–2326, 1988.

[45] K. A. Strain and B. J. Meers. *Experimental demonstration of dual recycling for interferometric gravitational-wave detectors. Phys. Rev. Lett.*, **66**(11):1391–1394, 1991.

[46] J. Hough, S. Rowan, and B. Sathyaprakash. *The search for gravitational waves. Journal of Physics B: Atomic, Molecular and Optical Physics*, **38**:S497–S519, 2005.

[47] N. A. Robertson, M. Barton, G. Cagnoli, et al. *Advanced LIGO Suspension System Conceptual Design.* LIGO-DCC T010103, 2010.

[48] M. Punturo, M. Abernathy, F. Acernese, et al. *The third generation of gravitational wave observatories and their science reach. Classical and Quantum Gravity*, **27**(8):084007, 2010.

[49] K. Kuroda, M. Ohashi, S. Miyoki, et al. *Large-Scale Cryogenic Gravitational Wave Telescope. International Journal of Modern Physics D*, **8**: 557–579, 1999.

[50] K. Danzmann and A. Rüdiger. *LISA technology - concept, status, prospects. Classical and Quantum Gravity*, **20**:1, 2003.

[51] B. Picinbono and C. Bendjaballah. *Photoelectron Shot Noise. Journal of Mathemtical Physics*, **11**(7), 1970.

[52] W.A. Edelstein, J. Hough, J.R. Pugh, and W. Martin. *Limits to the measurement of displacement in an interferometric gravitational radiation detector. Journal of Physics E Scientific Instruments*, **11**(7):710, 1978.

[53] R. Loudon. *Quantum limit on the Michelson interferometer used for gravitational-wave detection. Physical Review Letters*, **47**:815–818, 1981.

[54] V. Giovannetti, S. Lloyd, and L. Maccone. *Quantum-Enhanced Measurements: beating the Standard Quantum Limit. Science*, **306**:1330–1336, 2004.

[55] A. Einstein. *Investigations on the Theory of Brownian Movement. New York Press*, Dover, 1956.

[56] V. B. Braginsky, M. L. Gorodetsky, and S. P. Vyatchanin. *Thermodynamical fluctuations and photo-thermal shot noise in gravitational wave antennae. Physics Letters A*, **264**:1–10, 1999.

[57] V. B. Braginsky, M. L. Gorodetsky, and S. P. Vyatchanin. *Thermo-refractive noise in gravitational wave antennae. Physics Letters A*, **271**: 303–307, 2000.

[58] M. Evans, S. Ballmer, M. Fejer, et al. *Thermo-optic noise in coated mirrors for high-precision optical measurements. Physical Review D*, **78** (10), 2008.

[59] Courtesy of ligo. http://www.ligo.caltech.edu/.

[60] http://wwwcascina.virgo.infn.it/dataanalysis/calibration/sensitivity/.

[61] Courtesy of virgo. https://wwwcascina.virgo.infn.it/.

[62] http://www.geo600.org/images/recent-and-past-sensitivity-curves-of-geo600.

[63] Courtesy of geo600. http://www.geo600.org/.

[64] S. Kawamura. *Ground-based interferometers and their science reach. Classical and Quantum Gravity*, **27**(8), 2010.

[65] LIGO scientific collaboration. *Predictions for the Rates of Compact Binary Coalescences Observable by Ground-based Gravitational-wave Detectors. Classical Quantum Gravity*, **27**, 2010.

[66] B. Willke, P. Ajith, B. Allen, et al. *The GEO-HF Project. Classical Quantum Gravity*, **23**, 2006.

[67] G. M. Harry and the LIGO Scientific Collaboration. *Advanced LIGO: the next generation of gravitational wave detectors. Classical and Quantum Gravity*, **27**(8):084006, 2010.

[68] S. Whitcomb. *Advanced LIGO, LIGO-Australia and the International Network*. Indigo - ACIGA meeting on LIGO-Australia, 2011.

[69] R. Flaminio, A.Freise, A. Gennai, et al. *Advanced Virgo White Paper*. https://wwwcascina.virgo.infn.it/advirgo/docs/whitepaper.pdf, 2005.

[70] K Kuroda. *LCGT Status. Classical Quantum Gravity*, **7**, 2010.

[71] P McNamara, S Vitale, K Danzmann, and (on behalf of the LISA Pathfinder Science Working Team). *LISA Pathfinder. Classical and Quantum Gravity*, **25**:114034 (8pp), 2008.

[72] B. Jancovici. *Statistical Physics and Thermodynamics*. McGraw-Hill Book Company Limited, 1973.

[73] R. Brown. *A brief account of microscopical observations made in the months of June, July and August, 1827, on the particles contained in the pollen of plants; and on the general existence of active molecules in organic and inorganic bodies. Edinburgh new Philosophical Journal*, pages 358–371, 1828.

[74] A. Einstein. *¨Uber die von der molekularkinetischen Theorie der W¨arme geforderte Bewegung von in ruhenden Fl¨ussigkeiten suspendierten Teilchen. Annalen der Physik*, (17):549, 1905.

[75] H. B. Callen and T. A Welton. *Irreversibility and Generalised Noise. Physical Review*, **83**:34–40, 1951.

[76] H. B. Callen and R. F. Greene. *On a Theorem of Irreversible Thermodynamics. Physical Review*, **86**:702–710, 1952.

[77] S. Twyford. *Development Towards Low Loss Suspensions for Laser Interferoemtric Gravitational Wave Detectors*. PhD thesis, University of Glasgow, 1998.

[78] T.J. Quinn, C.C. Speake, R.S Davis, and W. Tew. *Stress-dependent damping in Cu-Be torsion and flexure suspensions at stresses up to 1.1 GPa. Physics Letters A*, **198**:474, 1995.

[79] A. S. Nowick and B. S. Berry. *Anelastic relaxation in crystalline solids.* Academic Press, New York and London, 1972.

[80] A. P. French. *Vibrations and Waves.* M.I.T Introductory Physics Series, (Van Nostrand International), 1965.

[81] P.R. Saulson. *Thermal noise in mechanical experiments. Physical Review D*, **42**:2437–2445, 1990.

[82] A. Ageev, B. C. Palmer, A. De Felice, et al. *Very high quality factor measured in annealed fused silica. Classical and Quantum Gravity*, **21** (16):3887, 2004.

[83] S. Rowan, S. M. Twyford, J. Hough, and D. H. Gwo. *Mechanical losses associated with the technique of hydroxide-catalysis bonding of fused silica. Physics Letters A*, **246**:471–476, 1998.

[84] P. Sneddon, S. Bull, G. Cagnoli, et al. *The intrinsic mechanical loss factor of hydroxy-catalysis bonds for use in the mirror suspensions of gravitational wave detectors. Classical and Quantum Gravity*, **20**:5027–5037, 2003.

[85] J. E. Logan, J. Hough, and N. A. Robertson. *Aspects of the thermal motion of a mass suspended as a pendulum by wires. Physics Letters A*, **183**:145–152, 1993.

[86] G. Cagnoli, J. Hough, D. DeBra, et al. *Damping dilution factor for a pendulum in an interferometric gravitational waves detector. Physics Letters A*, **272**:39–45, 2000.

[87] Y. Levin. *Internal thermal noise in the LIGO test masses: A direct approach. Physical Review D*, **57**:659–663, 1998.

[88] Y. Liu and K. S. Thorne. *Thermoelastic noise and homogeneous thermal noise in finite sized gravitational-wave test masses. Phys. Rev. D*, **62**: 122002, 2000.

[89] Advanced LIGO team. *Advanced LIGO Reference Design.* LIGO DCC M060056-v2, 2011.

[90] G. Harry, M. Abernathy, A. Becerra-Toledo, et al. *Titania-Doped Tantala/Silica Coatings for Gravitational Wave Detection. Classical and Quantum Gravity*, **24**:405, 2006.

[91] N. Nakagawa, A. Gretarsson, E. Gustafson, et al. *Thermal Noise in half-infinite mirrors with nonuniform loss: A slab of excess loss in a half-infinite mirror. Physical Review D*, **65**, 2002.

[92] I. W. Martin, E. Chalkley, R. Nawrodt, et al. *Comparison of the temperature dependence of the mechanical dissipation in thin films of Ta2O5 and Ta2O5 doped with TiO2. Classical Quantum Gravity*, **26**, 2009.

[93] I. W. Martin, R. Bassiri, R. Nawrodt, et al. *Effect of heat treatment on mechanical dissipation in Ta2O5 coatings. Classical and Quantum Gravity*, **27**(22), 2010.

[94] G. Harry, M. Abernathy, A. Becerra-Toledo, et al. *Titania-doped tantala/silica coatings for gravitational-wave detection. Classical Quantum Gravity*, **24**:405–415, 2007.

[95] D. R. M. Crooks, G. Cagnoli, M. M. Fejer, et al. *Experimental measurements of mechanical dissipation associated with dielectric coatings formed using SiO2, Ta2O5 and Al2O3. Classical and Quantum Gravity*, **23**(15):4953–4965, 2006.

[96] R. Flaminio, J. Franc, C. Michel, et al. *A study of coating mechanical and optical losses in view of reducing mirror thermal noise in gravitational wave detectors. Classical and Quantum Gravity*, **27**, 2010.

[97] F. Brückner, D. Friedrich, T. Clausnitzer, et al. *Demonstration of a cavity coupler based on a resonant waveguide grating. Optical society of America*, 2008.

[98] C. Zener. *Internal friction in solids. Physical Review*, **52**:230–234, 1937.

[99] http://www.gwastro.org/.

[100] D.H. Gwo. *Ultra-precision bonding for cryogenic fused silica optics.* In J.B. Heaney and L.G. Burriesci, editors, *Proc. of SPIE, Cryogenic optical systems and instruments VIII*, volume **3435**, page 136, 1998.

[101] D.H. Gwo. *Ultra precision and reliable bonding method U.S. Patent no. US 6,284,085 B1*, 2001.

[102] D.H. Gwo. *Hydroxide-catalysed bonding*, U.S. Patent no. US 6,548,176 B1, 2003.

[103] S.M. Twyford, S. Rowan, J. Hough, and D.H. Gwo. *Losses associated with the bonding of fused quartz fibres to fused quartz test masses.* In *Proceedings from the Second Edoardo Amaldi Conference on Gravitational Waves*, volume **4**, pages 479–484, 1997.

[104] P Amico, L Bosi, L Carbone, L Gammaitoni, et al. *Fused silica suspension for the VIRGO optics: status and perspectives. Classical and Quantum Gravity*, **19**:1669–1674, 2002.

[105] S. Kawamura and F. Raab. *Suspension Design Requirements.* LIGO DCC T950011-14, 1995.

[106] L. Cunningham, P. G. Murray, A. Cumming, et al. *Re-evaluation of the mechanical loss factor of hydroxide catalysis bonds and its significance for the next generation of gravitational wave detectors. Physics Letters A*, **374**(39):3993–3998, 2010.

[107] M. van Veggel, A. Bell, A. Cumming, et al. *Final Design Document ETM/ITM Ears*. LIGO DCC T0900447, 2009.

[108] R. K. Iler. *The Chemistry of Silica*. John Wiley and Sons, 1979.

[109] E. J. Elliffe, J. Bogenstahl, A. Deshpande, et al. *Hydroxide-catalysis bonding for stable optical systems for space. Classical and Quantum Gravity*, **22**:257, 2005.

[110] http://www.zygo.com.

[111] R. T. Fenner. *Mechanics of Solids*. CRC Press, 1993.

[112] *ASTM C1161-02c, Standard Test Method for Flexural Strength of Advanced Ceramics at Ambient Temperature*. ASTM International, 2008.

[113] D. Coyne. *LIGO Vacuum Compatibility, Cleaning Methods and Qualification Procedures*. LIGO DCC E960022-v14, 2011.

[114] A. Cumming. Private communication. 2009.

[115] http://www.corning.com/docs/specialtymaterials/pisheets.

[116] http://heraeus-quarzglas.com/media/webmedia_local/downloads.

[117] http://www.corning.com/specialtymaterials/.

[118] http://www.heraeusoptics.com/products/p_productsoptics.cfm.

[119] http://www.goochandhousego.com/.

[120] W. Winkler, K. Danzmann, A. Rüdiger, et al. *Heating by optical absorption and the performance of interferometric gravitational-wave detectors. Physical Review A*, **44**(11):7022–7036, 1991.

[121] K. Numata, G. Bianc, N. Ohishi, et al. *Measurement of the intrinsic mechanical loss of low-loss samples using a nodal support. Physics Letters A*, **276**(37), 2000.

[122] B. S. Lunin and S. N. Torbin. *Vestnik Moskovskogo Universiteta*, **41**:93, 2000.

[123] S. D. Penn, G. M. Harry, A. M. Gretarsson, et al. *High quality factor measured in fused silica. Review of Scientific Instruments*, **72**:3670, 2001.

[124] H. J. Pain. *The Physics of Vibrations and Waves.* Wiley, New York, 2000.

[125] V. B. Braginsky, V. P. Mitrofanov, and V. I. Panov. *Systems with Small Dissipation.* University of Chicago Press, 1985.

[126] A. Cavalleri, G. Ciani, R. Dolesi, et al. *Increased Brownian Force Noise from Molecular Impacts in a Constrained Volume. Physical Review Letters*, **103**, 2009.

[127] A. Cumming. *Aspects of mirrors and suspensions for advanced gravitational wave detectors.* PhD thesis, Department of Physics and Astronomy, University of Glasgow, 2008.

[128] J. E. Logan, N. A. Robertson, and J. Hough. *An investigation of limitations to quality factor measurements of suspended masses due to resonances in the suspension wires. Physics Letters A*, **170**:352–358, 1992.

[129] http://www.ansys.com.

[130] K. Numata, S. Otsuka, M. Ando, et al. *Intrinsic losses in various kinds of fused silica. Classical and Quantum Gravity*, **19**:1697–1702, 2002.

[131] S. Rowan, R. Hutchins, A. McLaren, et al. *The quality factor of natural fused quartz ribbons over a frequency range from 6 to 160 Hz. Physics Letters A*, **227**(3-4):153 – 158, 1997.

[132] P. Sneddon. *Investigations of Internal Mechanical Loss Factors of Test Mass Materials For Interferometric Gravitational Wave Detectors.* Phd thesis, University of Glasgow, 2001.

[133] A. Gillespie. *Thermal Noise in the Initial LIGO Interferometers.* Phd thesis, California Institute of Technology, 1995.

[134] W. J. Startin, M. A. Beilby, and P. R. Saulson. *Mechanical quality factors of fused silica resonators. Review of Scientific Instruments*, **69**: 3681–3689, 1998.

[135] K. Numata, K. Yamamoto, H. Ishimoto, et al. *Systematic measurement of the intrinsic losses in various kinds of bulk fused silica. Physics Letters A*, **327**:263–271, 2004.

[136] A. Gretarsson. *Thermal noise in low loss flexures.* PhD thesis, Syracuse University, 2002.

[137] A. Ageev, B. C. Palmer, A. De Felice, et al. *Very high quality factor measured in annealed fused silica. Classical and Quantum Gravity*, **21**: 3887–3892, 2004.

[138] A. M. Gretarsson and G. M. Harry. *Dissipation of mechanical energy in fused silica fibers. Review of Scientific Instruments*, **70**:4081–4087, 1999.

[139] S. Penn, A. Ageev, D. Busby, et al. *Frequency and surface dependence of the mechanical loss in fused silica. Physics Letters A*, **352**:3–6, 2006.

[140] B. S. Lunin. *Physical and Chemical Bases for the Development of hemisperical resonators for solid-state gyroscopes.* Moscow: Moscow Aviation Institute, 2005.

[141] J. Wiedersich, S. V. Adichtchev, and E. Rossler. *Spectral Shape of Relaxations in Silica Glass. Physical Review Letters*, **84**(12):2000, 2000.

[142] O. L. Anderson and H. E. Bommel. *Ultrasonic absorption in fused silica at low temperatures and high frequencies. Journal of the American Ceramic Society*, **38**:125–131, 1955.

[143] R. E. Strakna. *Investigation of low temperature ultrasonic absorption in fast-neutron irradiated SiO_2 glass.* *Physical Review*, **123**:2020–2026, 1961.

[144] M. R. Vukcevich. *A new interpretation of the anomalous properties of vitreous silica.* *Journal of Non-Crystalline Solids*, **11**:25–63, 1972.

[145] S. Reid. *Studies of materials for future ground-based and space-based interferometric gravitational wave detectors.* PhD thesis, Department of Physics and Astronomy, University of Glasgow, 2006.

[146] S. Rowan for LIGO Laboratory and LSC Partners. *Substrate mechanical loss studies.* LIGO DCC G020420-00-R, 2002.

[147] Stuart Reid. *Private Communication following discussions between Stuart Reid and David Bright in 2008*, 2011.

[148] S. Hild, H. Lück, W. Winkler, et al. *Measurement of a low-absorption sample of OH-reduced fused silica.* *Applied Optics*, **45**(28):7269–7272, 2006.

[149] H. Armandula, G. Billingsley, G. Harry, et al. *Core Optics Components Design*, 2010.

[150] P. Fritschel. *Advanced LIGO Systems Design.* LIGO DCC T010075-v2, 2009.

[151] http://einstein.standford.edu/content/topics/pg4.html.

[152] A. Heptonstall, G. Cagnoli, J. Hough, et al. *Characterisation of mechanical loss in synthetic fused silica ribbons.* *Physics Letters A*, **354**, 2006.

[153] A. Cumming, R. Jones, M. Barton, et al. *Apparatus for dimensional characterization of fused silica fibers for the suspensions of ad-*

vanced gravitational wave detectors. Review of Scientific Instruments, **82**(044502), 2011.

[154] M. M. Fejer, S. Rowan, G. Cagnoli, et al. *Thermoelastic dissipation in inhomogeneous media: loss measurements and displacement noise in coated test masses for interferometric gravitational wave detectors. Physical Review D*, **70**, 2004.

[155] J. K. White. *Thermal expansion of reference materials: copper, silica and silicon. Journal of Physics D, Applied physics*, **6**, 1973.

[156] A. Gretarsson. *Thermal Noise in Low Loss Flexures.* PhD thesis, Syracuse University, 2002.

[157] A. Heptonstall, M. Barton, C. Cantley, et al. *Investigation of mechanical dissipation in CO_2 laser-drawn fused silica fibres and welds. classical and Quantum Gravity*, **27**(035013), 2010.

[158] P. Holt. *Quantifying Surface Loss Of Mechanically Polished Silica Cantilevers.* PhD thesis, Department of Physics and Astronomy, University of Glasgow, 2007.

[159] G. Hammond. *Enhancements to the aLIGO Suspension.* Presented at a LVC meeting G1100343-v2.

[160] M. Fine. *Low-Temperature Internal Friction and Elasticity Effects in Vitreous Silica. Journal of Applied Physics*, **25**:402, 1953.

[161] A. Schroeter, R. Nawrodt, R. Schnabel, et al. *On the mechanical quality factors of cryogenic test masses from fused silica and crystalline quartz. arXiv:0709.4359v1 [gr-qc]*, 2007.

[162] V. B. Braginsky, M. L. Gorodetsky, and S. P. Vyatchanin. *Thermo-refractive noise in gravitational wave antennae. Physics Letters A*, **271**: 303–307, 2000.

[163] D. F. McGuigan, C. C Lam, R. Q. Gram, et al. *Measurements of the Mechanical Q of Single-Crystal Silicon at Low Temepratures. Journal of Low Temperature Physics*, **30**(5/6), 1978.

[164] S. Rowan, S. M. Twyford, R. Hutchins, et al. *Q factor measurements on prototype fused quartz pendulum suspensions for use in gravitational wave detectors. Physics Letters A*, **233**:303–308, 1997.

[165] S. Rowan, R. Byer, M. Fejer, et al. *Test Mass Materials for a New Generation of Gravitational Wave Detectors. Proceedings of SPIE, edited by M. Cruise and P. Saulson*, **4856**:292, 2003.

[166] S. Rowan and S. Reid for GEO600/Stanford Groups. *Aspects of silicon for use in the suspensions of gravitational wave detectors.* LIGO DCC G050054-00-Z, 2005.

[167] S. Reid, G. Cagnoli, D. R. M. Crooks, et al. *Mechanical dissipation in silicon flexures. Physics letters A*, **351**:205–211, 2006.

[168] N. L. Beveridge, A. A. van Veggel, M. Hendry, et al. *Low temperature strength tests and SEM imaging of hydroxide-catalysis bonds between silicon. Classical and Quantum Gravity*, **28**(8), 2011.

[169] Y.S. Touloukian et al. *Thermophysical properties of matter.* Plenum., New York, 1970.

[170] S. Hild, M. Abernathy, F. Acernese, et al. *Sensitivity studies for third-generation gravitational wave observatories. Classical and Quantum gravity*, **28**, 2011.

[171] J. Czochralski. *Ein neues Verfahren zur Messung der Kristallisationsgeschwindigkeit der Metalle. Z. Physik. Chem.*, **92**:219–221, 1918.

[172] http://www.semicor.ukrpack.net/.

[173] http://www.spanoptic.com.

[174] C. Kittel. *Introduction to Solid State Physics*. John Wiley and sons, 1966.

[175] B. A. Auld. *Acoustic Fields and Waves in Solids*, volume **1**. Wiley, New York, 1973.

[176] W. L. Bond. *The Mathematics of the Physical Properties of Crystals. Bell System Technical Journal*, **22**:1–72, 1943.

[177] T. Lackner. *Determination of Axisymmetric Elastic Constants in Anisotropic Silicon for a Thyristor Tablet. Journal of Electronic Materials*, **18**(1), 1989.

[178] http://www.advent-rm.com/.

[179] http://www.olympus.co.uk.

[180] http://www.sios.de/.

[181] R. C. Jaeger. *Introduction to microelectronic fabrication*. Upper saddle river: Prentice Hall, 2001.

[182] http://www.sentech.de/.

[183] htp://www.taylor-hobson.com.

[184] Robert Hull (Editor). *Properties of Crystalline Silicon*. INSPEC, The Institute of Electrical Engineers, London, United Kingdom, 1999.

[185] D. Crooks. *Mechanical Loss and its Significance in the Test Mass Mirrors of Gravitational Wave Detectors*. PhD thesis, Department of Physics and Astronomy, University of Glasgow, 2003.

[186] G. W. McMahon. *Experimental study of vibrations of solid, isotropic, elastic cylinders. Journal of Accoustical Society of America*, **36**:85–92, 1964.

[187] L. Cunningham, C. Torrie, and A. Cumming. *Development of an FEA model to investigate the thermal noise in the bond layer of the ETM TM for AdLIGO thermal noise simulation.* LIGO DCC LIGO-T080163-V2, 2008.

[188] P. Murray. *Measurement of the Mechanical Loss of Test Mass Materials for Advanced Gravitational Wave Detectors.* PhD thesis, Department of Physics and Astronomy, University of Glasgow, 2008.

[189] B.E. White Jr. and R.O. Pohl. *How do two-level-systems come about? Physica B: Condensed Matter*, **219-220**:267–269, 1996.

[190] E. Chalkley. *Investigations of the Properties of Materials for the Optics and Suspensions of Future Gravitational Wave Detectors.* PhD thesis, University of Glasgow, 2010.

[191] R. Nawrodt. Private communication. 2011.